STRATOSPHERIC BEHAVIOR DURING TROPOSPHERIC PERSISTENT ANOMALY EVENTS

by Robert John Conzemius

B. A. Chemistry, St. John's University
Collegeville, Minnesota
(1988)

Submitted to the Department of
Earth, Atmospheric and Planetary Sciences
in partial fulfillment of the requirements
for the Degree of

MASTER OF SCIENCE
in Meteorology

at the

Massachusetts Institute of Technology

June 1990

Signature of Author.....
Department of Earth, Atmospheric and Planetary Sciences
May 29, 1990

Certified by.....
Randall M. Dole
Professor of Meteorology
Thesis Supervisor

Certified by.....
R. Alan Plumb
Professor of Meteorology
Thesis Supervisor

Accepted by.....
Thomas H. Jordan
Chairman, Departmental Committee on Graduate Students

ACKNOWLEDGEMENTS

I would like to thank my advisors Alan Plumb and Randy Dole for their guidance and direction towards completion of this thesis. I would also like to thank those students who helped get this research started, particularly Peter Neilley, who helped me extensively with the construction of the datasets, and Rob Black, who provided information about the persistent anomaly events I studied. I must also not forget Mike Morgan and Chun Wu. They helped me in my coursework when I found it very difficult. Also, I thank my family for the spiritual encouragement they gave from Minnesota. Finally, thanks goes to Jane McNabb, who helped me extensively with getting the thesis in final form and to Diana Spiegel, system manager of the VAX cluster here at the Center for Meteorology and Physical Oceanography.

Support for this research was provided by NASA Grant NAGW-1727 and NSF Grant 8911459-ATM. Many of the calculations were performed on the National Center for Atmospheric Research computing system. NCAR is supported by the National Science Foundation.

CONTENTS

STRATOSPHERIC BEHAVIOR DURING TROPOSPHERIC PERSISTENT ANOMALY EVENTS

by

Robert John Conzemius

Submitted to the Department of Earth, Atmospheric and Planetary Sciences on May 29, 1990 in partial fulfillment of the requirements for the Degree of Master of Science in Meteorology

ABSTRACT

This thesis extends previous observational studies of persistent anomalies by examining whether the developments of persistent anomaly events in the troposphere are associated with significant stratospheric flow anomalies. We focus here on wintertime persistent anomaly cases occurring over the North Pacific (PAC) and North Atlantic (ATL) regions.

For both positive and negative anomaly cases in these regions, composite evolution analyses are constructed of the geopotential heights and height anomalies at both the 70 mb and 10 mb levels. In addition, composite analyses of temperatures and temperature anomalies and longitude-pressure cross sections of height anomalies are obtained for the PAC events. These analyses reveal some surprising new features, referred to as initial stratospheric polar anomalies (ISPA's), which are evident at both 70 and 10 mb in the polar regions throughout the ATL cases and before onset of the PAC cases. The ISPA's are the most intense and highly significant features at 10 mb. The PAC positive (PACPOS) and ATL negative (ATLNEG) anomaly patterns both have positive ISPA's, while the PAC negative (PACNEG) and ATL positive (ATLPOS) both have negative ISPAs. This suggests that there may be some relationship between the prior large-scale stratospheric circulation and the polarity of the ATL and PAC patterns that subsequently develop.

Aside from the ISPAs, the ATL patterns do not exhibit a strong systematic association with anomalies in the stratospheric circulation. In the PAC events, however, an anomaly pattern develops at 70 mb a few days following the onset of the tropospheric anomalies. This pattern strongly resembles the 500 mb pattern described in Dole (1986a,1986b), and appears to have a predominantly equivalent barotropic character. At 10 mb, there is some evidence for anomalous upward-propagating waves. Overall, the general 10 mb circulation in the PACPOS cases begins with a large zonal wave 1 ridge centered over Alaska and gradually changes to a more zonal flow by day +10. In the PACNEG cases, the 10 mb flow is predominantly zonal before onset, and gradually changes to a pattern characterized by more highly amplified planetary scale waves.

Diagnostic analyses performed on the PAC cases indicate that the PACNEG events are associated with anomalously strong upward wave propagation, while the PACPOS cases have a generally reduced upward flux of wave activity. Cross sections of zonally averaged wave activity and zonal mean wind anomalies for the PACPOS cases show an anomalously weak polar vortex and positive ISPAs before onset. Following onset, the developing

tropospheric flow anomalies associated with the PACPOS cases appear to be mainly trapped within the troposphere, while those associated with the PACNEG cases extend upward to 10mb. Eliassen - Palm (EP) flux diagnostics confirm this view, showing anomalously strong upward propagation in the PACNEG cases, but reduced upward EP fluxes during and following the onset of the PACPOS cases. In the PACPOS cases, the stratospheric flow anomalies are associated synoptically with a predominantly zonal flow. On the basis of these analyses, we suggest that the stratospheric flow anomalies that occur following the developments of the PACPOS cases are unlikely to represent enhanced upward wave propagation from anomalous tropospheric sources, but rather indicate the circulation that would occur if upward propagation of planetary wave activity is significantly reduced.

The connections between four major stratospheric warmings and persistent anomaly cases are then examined. It is found that for all of these warmings amplified ridges are present over both the eastern Pacific and the eastern Atlantic or Europe. The persistent anomaly patterns appear as prominent features of the large scale wave patterns associated with these events.

Thesis Supervisor: Randall M. Dole
Title: Professor of Meteorology

Thesis Supervisor: R. Alan Plumb
Title: Professor of Meteorology

CHAPTER 1

INTRODUCTION

1.1 Background and Motivation

Atmospheric patterns associated with low frequency variability have been the subject of intensive study in recent years. Perhaps the most thoroughly documented of these are blocking patterns (e.g., Rex1950a,b), although studies of teleconnections (Wallace and Gutzler, 1981) and persistent anomalies (Dole and Gordon, 1983; Dole, 1986a) have provided convincing evidence for the existence of other recurrent low-frequency circulation anomalies. Until now, the focus for these studies has been on determining characteristic features of the tropospheric circulation. In particular, previous observational studies of persistent anomalies have documented the geographical distributions, mean horizontal and vertical structures, and time evolution of significant features associated with the development and decay of the anomalies.

In their original study, Dole and Gordon (1983, henceforth DG) described the geographical distributions of persistent anomalies of the extratropical Northern Hemisphere wintertime circulation. They found three regions of maximum occurrence: 1) over the North Pacific to the south of the Aleutian Islands (PAC), 2) over the eastern North Atlantic (ATL), and over the northern Soviet Union (NSU). Dole (1986a, henceforth DA) then described the time-mean structures of flow patterns associated with persistent anomalies in these regions. He found that, to a first approximation, the

composite positive and negative anomaly patterns in a given region can be described as opposite phases of the same basic pattern, which he described as the primary regional pattern of low-frequency variability. For the PAC and ATL regions, the primary patterns resembled, respectively, the PNA and EA teleconnection patterns described by Wallace and Gutzler (1981).

DA also found that the vertical structures associated with the persistent anomalies appeared to be predominantly equivalent barotropic in character, with only slight evidence of a westward tilt with height between the 1000 mb and 100 mb levels (on the order of 5° to 10° longitude over this layer). This agrees with results of other studies of vertical structures of transient disturbances (Blackmon et al., 1979; Lau and Nath, 1987), which show that the patterns with low frequency variability typically have little or no westward phase tilt with height. DA and Blackmon et al. also found that the amplitude of the height anomalies was largest near 300 mb, as would be expected if the anomalies were predominantly the manifestation of external Rossby waves (Held, 1983).

Subsequently, Dole (1986b, henceforth DS; 1989, henceforth DE) and Dole and Black (1990, hereafter DB) examined the time evolution of flow patterns associated with persistent anomalies, focusing on times around the development and breakdown of the anomalous patterns. In particular, DB presented extensive synoptic and diagnostic analyses of the development of Pacific negative cases (hereafter PACNEG). They found that the early stages of the developments were associated with the intensification of the east Asian jet and the development of a midlatitude baroclinic disturbance over the western Pacific. As this disturbance propagated toward the mid-Pacific, it appeared to increase in scale while acquiring a more equivalent barotropic structure. Anomaly centers then intensified in sequence downstream from the key region, eventually forming the mature PAC negative anomaly pattern, which was characterized synoptically by an abnormally intense Aleutian low, an enhanced ridge over western North America, and a

deepened trough over the east coast of the United States.

Diagnostic analyses by DB indicated that there were net poleward heat fluxes associated with the anomalies during both the early and late stages of the developments. DB suggested that the poleward heat fluxes at early stages were likely to be related to baroclinic development on long synoptic-scales. Such synoptic-scale disturbances would be unlikely to propagate above the tropopause and therefore would not be expected to significantly influence the stratospheric circulation (e.g., Holton, 1979). At later stages, however, DB indicated that the poleward heat fluxes appeared to be associated with a disturbance of considerably larger scale (predominantly zonal wavenumbers k - 1 - 4).

While the above studies have only documented the vertical structures and evolution of persistent anomalies only up to the 100 mb level, the presence of substantial poleward heat fluxes together with the relatively large zonal scales of the disturbances suggests that at later stages in the developments, more significant vertical propagation into the stratosphere may occur. It is the purpose of this thesis to examine this possibility by determining the changes in the stratospheric circulation that are associated with the development of tropospheric persistent anomalies.

CHAPTER 2

DATA AND METHODS

2.1 Data

Tropospheric data for this study were obtained from twice daily (0000Z and1200Z) NMC tropospheric height and temperature grids at all ten standard levels from 1000 to 100 mb for 25 152-day winter seasons (1 November to 31 March) covering the winters 1962-63 through 1986-87. In addition, once daily (1200Z) stratospheric height and temperature grids at 70, 50, 30, and 10 mb were available starting 8 January 1973 and continuing through 31 March 1986. Except for the period 21 September 1974 through 17 December 1975 at 70 mb and 50 mb, 0000Z observations were unavailable for stratospheric levels above 100 mb.

Missing grids were interpolated linearly and hydrostatically if heights and/or temperatures were missing at one level. For levels above 100 mb, if two or more consecutive levels of height grids were missing, a hydrostatic interpolation was used if temperature grids were present at those levels. Whenever data could not be interpolated hydrostatically from contemporaneous data, missing grids were interpolated in time. Levels at and below 100 mb were interpolated linearly in time from surrounding available grids if three or fewer consecutive 12-hourly observations were absent. Stratospheric levels were interpolated linearly in time if two or fewer consecutive 1200Z times (or if 0000Z grids existed, five or fewer consecutive 12-hourly observations) were missing.

Since levels above 100 mb generally were present only at 1200Z, most 0000Z times are interpolated from surrounding 1200Z times.

2.2 Methods

Climatological normals of height and temperature were found by computing the first four Fourier coefficients of the annual variation from a year-round dataset. For the levels at and below 100 mb, the period 1 January 1962 through 31 December 1987 was used to calculate the coefficients. For levels 70 mb and above, the period was 8 January 1973 through 7 January 1986. Grids that were interpolated were not used in the calculation of the Fourier coefficients.

Normal grids constructed from these coefficients were subtracted from the observed fields to obtain the anomalies. A persistent anomaly was defined as in DG as a 500 mb height anomaly of magnitude equal to or greater than M which exists for a duration equal to or greater than D. For this study as in previous studies, M and D were chosen as 100m and 10 days respectively. Cases began when the height anomaly first crossed the M threshold, defined as day 0 (all other days are relative to this time), and ended when the anomaly again became less than M. Anomalies were scaled by the sine of latitude as in DG before these criteria were applied.

DG selected cases at the original keypoints, indicated in Appendix B, for the winters up until 1976/77. Prior to the case selection, the anomaly time series was low-pass filtered as in Blackmon et al. (1976) in order to remove effects of transient synoptic-scale disturbances on the starting (day 0) and ending times. Also, the climatology used for the selection of these cases was from a least-squares quadratic fit to the 14 winter time series from 1963/1964 through 1976/77.

For cases selected since that time, a slightly different filter, described by Blackmon et al. (1986) was used. The climatology used was constructed from the first four Fourier coefficients from a 23 year dataset starting in 1963 and ending in 1986 (Black, personal communication). Using this slightly newer selection procedure and the same selection criteria, Black found a slightly different regional distribution in cases for the winters 1977/78 through December 1986. The new keypoints and their cases are listed in appendix B.

The cases used in this study are those identified by DG and Black for which good stratospheric data were available up to 10 mb. In total, 7 PACPOS, 13 PACNEG, 9 ATLPOS, and 8 ATLNEG cases were selected for the original keypoint, and 7 PACPOS, 11 PACNEG, 8 ATLPOS, and 8 ATLNEG cases were chosen at the new keypoint.

The procedure used to analyse the cases was a simple compositing technique. First, heights and temperatures were obtained from the dataset for a particular case. The climatological normal was constructed using the first four Fourier coefficients of the annual cycle, and then was subtracted from the heights and temperatures to obtain their anomalies. The heights and temperatures and their anomalies were then averaged together for each category of cases (i.e. PACPOS, etc.) to form the analyses that appear in the next chapter.

CHAPTER 3

STRATOSPHERIC COMPOSITE ANALYSES

3.1 Overview

Composite analyses were constructed for both the ATL and PAC cases for the period from six days before case onset (as defined for the 500 mb data) until fourteen days after case onset (day +14). Composite height and temperature fields were formed by averaging together all available cases. Anomalies were computed by subtracting the daily climatology for each day from each individual case and then averaging that difference over all cases. The climatology was from the first four Fourier coefficients of the annual cycle. Confidence levels of the composites were estimated using a two-sided student's t-test.

Longitude-pressure cross sections were constructed around latitude circles at 40°N, 50°N, 60°N, and 70°N for composite PACPOS and PACNEG height anomalies. Maximum height anomaly magnitudes at 500 mb occur between 40°N and 50°N, while at 10 mb, the largest magnitudes occur near 70°N. Thus, a cross section at 60°N may be the most representative of the relationships that exist between the troposphere and the stratosphere. 60°N is near where the maximum anomalies occur in the stratosphere that we want to look at, but it is still far enough to the south to see anomalies in the lower troposphere quite well. Observations of other latitudes confirm this point of view.

In order to get a better view of growth and dissipation of the waves, height anomalies in the longitude-pressure cross sections were scaled by the square root of

pressure (in mb) relative to 300 mb. Specifically, the coefficient for scaling was defined as the square root of pressure divided by the square root of 300. Thus, a 300 mb scaled anomaly, is equal to a 300 mb unscaled anomaly.

3.2 Pacific Events

3.2.1 PACPOS

Height Anomalies

Composite height anomaly fields and t-test results for the PACPOS cases are shown in Fig. 3.1 for 70 mb and in Fig. 3.2 for 10 mb. In Fig. 3.3 are the composite height fields for the PACPOS cases at day -2 and day +10 at 70 mb and 10 mb. Longitude-pressure cross sections are shown in Fig. 3.4 for the same days in Figs. 3.1 and 3.2.

Somewhat surprisingly, the most persistent feature in the 70 mb composites is the strong positive anomaly found before day 0 in the Western Hemisphere between 70°N and the North Pole, indicating a weakened polar vortex. This anomaly is present back to day -10 (not shown) and persists through day +4 (not shown) when it moves to a point just north of Iceland. From now on, these high latitude anomalies before case onset will be referred to as initial stratospheric polar anomalies (ISPA's). The anomaly in PACPOS cases is a positive ISPA. Also present at day -6 (Fig. 3.1a) is a negative height anomaly over Siberia. While not highly significant, it maintains its identity while drifting to the northeastern Soviet Union, where it increases in strength through day +2 (Fig. 3.1c) and then slowly weakens. By this time, a positive anomaly has developed over the keypoint. It grows in amplitude and is followed downstream by a negative height anomaly over

western North America, reminiscent of the downstream wavetrain found at 500 mb. The North American trough then deepens until the end of the period, when a strong wavenumber two signature is present. In the 70 mb height fields, this mature pattern is seen in the form of an enhanced Pacific ridge, deeper trough in western North America, and a ridge over the North Atlantic, with a highly distorted vortex that appears in nearly two pieces.

At 10 mb (Fig. 3.2), the dominant pattern is one of a large positive anomaly near the pole surrounded by negative anomalies in lower latitudes. The same ISPA as at 70 mb is much higher in amplitude and has greater areal coverage. However, it is important to take into consideration at this point the pressure-dependence of amplitude. For an upward propagating Rossby wave whose kinetic energy density remains constant, geopotential amplitude increases by a factor proportional to the inverse square root of pressure (Charney and Drazin, 1961). Thus, a Rossby wave propagating upward from 70 mb to 10 mb will increase in amplitude by a factor of approximatly 2.5. Thus, when the anomalies are scaled to the square root of pressure, one sees that the strength of the positive anomaly is basically unchanged from 70 mb (Fig. 3.1b) to 10 mb (Fig. 3.2b).

Because this large positive anomaly was not expected, one might tend to discount its significance. However, not only is it the largest amplitude anomaly, but it is also the most statistically significant feature (aside from the negative anomalies at the same time over the western Atlantic and eastern United States).

Over Siberia, the same negative anomaly as at 70 mb is present. After day +2 (Fig. 3.2c), the positive anomaly weakens and drifts eastward to near the Greenwich Meridian by day +14 (Fig. 3.2f). At day +6 (Fig. 3.2d), a negative anomaly begins to strengthen over western North America as at 70 mb and continues to strengthen through day +12 (not shown). In the longitude-pressure cross sections (Fig. 3.4), it appears that this negative anomaly is related to the tropospheric negative anomaly over western North

America. Note that a positive anomaly over the keypoint at 10 mb is either very weak or totally absent throughout the time series, with the mature pattern dominated by wavenumber one.

In the 10 mb composite on day -2 (Fig. 3.3b), there is an abnormally strong Pacific ridge and a highly distorted vortex with strong warming apparent over the pole. By day +10 (Fig. 3.3d), the flow is more zonal. However, the polar vortex has not deepened during this period but has simply moved closer to the pole.

Vertical Structure

In the longitude-pressure cross section in Fig. 3.4a, a trough (negative anomaly) is found over the keypoint longitude with a large-scale ridge (the ISPA) to the east, which penetrates strongly into the stratosphere. The trough loses intensity in the troposphere at 180°W by day -2 (Fig. 3.4b), but negative height anomalies become more dominant in both the troposphere and the stratosphere between the dateline and 75°E. The ISPA maintains its strength through day -2. By day 0 (not shown), the ISPA has disappeared in the troposphere and the trough remains diffuse. On day +2 (Fig. 3.4c), a new ridge is observed near 165°W and the Rockies (120°W to 100°W) are covered by a trough. The ISPA is, however, still present in the stratosphere. Negative height anomalies then extend upward to 10 mb on day +6 (Fig. 3.4d), and the keypoint ridge reaches full strength. On following days, the ridge-trough pattern expands in vertical as well as horizontal scale, with the Rockies trough extending with nearly full strength up to at least 10 mb. On days +10 (Fig. 3.4e) and +14 (Fig. 3.4f), the cross sections show that the primary anomaly over the keypoint is mostly trapped in the troposphere, but the secondary anomaly, namely, the trough over the Rockies, displays much more evidence of upward propagation. This difference is clearly visible when looking at the +60m and -60m contours.

On day +14 the decrease in the zonal wavenumber with height is clearly evident. At the surface, several troughs and ridges are present, but at higher levels, the dominant wavenumbers are one and two. Only the strongest and largest scale anomalies penetrate significantly above the tropopause.

Latitude-pressure cross sections (not shown) were then taken at 170°W and 120°W, the longitudes of the ridge and trough respectively. At 170°W, the ridge grows rapidly during onset and covers the latitudes from 30°N to 60°N, with maximum strength at 45°N. Following this development, the ridge expands in horizontal scale as its center of maximum strength drifts northward to near 70°N. However , it appears to be strongly trapped, never reaching 10 mb. At 120°W, the trough develops around day +2 below 150 mb between 40°N and 80°N. It then expands in vertical as well as horizontal scale, reaching at least up to 10 mb and covering most of the latitude-pressure cross section. Peak amplitude is near 60°N at 300 mb.

Thermal Structure

Similar composites were constructed for temperatures at all levels for the Pacific persistent anomalies. Temperature anomalies and their confidence levels for PACPOS cases at 70 mb are displayed in Fig. 3.5. The positive ISPA is visible in the temperature fields as a warm core feature at 70 mb. This warm core is surrounded by colder than normal temperatures until it is distorted by other anomalies associated with the primary anomaly at the keypoint and secondary anomalies of the downstream wavetrain. Around day +2 (Fig. 3.5c), a cold anomaly develops over the keypoint region. Also, during the same period, a pattern of alternating warm and cold centers can be seen downstream from the keypoint temperature anomaly, with warm temperature anomalies over western North America and cold anomalies over the southeastern United States. These anomalies are negatively correlated with the height anomalies at that level, consistent with the fact that

the height anomalies that are decaying upward.

At 10 mb (not shown), the warm core anomaly near the pole is also present but is less stationary than at 70 mb. There is also a cold anomaly over the western Pacific at day -6, which is relatively stationary. It is notable that this anomaly, south and west of the keypoint, is the only consistently significant anomaly in the 10 mb temperature anomaly field.

The 70 mb composite temperature fields, shown in Fig. 3.6, show some systematic changes from day -2 to day +10. On day -2 (Fig. 3.6a), the pool of coldest air is displaced slightly towards the northern Soviet Union. There is a zonally elongated warm center just south of the Bering Straits. By day +10 (Fig. 3.6b), the warm center has migrated westward to the east coast of Asia and is 3°C colder. The coldest air, by then, is over the polar region, with large temperature decreases over North America between day -2 and day +10. At 10 mb (not shown), qualitatively similar changes occur during the same time period.

3.2.2 PACNEG

Height Anomalies

Height anomalies and their confidence levels are shown for PACNEG cases at 70 mb in Fig. 3.7., and at 10 mb in Fig. 3.8. Figure 3.9 shows the composite height fields at days -2 and +10 for both 70 mb and 10 mb. For comparison between the signs of cases, Fig. 3.10 shows the difference between PACPOS and PACNEG heights at 70 mb and the significance of those differences. Fig. 3.11 shows these differences at 10 mb.

At 70 mb (Fig. 3.7), the negative cases have the same basic anomaly pattern as the positive cases, but with reversal of the sign of the anomalies. Again, significant

anomalies appear over the polar regions shortly before case onset, with the negative cases having a deeper, stronger vortex than the positive cases. At day -6 (Fig. 3.7a), there is a negative height anomaly over northwestern Canada, a negative ISPA. This anomaly is slightly farther south and west and is somewhat weaker than its counterpart in positive cases. Through day -2 (Fig. 3.7b), this anomaly center strengthens and drifts slightly northwestward. At the same time, a positive anomaly strengthens over Siberia and remains more or less stationary. This ridge over Siberia is the most statistically significant feature on the map before case onset. Longitude-pressure cross sections, displayed in Fig. 3.12, show that this ridge is coherent with the 500 mb Siberian ridge in DS. On days 0 (not shown) and +2 (Fig. 3.7c), a highly significant trough develops over the North Pacific that appears at first as an extension of the ISPA. Almost immediately, a ridge develops downstream over the Rocky Mountains, followed on day +6 (Fig. 3.7d) by a negative height anomaly over the southeastern United States, although this latter feature is not as highly significant. By day +6, a strong wavenumber two pattern exists, with three of the four anomaly centers being significant beyond the 99% confidence level on day +10 (Fig. 3.7e). In the composite 70 mb height field (Fig. 3.9c), the mature PACNEG pattern is marked by a deep trough over the western two thirds of the Pacific, a strong ridge over the west coast of North America, and an enhanced trough over eastern North America. This is the same basic pattern as at 500 mb, suggesting that the major contribution to the anomaly pattern at 70 mb is equivalent barotropic in character.

At 10 mb, the polar vortex is deeper in the PACNEG composite (Fig. 3.9b) than in the PACPOS composite (Fig. 3.3b). The same negative ISPA exists but is not highly significant, due to the relative weakness of the ISPA in PACNEG cases compared to the same feature in PACPOS cases. Nevertheless, it is still more than 95% significant on day -2 (Fig. 3.8b) and is the strongest of any stratospheric anomaly throughout the time series. Scaling to the square root of pressure reveals that this anomaly is relatively

constant with height, and the longitude-pressure cross sections (Fig. 3.12) bear this out. The Siberian positive anomaly is also present. Between day 0 (not shown) and day +6 (Fig. 3.8d), the anomaly centers weaken considerably and only the negative ISPA shows any marginal level of significance (90%). Then, a positive anomaly appears over northwestern North America and grows in amplitude and/or areal coverage up to day +14 (Fig. 3.8f) while a negative anomaly covers northern Europe. This feature, when traced back in time, is seen to be a part of the ISPA. The mature pattern in the 10 mb height anomaly field is clearly dominated by a wavenumber one, but neither anomaly center is significant to a high confidence level, due to the high variance in geopotential heights at 10 mb.

In the composite 10 mb height field (Fig. 3.9), the only obvious change through the period is enhanced ridging over the eastern Pacific and northwestern North America. Looking at the 10 mb composite heights (Fig. 3.9d) compared to the 70 mb heights (Fig. 3.9c) at day +10, as well as with the 70 mb and 10 mb height anomalies, the relatively larger scales in the propagation of disturbances to higher levels of the atmosphere is again evident. The scale of the eastern Pacific ridge is much larger at 10 mb than at 70 mb. Also, the negative height anomaly over the keypoint does not appear at 10 mb.

During the development of PACNEG events, then, the tendency at 10 mb is to bring the westerlies over Alaska closer to the pole. On day -2 (Fig. 3.9b), there is a deep vortex over the pole and the flow is relatively zonal. By day +10 (Fig. 3.9d), there is enhanced ridging over Alaska, and there is flow of lower latitude air over the pole. It would appear that the vortex should be weaker with such a pattern, but it is more displaced than weakened.

It is interesting to note the similarity between the PACPOS cases on day -2 (Fig. 3.3a,b) and the PACNEG cases on day +10 (Fig. 3.9c,d), especially at the 10 mb level. Both have an enhanced eastern Pacific ridge. The same relationship exists, qualitatively,

for PACNEG day -2 (Fig. 3.9a,b) and PACPOS day +10 (Fig. 3.3c,d), with a more zonal flow present on those days.

Vertical Structure

Longitude-pressure cross sections at 60°N for PACNEG composite height anomalies in Fig. 3.12 have few differences from the PACPOS cases, but these differences are significant. Before onset, the troposphere and the stratosphere appear to be dominated by different wavenumbers. In the troposphere, several disturbances of smaller scale extend from the surface up to 150 mb. These smaller wavenumbers are vertically trapped, and in the stratosphere, the height anomalies are of a much larger horizontal scale and are dominated by wavenumber two.

The negative ISPA is evident from 180° to 60°W. On day -2 (Fig. 3.12b), a trough appears east of the keypoint that appears to be connected with the ISPA, although this could be just an artifact of the analysis, as superposition of two separate disturbances, one in the stratosphere and the other in the troposphere, would produce the same structure. There is no clear evidence of any direct causal connection between the ISPA and the developing trough in the troposphere. Cross sections at 50°N and 40°N reveal that the disturbance that is associated with the development of the persistent anomaly pattern moves in from the west as in DS.

By day +2 (Fig 3.12c), the trough-ridge couplet is in place in the troposphere, and the trough already extends into the lower stratosphere. The primary anomaly extends into the stratosphere more than its counterpart in the PACPOS cases, although it is still more damped than the secondary anomaly to its east. By day +6 (Fig. 3.12d), the positive anomaly in the vicinity of 120°W extends into the highest levels of the cross section, where it continues to build until day +10 (Fig. 3.12e). At this time, the overall vertical structure bears strong resemblance to day -6 of PACPOS (Fig. 3.4a). Also notable

throughout the time series are the large scale ridge between 60°E and 150°E and the trough to its west. By days +6 and +10, the persistent anomaly pattern combines with these features to form a strong wavenumber two signature throughout all levels of the cross section.

In addition to the fact that the troposphere and the stratosphere are in phase around the latitude circle, the degree to which the troposphere and the stratosphere are dominated by waves of the same scale is remarkable. Also, there is some suggestion of a slight westward tilt with height. This sort of a pattern is suggestive of upward propagation of planetary waves that was not as evident in the PACPOS composite cross sections.

Otherwise after day 0, the basic structure in these cross sections qualitatively resembles the vertical structure of streamfunction anomalies forced by a "delta function" source in a baroclinic model in a beta-plane channel (Held, 1983). In this model, barotropic components of Rossby waves are trapped at lower levels, but a baroclinic portion reaches the highest levels of the model, where larger scale waves dominate. The same similarity exists for PACPOS cross sections with reversal of sign.

Latitude-pressure cross sections (not shown) at 170°W for PACNEG are much as they are in PACPOS cases, except for the reversal of sign. The ISPA is present at day -2. Then, the keypoint anomaly develops, but there is less northward drift with time than in PACPOS case composite anomalies. At 120°W, the ISPA is strong at first and fades away around or just after case onset. There is already a weak ridge at day -2 in the troposphere, but at day +2 and onward, the ridge undergoes strong horizontal and vertical development, and its center gradually drifts northward from 50°N to 70°N as it propagates into the stratosphere.

Thermal Structure

PACNEG 70 mb temperature anomalies and their confidence levels are shown in

Fig. 3.13. Figure 3.14 shows the composite temperature fields at days -6 and +6. The 70 mb temperature anomaly pattern is qualitatively the same in PACNEG as in PACPOS cases, except for sign reversal. Cold anomalies cover North America on day -2 (Fig. 3.13b) and warm anomalies cover most of Asia. By day +2 (Fig. 3.13c), warm anomalies appear over the keypoint region, with cold anomalies over a broad area to the south. The cold area over North America then weakens and disappears after onset. A new negative center develops over the North Atlantic and Europe as a result of displacement of the vortex in that general direction and development of a trough in that area. All these features are significant at or above the 99% confidence level.

The 70 mb temperature composite analyses show at day -2 (Fig. 3.14a), a cold center at the pole and zonally elongated warm centers near the northeastern Soviet Union and the northeastern United States. By day +10 (Fig. 3.14b), the warm center, originally over the northeastern coast of the Soviet Union, has moved eastward and is located just to the west of the Aleutian Islands.

At 10 mb (not shown), the temperature anomaly pattern is not as clearly defined. The only significant feature is the cold anomaly that covers northwestern North America, northeastern Asia, and the northern North Pacific from day -2 to day +4. By day +10, a warm anomaly covers the easternmost areas of Asia, but this latter anomaly does not appear well on the maps of statistical significance.

Temperature cross sections (Fig. 3.15) reveal rather interesting thermal structures during at least the first few days of these events. The longitude-pressure temperature anomaly cross section in Fig. 3.15 is from day +4 of PACNEG at 50°N, stretching from 150°E to 30°W, where the thermal pattern is most obvious. Below 300 mb, the temperature anomalies are in phase with the height anomalies. The result of this relationship between height and temperature anomalies is that the magnitude of the height anomalies peaks at 300 mb. Above that level, however, the temperature anomalies have

the opposite sign, and the height anomalies decay.

The reversal of sign can be explained by the relative balances between horizontal advection and vertical motion on the temperature fields. In the troposphere, cold advection typically occurs at lower levels under deepening 500 mb troughs, and although the pattern by day +4 is reasonably mature and has become more barotropic in character, the cold advection that has taken place during the long synoptic-scale development on previous days accounts for the cold anomaly over the keypoint below 300 mb. Similarly, warm advection to the east of the trough has produced a warm anomaly between 150°W and 90°W. Associated with cold advection in a trough, there typically is sinking motion, which warms the air adiabatically. Likewise, rising motion to the east of a trough produces adiabatic cooling. At lower levels, this adiabatic warming/cooling is not enough to overcome the opposing horizontal temperature advection.

In the stratosphere, though, the warm temperature anomalies over the keypoint cannot be explained by advection since, as seen in the 70 mb composite temperature fields, there is a climatological warm maximum in mid-latitudes. Any advection into this region would likely be cold. The warm anomalies over the keypoint region in PACNEG cases can be explained by vertical motion. Given that there is cold advection producing height falls and sinking motion in the trough, the lapse rate of the stratosphere is such that any sinking motion would cause significant adiabatic warming. Likewise, rising motion produces the cold anomalies seen in the ridge at stratospheric levels.

At higher latitudes, this sign reversal is not as noticeable, nor is it as noticeable after day +4 in PACNEG. In PACPOS cases, the same basic temperature structure, with a reversal in sign, exists.

The decay with height of height anomalies above 300 mb is consistent with features of the temperature structure by simple hydrostatic balance.

3.2.3 COMMENT

The most remarkable features in the Pacific cases, then, are the ISPA's before onset. It was expected that the strongest and most significant features in the stratosphere would be found well after case onset, due to the time required for upward propagation of planetary scale waves. Indeed, there is evidence of the mature patterns in the middle stratosphere after the developments, but the strongest anomalies appear prior to the onset of the cases.

3.3 Atlantic Events

3.3.1 ATLPOS

The ATLPOS cases display similarities to their Pacific counterparts at 70 mb. Figure 3.16 shows 70 mb height anomalies and their associated confidence levels on days -2 and +10. The 10 mb height anomalies are shown in Fig. 3.17, and Fig. 3.18 shows corresponding analyses of 10 mb and 70 mb heights. The most remarkable feature in these cases is a negative ISPA, indicating a strong vortex that can be seen in the ATLPOS day -2 70 mb height fields (Fig. 3.18a). This feature is significant at the 99% level on most days, even as far back as day -10 (not shown), and changes very little throughout the period. It is interesting that the corresponding anomaly in the *Pacific* positive cases is of the opposite sign. At day +2 (not shown), a positive anomaly appears over the north-central Atlantic, extending westward over the eastern part of North America. This anomaly persists through day +10 (Fig. 3.16b), while during the same period, a weak pattern resembling the downstream wavetrain is observed as in the 500

mb analyses of DT. However, the downstream centers are not highly significant at 70 mb. Apparently, the ATLPOS pattern is weaker at 70 mb than its Pacific counterpart.

At 10 mb (Fig. 3.17), there is little difference between the anomalies before and after onset. The ISPA is found throughout the period centered near the North Pole. This negative center is surrounded by positive centers, much as the ISPA's in PACNEG and PACPOS cases are surrounded by anomalies of opposite sign. The ISPA has confidence levels above 95%, and the surrounding positive centers, which are more or less transient, have areas above the 90% confidence level. At no time, however, is there a significant anomaly over the keypoint region associated with the 500 mb keypoint positive anomaly.

3.3.2 ATLNEG

At 70 mb, the ATLNEG height anomalies, displayed in Fig. 3.19, are opposite to the ATLPOS height anomalies. Throughout the period, a positive ISPA is nearly surrounded by negative anomalies. This positive ISPA represents a weaker vortex. On day 0 (not shown), a small negative anomaly is found over the keypoint. This center grows until day +4 (not shown) and then remains constant. By day +10 (Fig. 3.19b), two downstream centers of alternating sign have developed, but they are, as in ATLPOS cases, not as highly significant as the keypoint anomaly.

At 10 mb, shown in Fig. 3.20, there exists the same basic pattern: a positive anomaly in polar regions surrounded by negative anomalies. The geopotential heights at the center of the polar vortex at 10 mb are 400m less in ATLPOS cases than in ATLNEG cases. Over the keypoint, there is no highly significant anomaly. Even the ISPA has a generally smaller confidence level.

In the composite height fields, shown in Fig. 3.21, very little obvious change is

seen in the pattern, which, when compared with the Pacific patterns, is consistent. Confidence levels of the 10 mb ISPA's are generally lower in Atlantic cases than in Pacific cases. The 10 mb heights during Pacific cases undergo a definite, systematic change between day -2 and day +10, while the Atlantic patterns remain relatively constant. At 70 mb, however, minor height falls occur between day -6 (Fig. 3.21a) and day +10 (Fig. 3.21c) over the keypoint in ATLNEG composites, while height rises occur in the same place during ATLPOS composites (Fig. 3.18a,c).

Overall, the main difference between the ATLPOS and ATLNEG cases in the middle stratosphere is the sign of the ISPA. In the ATLPOS cases, the sign is negative, and the polar vortex is stronger with a faster westerly flow. In the ATLNEG cases, the sign of the ISPA is positive and the vortex is weaker. The 10 mb westerly flow is less than in ATLPOS cases. In comparing the ATLPOS and ATLNEG 10 mb heights, there is no major dominance of any particular wavenumber other than 0. If a deeper vortex as in ATLNEG generally results from reduced wave activity into polar latitudes, and a shallower vortex results from enhanced wave activity flux into the polar regions, then given that there is no appearence of any dominant wavenumber greater than 0, any wave activity in the PACNEG cases may be random in phase and hence not show up in the composite analyses. If this is the case, the ATLPOS patterns would be associated with enhanced wave activity in the stratosphere, while ATLNEG patterns would be associated with weaker than normal stratospheric planetary waves.

3.4 Alternate Keypoint Selection

Similar methods were used to form composite analyses of persistent anomaly cases at different keypoints. In the Pacific, the second keypoint is at 42°N 145°W, and in the

Atlantic, it is at 46°N 35°W.

For the Pacific cases at the new keypoint (dates shown in appendix B), the same basic pattern as at the original keypoint was found for both PACPOS and PACNEG events, but the pattern is somewhat weaker and less well defined at the new keypoint. It appears, then, that the original keypoint selection is best at capturing the characteristics of the PACPOS and PACNEG patterns. Nevertheless, PACPOS cases at the new keypoint also have a positive ISPA, which decays after day 0, as well as an anomaly over the keypoint at 70 mb and a downstream center of opposite sign. The same is true, with sign reversed, for PACNEG cases.

For the Atlantic events, the same basic pattern as at the old keypoint also exists. For ATLNEG, the results are the same in both keypoint selections. In ATLPOS cases, however, the new keypoint selection has anomalies which are much stronger and much more highly significant. Day +8 of the new keypoint ATLPOS composites are shown in Fig. 3.22. This day is representative of the ATLPOS time series. Particularly notable are the strength of the ISPA and the strength of the ridge covering the eastern Pacific and western North America. On days after onset, the difference in height anomalies between the ridge and the ISPA exceed 1 km at 10 mb, and both features are highly confident. In fact, the ISPA in ATLPOS events at the new keypoint has the highest confidence of any anomaly in the persistent anomaly composites in this study. The areal coverage of 99% or higher confidence is the largest and the location and shape of the anomaly is most consistent. Thus it appears that the new keypoint selection is better at capturing the ATLPOS pattern, at least in the stratosphere.

The pattern for Atlantic events is particularly puzzling, especially for ATLPOS events, which, except for some weak anomalies at 70 mb, lacks any direct resemblance to the pattern that occurs at 500 mb.

Many of the cases for the new keypoint overlap with the cases at the original

keypoint, so they should not be viewed as a totally independent set of data. In addition, since case composites at the original keypoints generally have stronger stratospheric signatures than those at the new keypoints (except for ATLPOS), the rest of this study will concentrate exclusively on the original keypoint cases, and any mention of PACPOS, PACNEG, ATLPOS, or ATLNEG will refer to cases at the original keypoints unless explicitly stated otherwise.

3.5 Discussion

Results of these analyses show that the large scale pattern of persistent anomaly events *does* indeed appear at 70 mb. However, there are differences between the Atlantic and Pacific. Pacific events are associated with a much larger change in the 70 mb flow from day -2 to day +10. At 10 mb, the Pacific events show a clear change in the flow over the same time period. The ISPA at day -2 over the northwestern part of Canada becomes displaced well to the east as a new anomaly of opposite sign appears and grows, resulting in significant changes in the 10 mb height fields by day +10. However, such a change is, for the most part, absent during Atlantic cases. There are still strong ISPA's, especially in the ATLPOS new keypoint composites, but these anomalies are not replaced after day 0, as they are in Pacific cases. The 10 mb height field remains qualitatively unchanged between day -2 and day +10 aside from some minor height rises in ATLPOS events and minor height falls in ATLNEG cases.

There are two possible explanations for this discrepancy. The first is the difference in scale between the Atlantic and the Pacific events. Larger scale waves are more likely to propagate upward into the stratosphere (Charney and Drazin, 1961), and the Pacific events could have a larger scale. A look at the wavenumber contributions of the events

shown in DS and DT, however, reveals that the contributions from large wavenumbers are about the same in Atlantic and Pacific cases, so there is no real scale difference. The mature 500 mb Atlantic and Pacific patterns in DG and DT both cover about the same fraction of the hemisphere, so this explanation is, at best, uncertain.

The second explanation involves orographic forcing. The first secondary anomaly in Pacific persistent anomaly patterns covers the Rocky mountains, but Atlantic events do not have such a large scale mountain range oriented perpendicular to the flow downstream from the keypoint anomaly. Although the patterns in both Atlantic and Pacific events bear resemblance to Rossby wave dispersion from a localized souce of vorticity (Hoskins, 1977), the secondary anomalies in Pacific cases, located over the Rocky mountains, may be enhanced by orographic forcing. Observations just displayed show that it is the secondary anomaly that penetrates up to 10 mb.

It is because of this major difference between the Atlantic and Pacific persistent anomalies that we will concentrate exclusively on Pacific events in the next chapter.

Another interesting difference between Atlantic and Pacific cases is the difference in sign between the ISPA's. PACPOS patterns have a strong positive ISPA over northwestern North America before case onset and PACNEG patterns have a negative ISPA over the same area. In the Atlantic composites, the relationship between sign of the case and sign of the ISPA is reversed. ATLPOS patterns have negative ISPA's, while ATLNEG patterns have positive ISPA's.

There are a couple of possible explanations for this. First, among times when Pacific cases overlap with Altantic persistent anomaly cases (nine of them in all), seven are situations in which a Pacific persistent anomaly event of one sign (i.e. PACPOS) overlaps with an Atlantic event of the opposite sign (i.e. ATLNEG). It is quite possible that the same atmospheric conditions that favor PACPOS events also favor ATLNEG events, and the same for PACNEG and ATLPOS events. Additionally, the existence of

PACPOS events may favor the development of ATLNEG events over the development of ATLPOS events, and the existence of PACNEG events may favor the development of ATLPOS events over the development of ATLNEG events. For example, ridging over the southeastern United States as per PACPOS events, in consideration of Rossby wave dispersion from a localized source of vorticity (Hoskins,1977), would lead to downstream trough development over the Atlantic, and thus, ATLNEG. However, the Atlantic keypoint is far removed from the primary Pacific anomaly center, and the systematic relationships of anomalies in this area during Pacific events is relatively uncertain.

This brings up another possibility: sampling variability. In such a case, the correlation between ISPA's of Pacific and Atlantic cases can be regarded as false. Assuming that the probability of opposite sign in Atlantic-Pacific case overlap is 0.5 and that the number of case overlaps of opposite sign has a binomial distribution, then the probability of at least seven out of nine overlaps being of opposite sign is 0.10, which is fairly low. Nevertheless, a more extensive set of cases would be required to rule out this possibility.

However, the actual existence of the ISPA's is a mystery. Well defined anomalies exist in the stratosphere well before onset of persistent anomalies at 500 mb. In fact, the ISPA's are present back to at least day -10. We believe that the ISPA is the result of random phase wave activity in the troposphere well before cases begin that is not able to be seen in the analyses. In the PACPOS and ATLNEG cases, the sign of the ISPA is positive, indicating a weaker polar vortex which may have been eroded by enhanced large scale planetary wave activity propagating from the troposphere into the stratosphere. In the PACNEG and ATLPOS events, the vortex is deeper, indicating a lack of such large scale planetary waves.

The observations in ATLNEG cases show the positive ISPA's are more or less

directly over the pole, and there is no overwhelming large scale wave in the composite heights. The flow is quite zonal. However, in PACPOS cases, there is a large ridge over Alaska before day 0, and the presence of this ridge suggests wave 1 activity is consistently occurring with the same phase from case to case. In ATLPOS and PACNEG events, the flow shows no anomalously large wave activity, and therefore, the hypothesis that decreased wave activity occurs before ATLPOS and PACNEG cases fits the observations of these events. Perhaps the atmosphere is preconditioning itself before these events, or it may be possible that such an ISPA structure in the stratosphere may be a favorable condition for the development of persistent anomalies that otherwise may not have materialized.

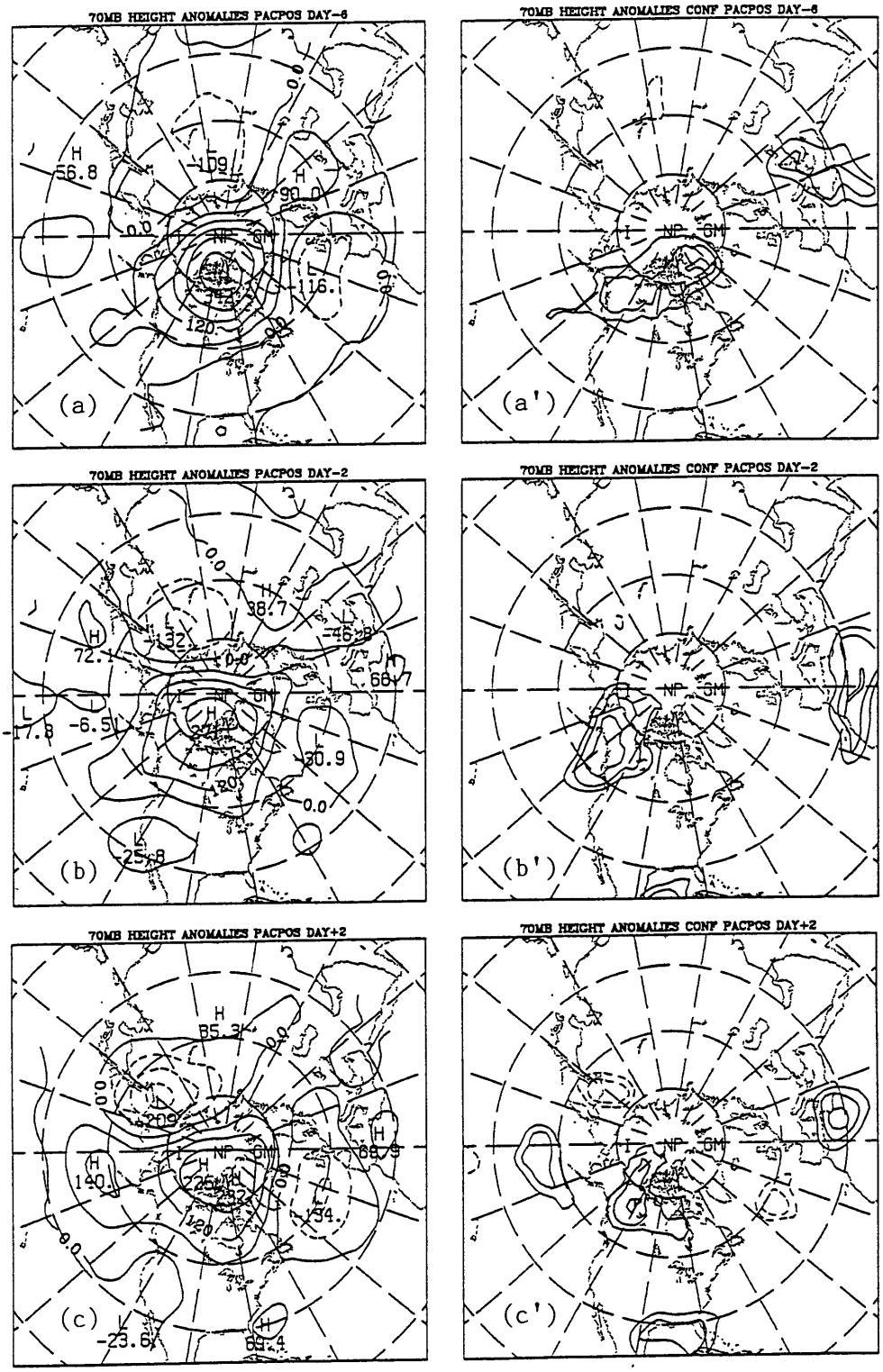

Fig. 3.1 Composite mean time evolution of 70 mb height anomalies (in meters) obtained from 7 PACPOS cases for days (a) -6, (b) -2, (c) +2, (d) +6, (e) +10, and (f) +14, relative to onset time. Areas where composite mean anomalies are greater or less than

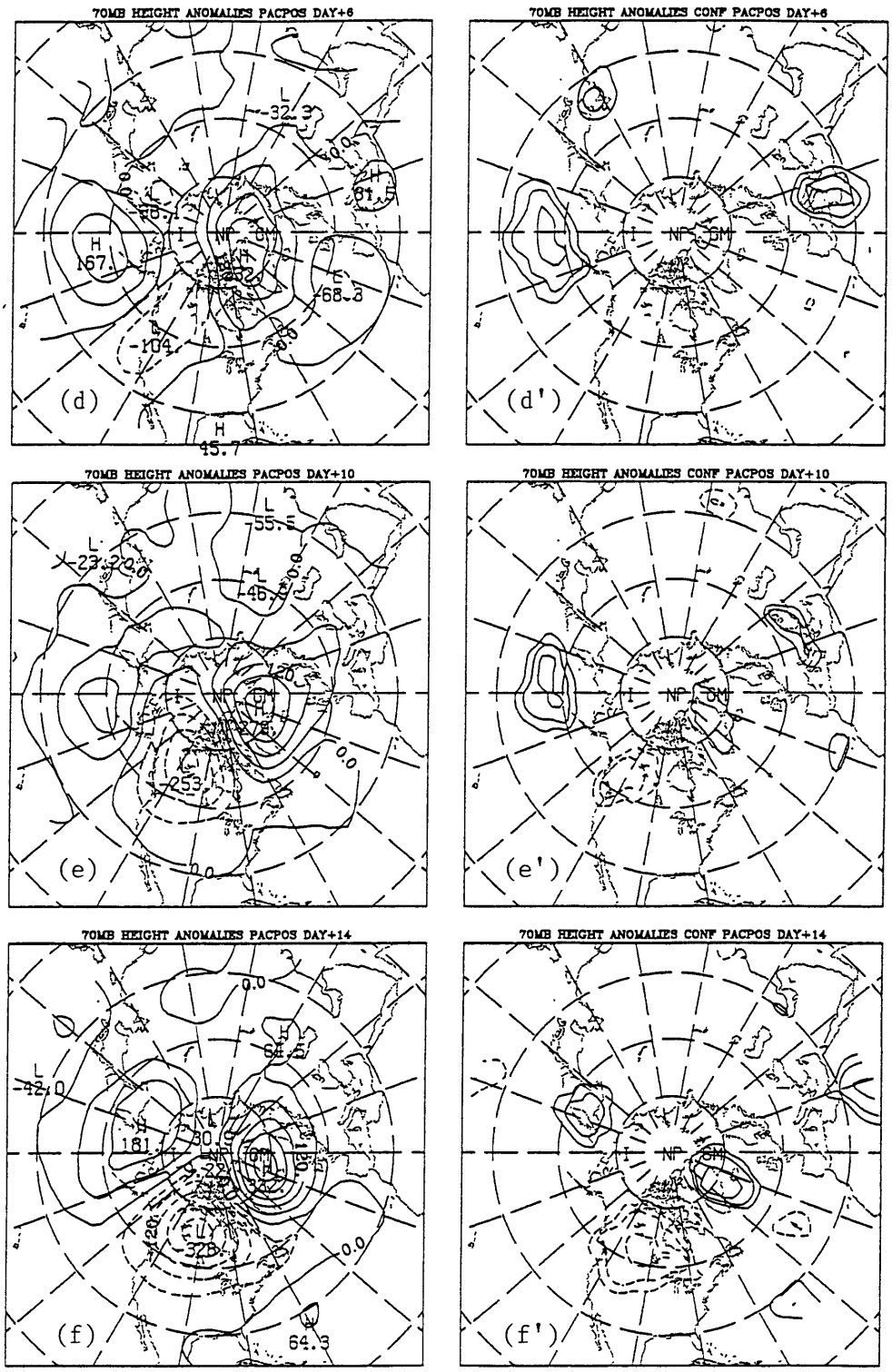

Fig. 3.1 (*Continued*) zero at varying confidence levels are shown for the same times in (a')-(f'). In these areas, the outermost contours represent a confidence level of 90%, the second contour represents 95% confidence, and the third 99%.

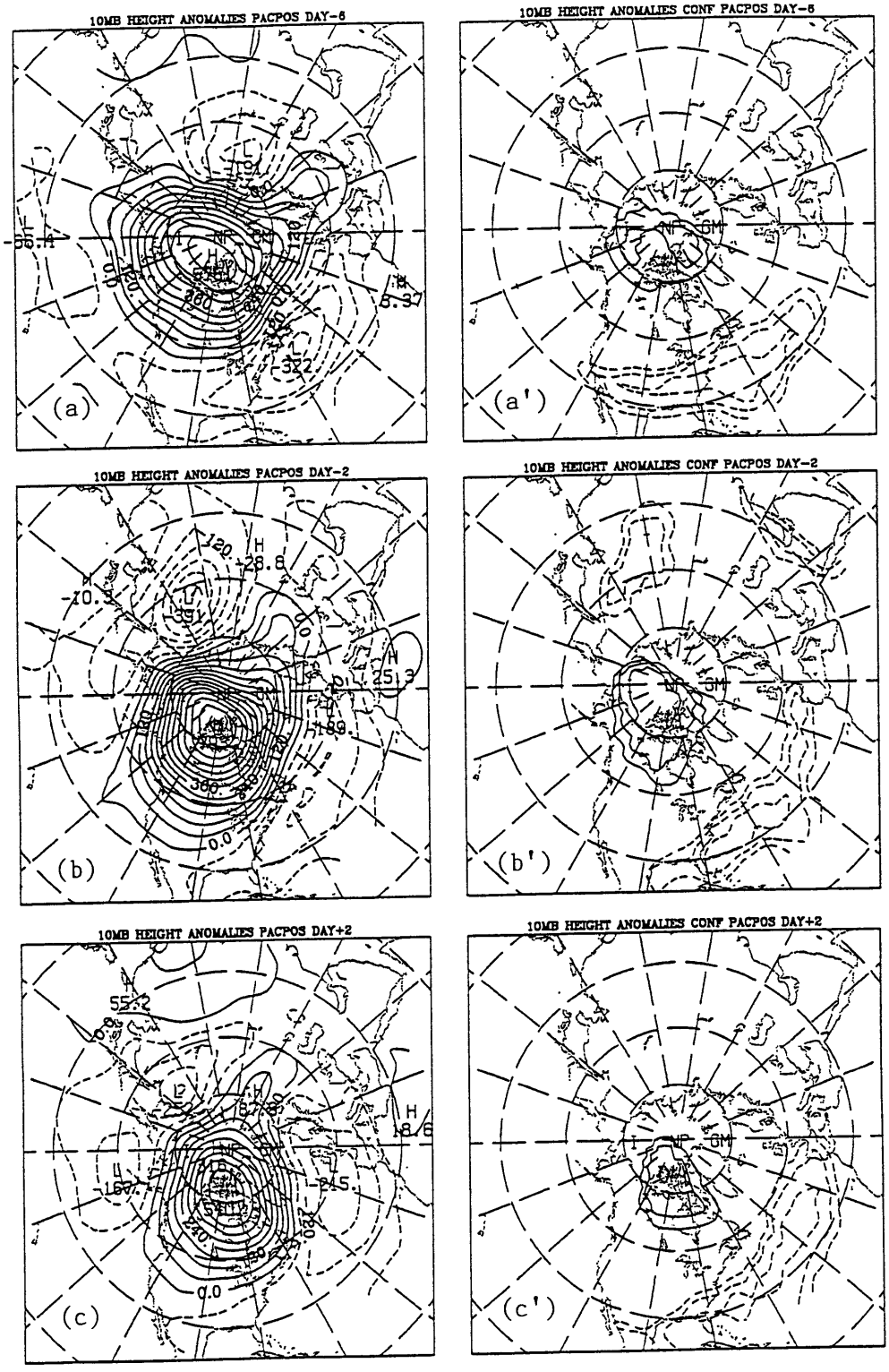

Fig. 3.2 As in Fig. 3.1 for the composite time evolution of 10 mb height anomalies (in meters) for the PACPOS cases on days (a) -6, (b) -2, (c) +2, (d) +6, (e) +10, and (f) +14.

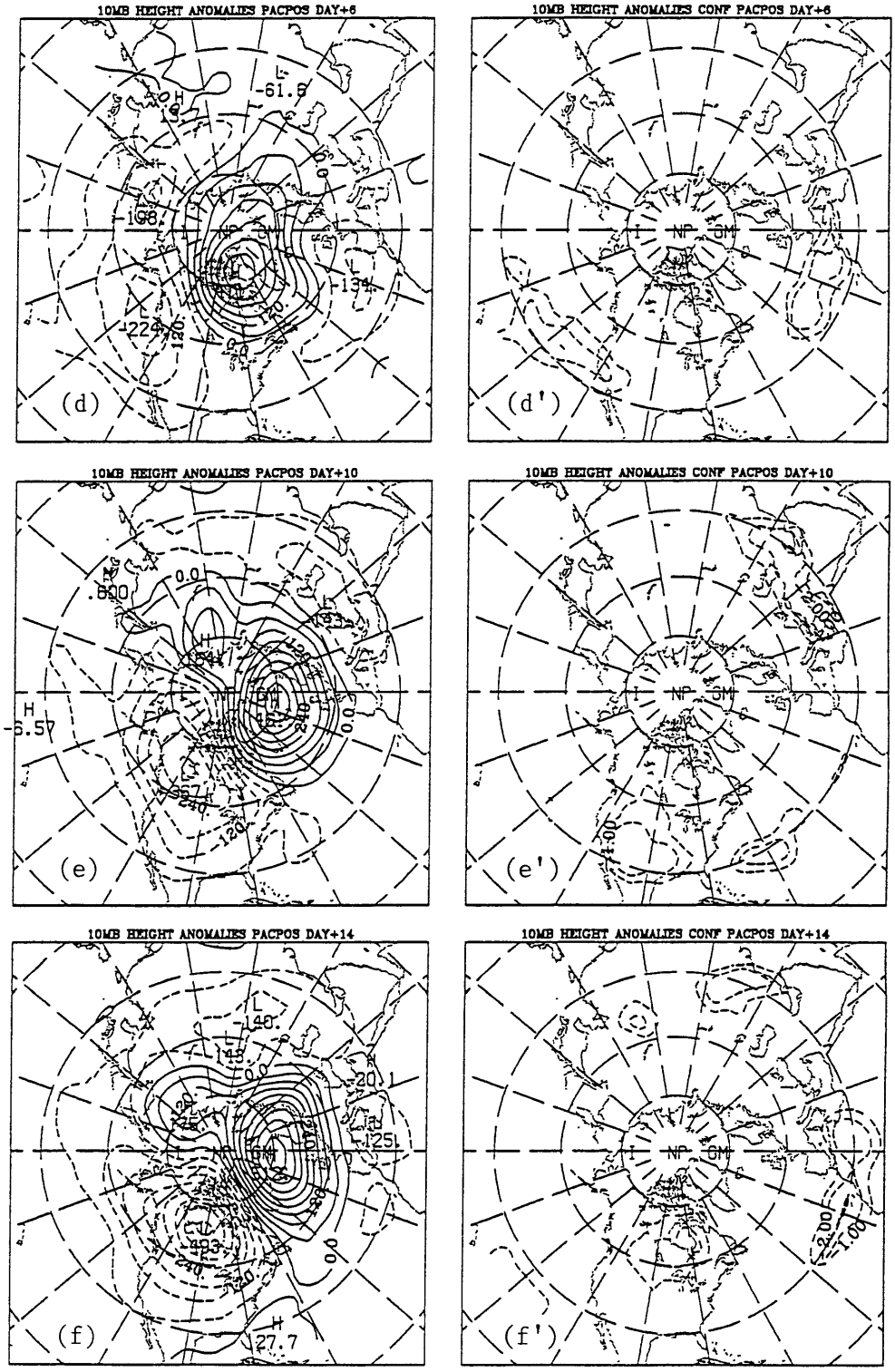

Fig. 3.2 (*Continued*)

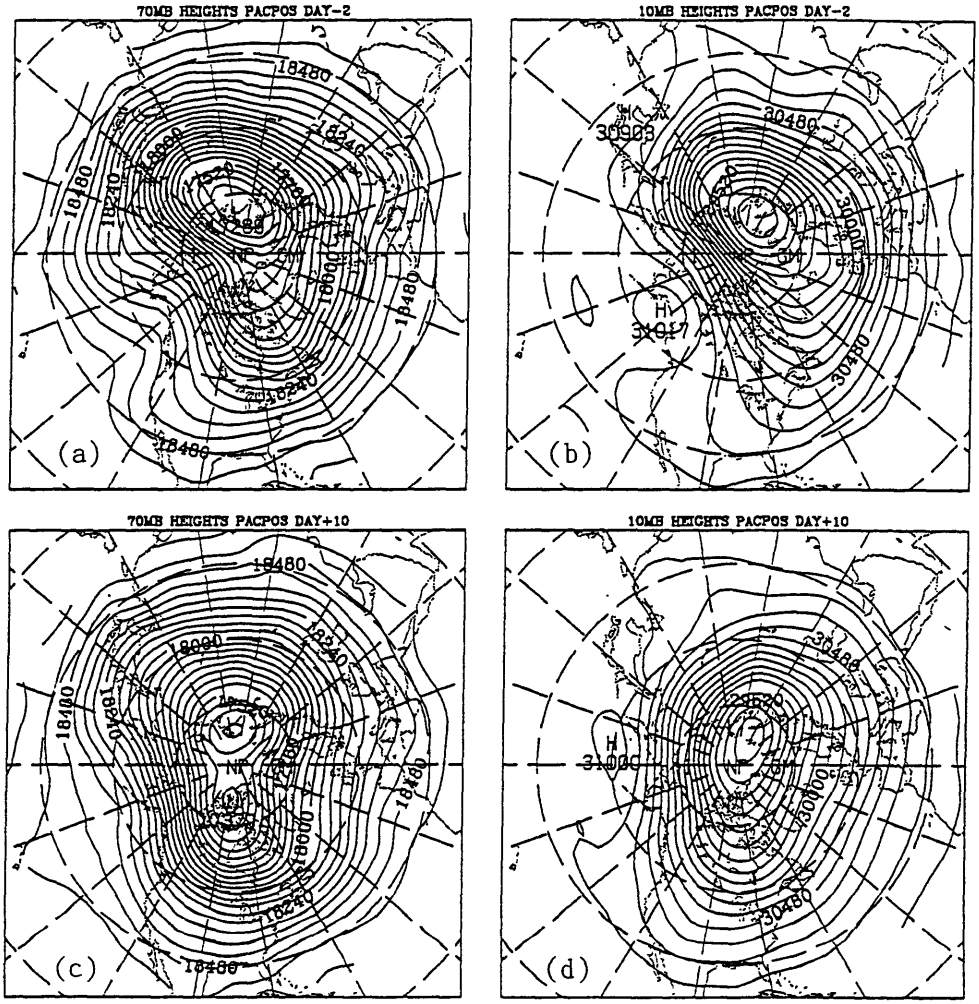

Fig. 3.3 Composite mean time evolution of geopotential heights (in meters) for the PACPOS cases for (a) 70 mb, day-2; (b) 10 mb, day-2; (c) 70 mb, day+10; and (d) 10 mb, day+10.

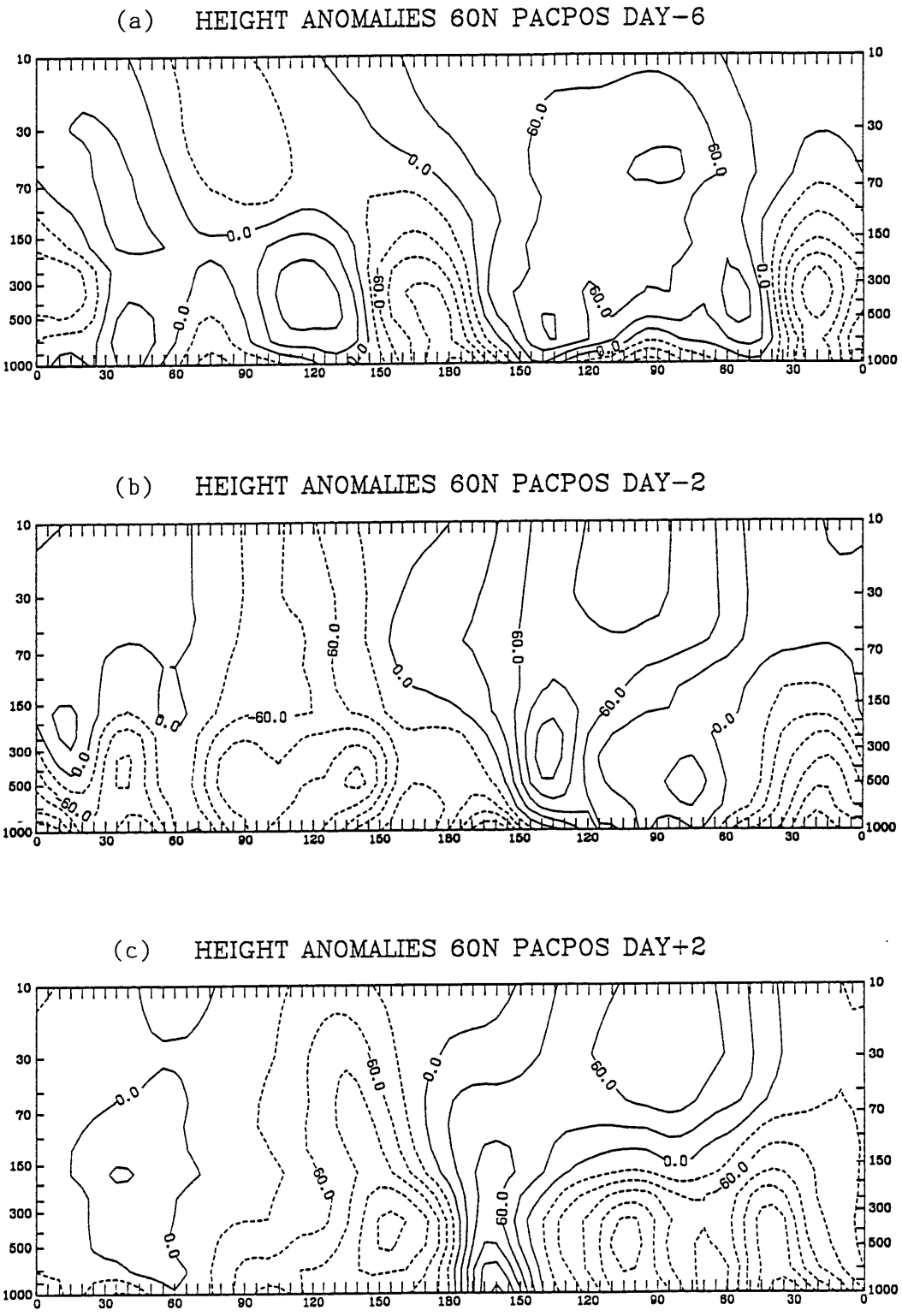

Fig. 3.4 Composite mean longitude-pressure (millibars) cross sections of height anomalies (in meters) for the PACPOS cases at 60°N for days (a) -6, (b) -2, (c) +2, (d) +6, (e) +10, and (f) +14, scaled by the square root of pressure to 300 mb.

(d) HEIGHT ANOMALIES 60N PACPOS DAY+6

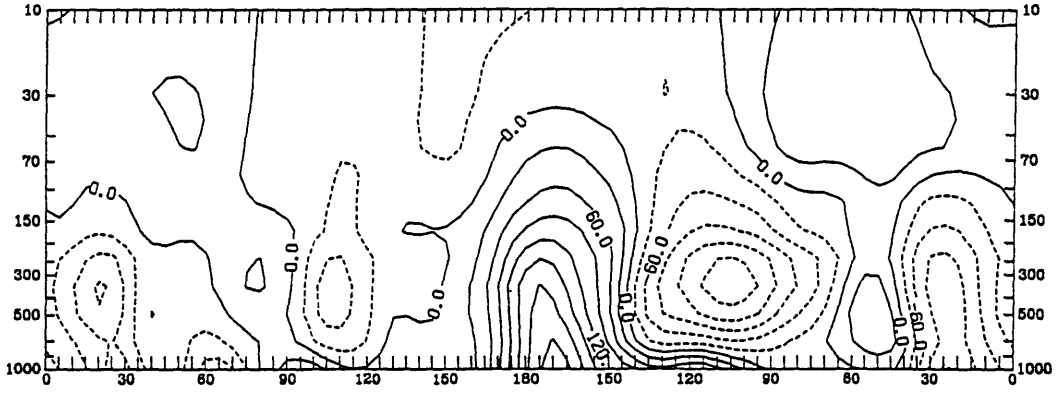

(e) HEIGHT ANOMALIES 60N PACPOS DAY+10

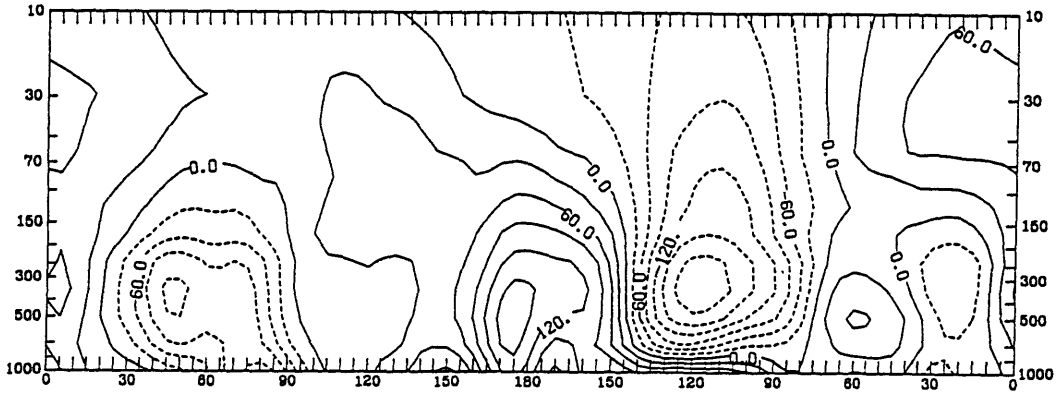

(f) HEIGHT ANOMALIES 60N PACPOS DAY+14

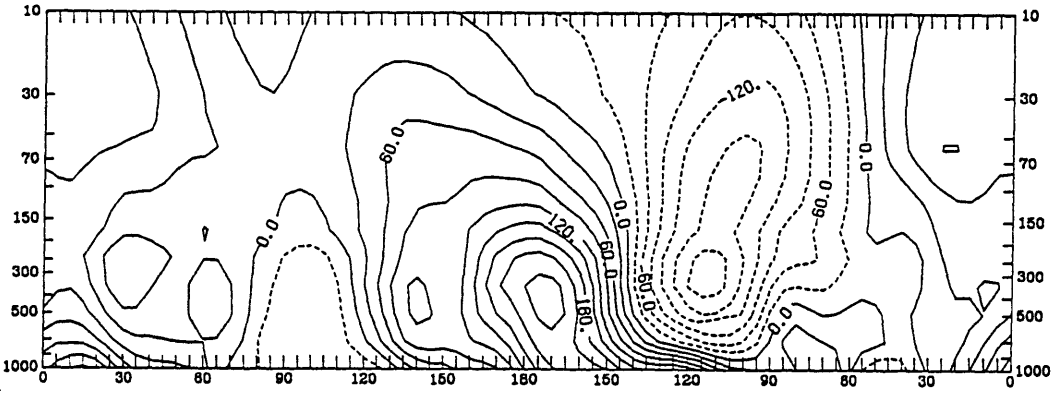

Fig. 3.4 (*Continued*)

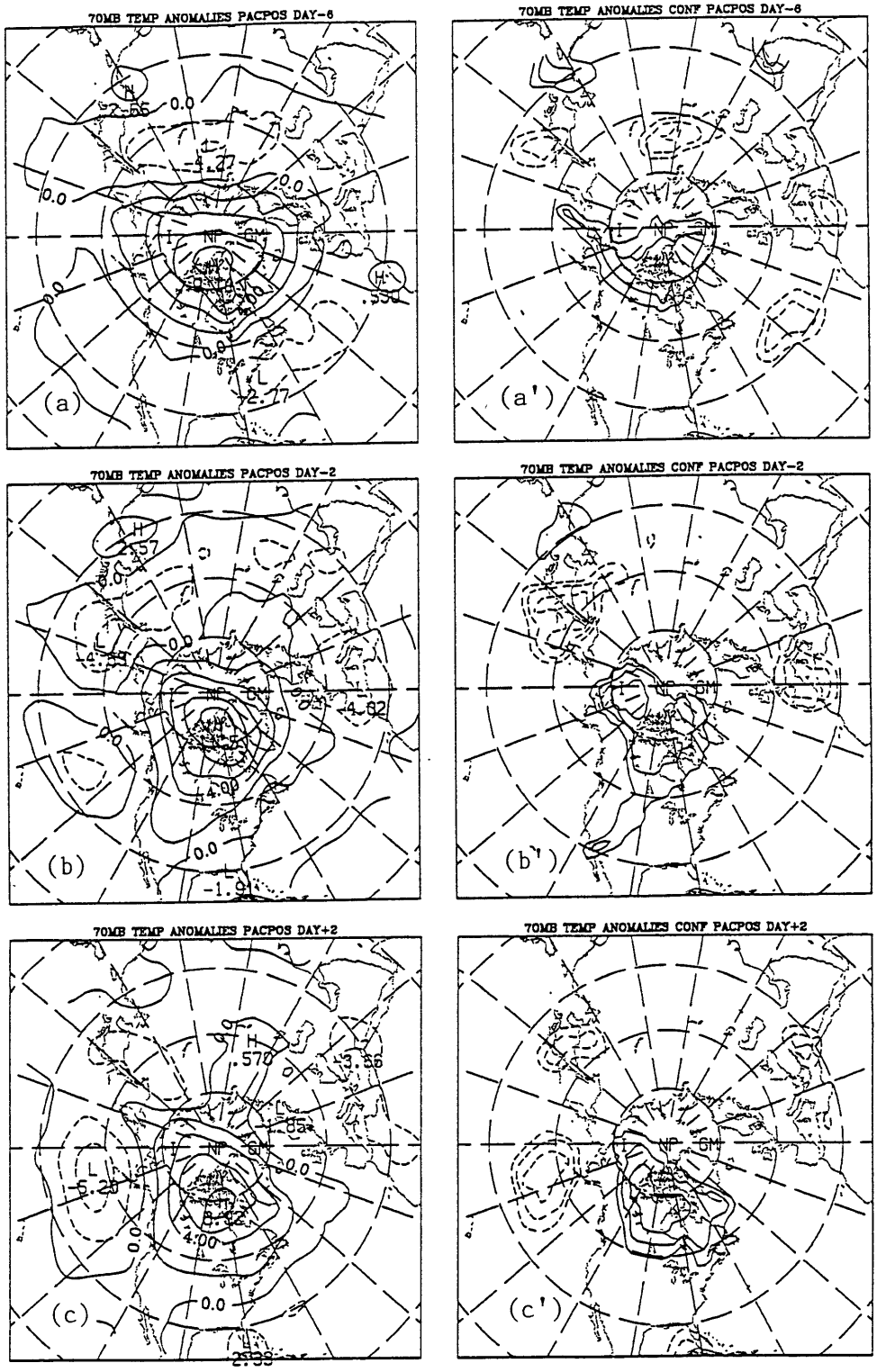

Fig. 3.5 As in Fig. 3.1 for the composite mean time evolution of 70 mb temperature anomalies (°C) for the PACPOS cases on days (a) -6, (b) -2, (c) +2, (d) +6, (e) +10, and (f) +14.

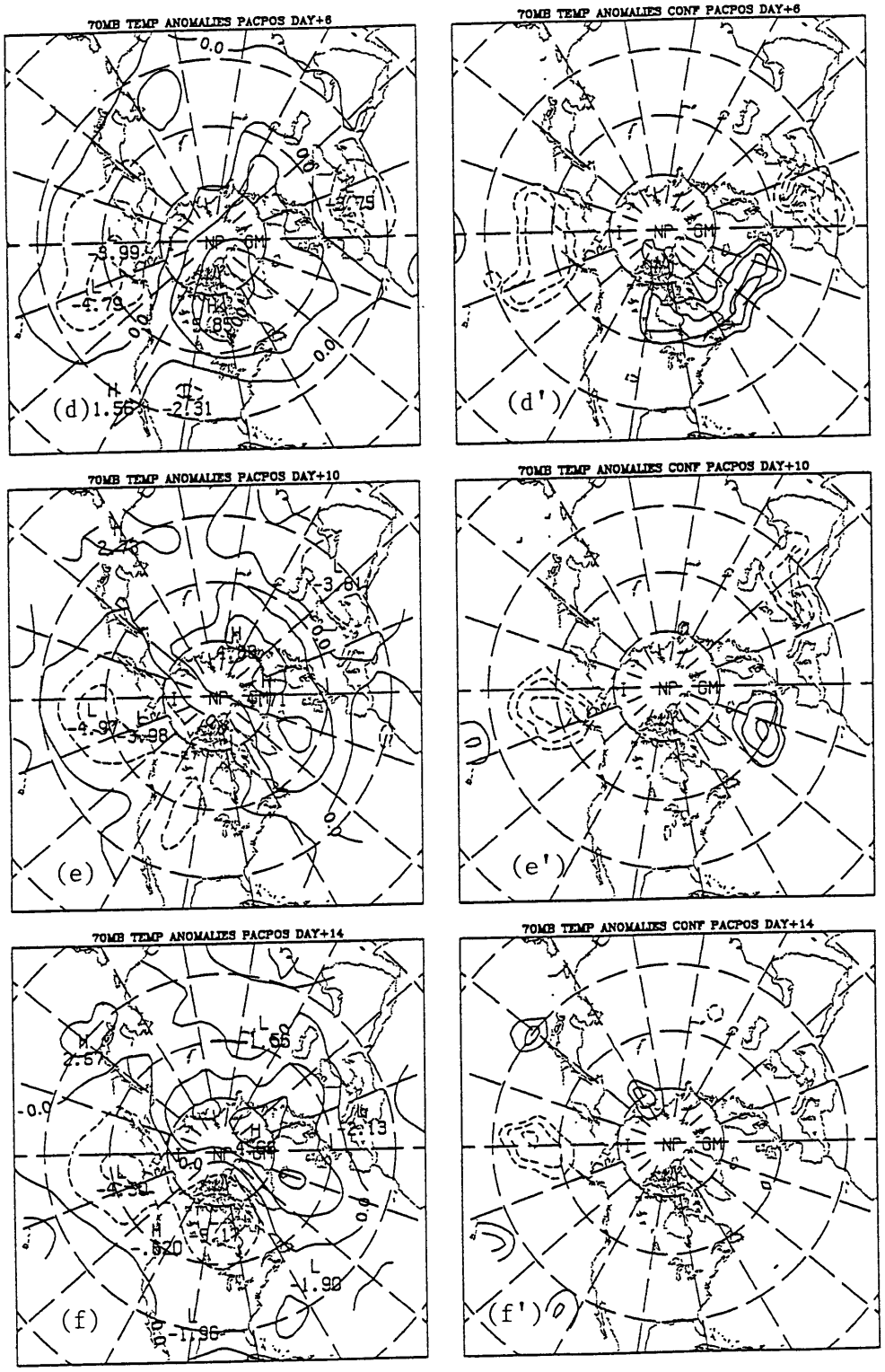

Fig. 3.5 (*Continued*)

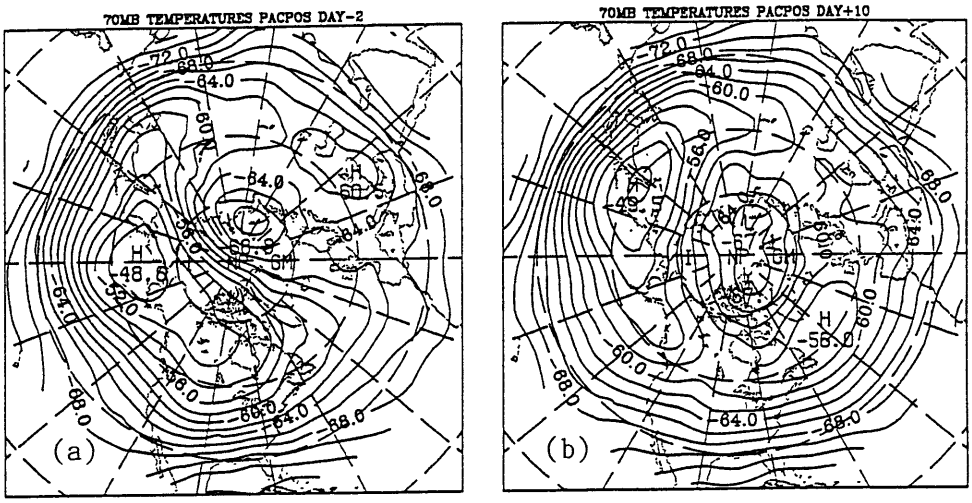

Fig. 3.6 Composite mean 70 mb temperature (°C) evolution for the PACPOS cases on days (a) -2, (b) +10.

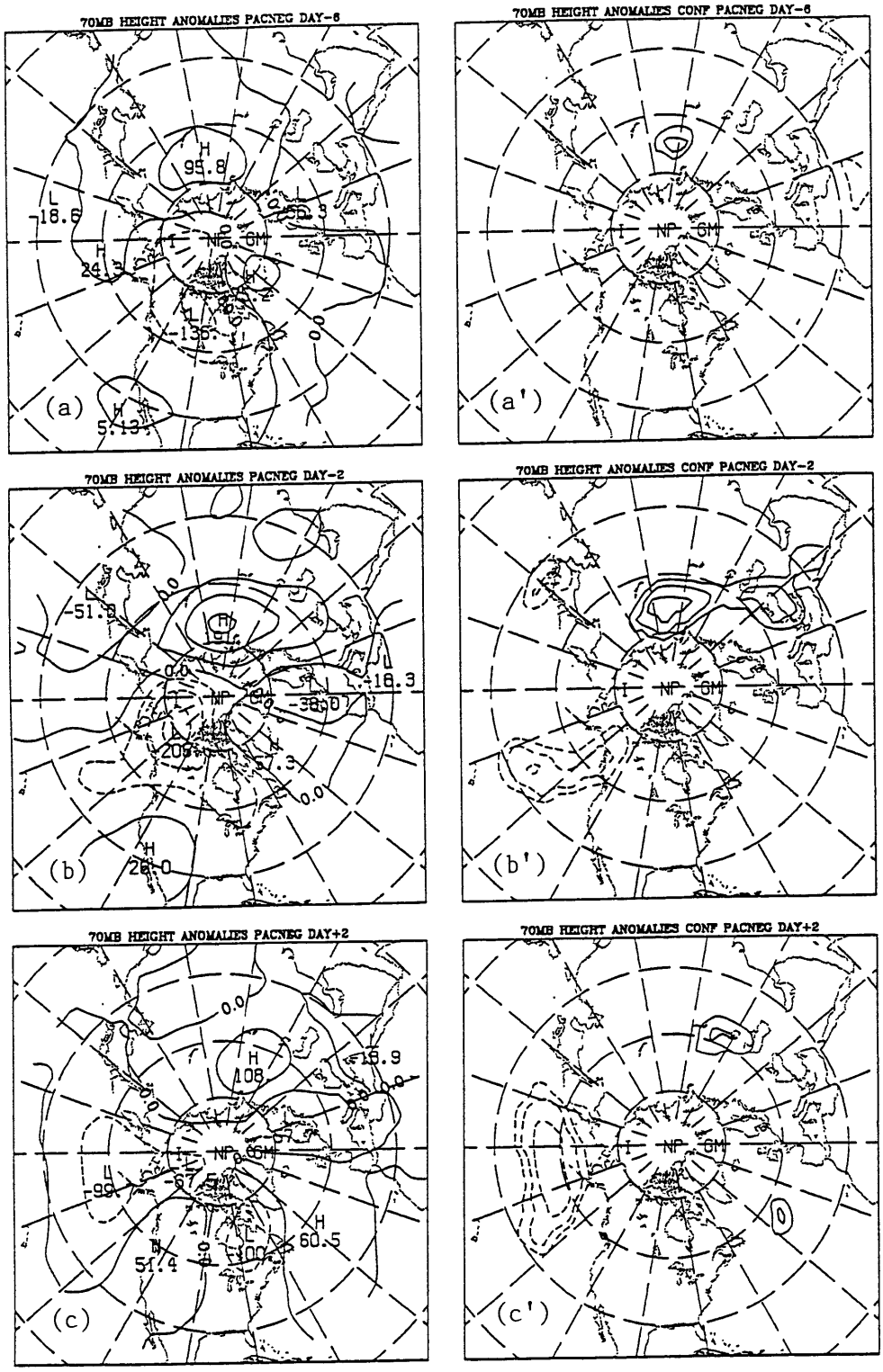

Fig. 3.7 As in Fig. 3.1 for the composite time evolution of 70 mb height anomalies from 13 PACNEG cases for days (a) -6, (b) -2, (c) +2, (d) +6, (e) +10, and (f) +14.

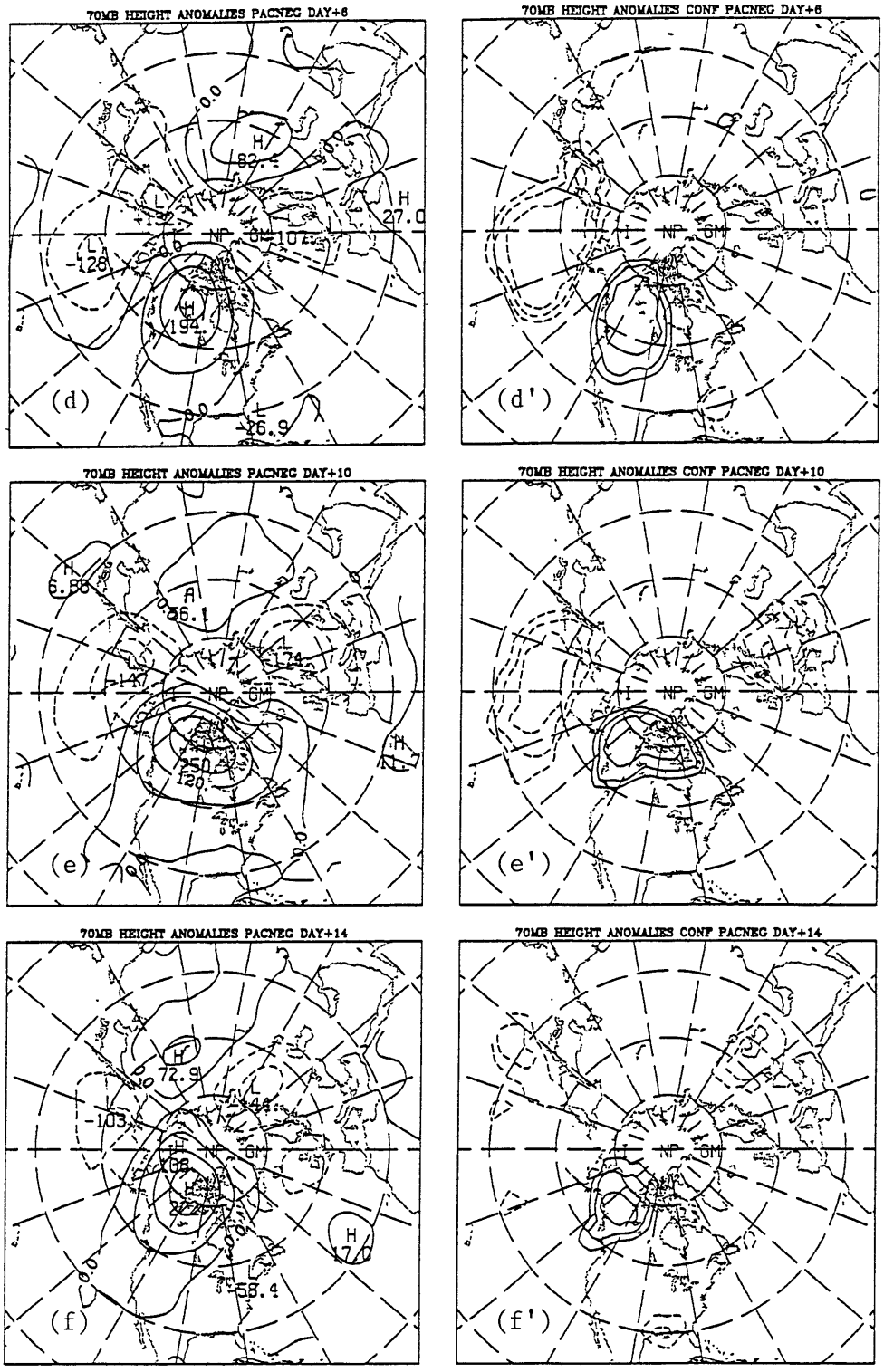

Fig. 3.7 (*Continued*)

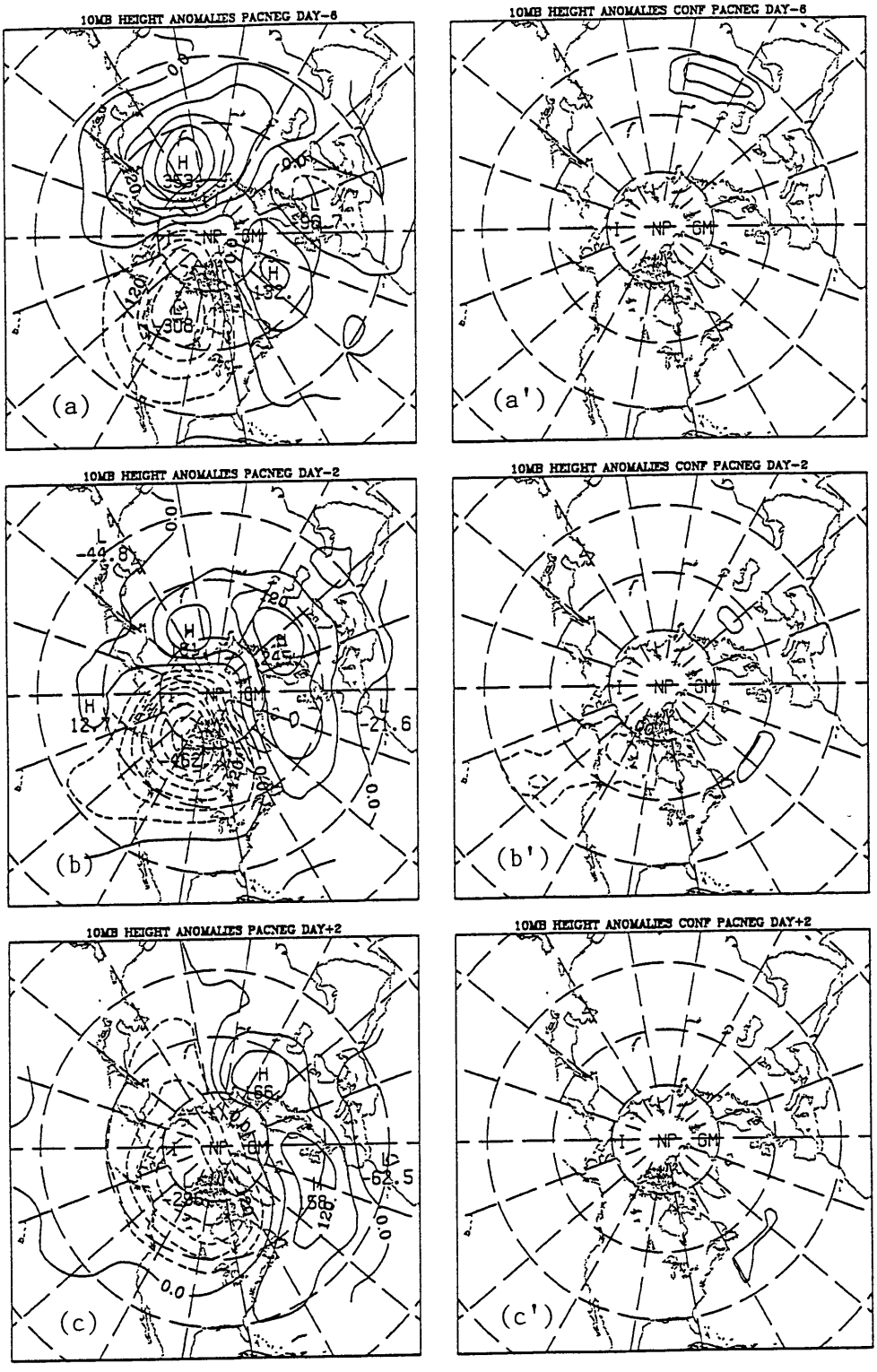

Fig. 3.8 As in Fig. 3.1 for the composite mean time evolution of 10 mb height anomalies for the PACNEG cases on days (a) -6, (b) -2, (c) +2, (d) +6, (e) +10, and (f) +14.

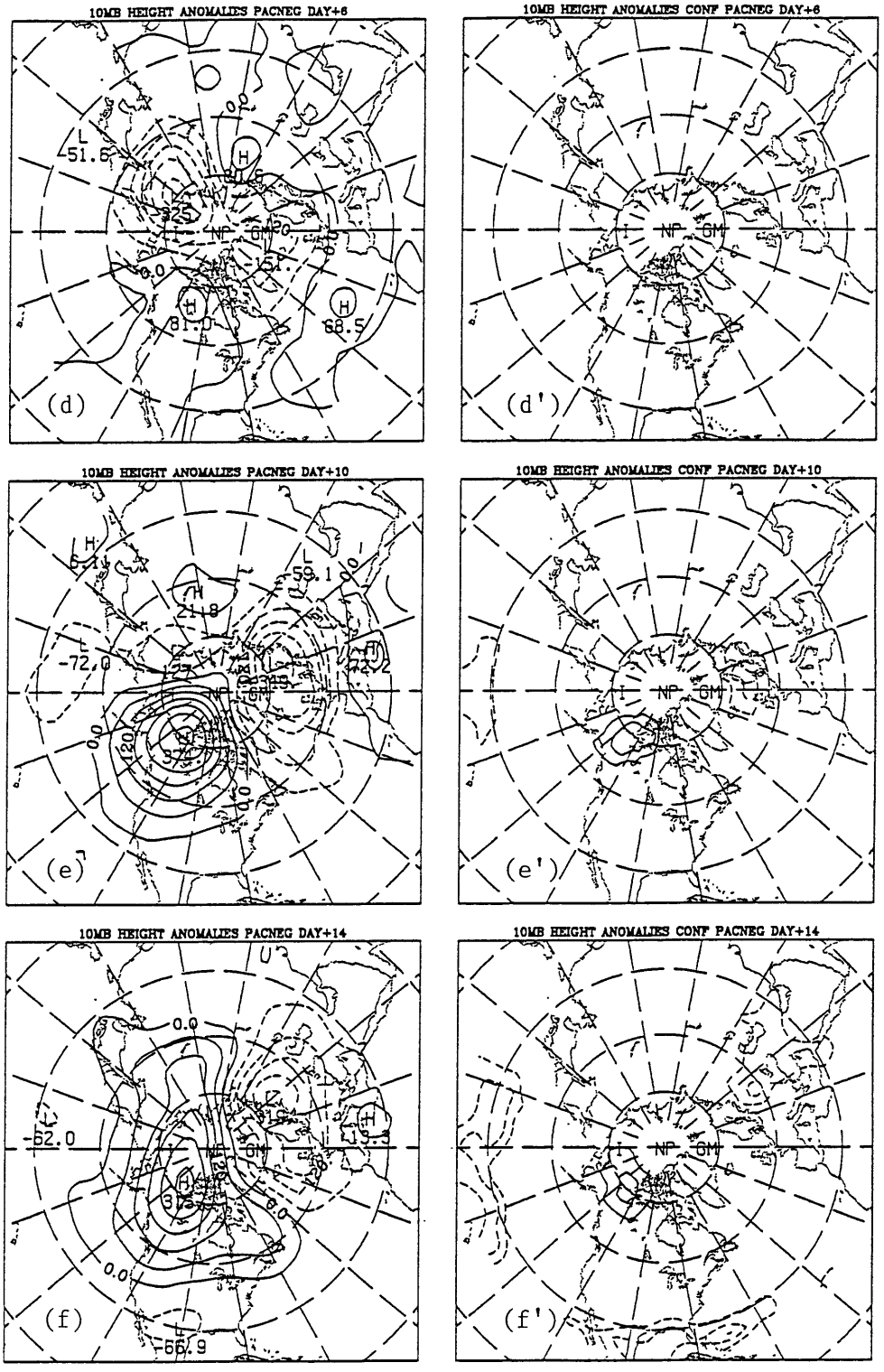

Fig. 3.8 (*Continued*)

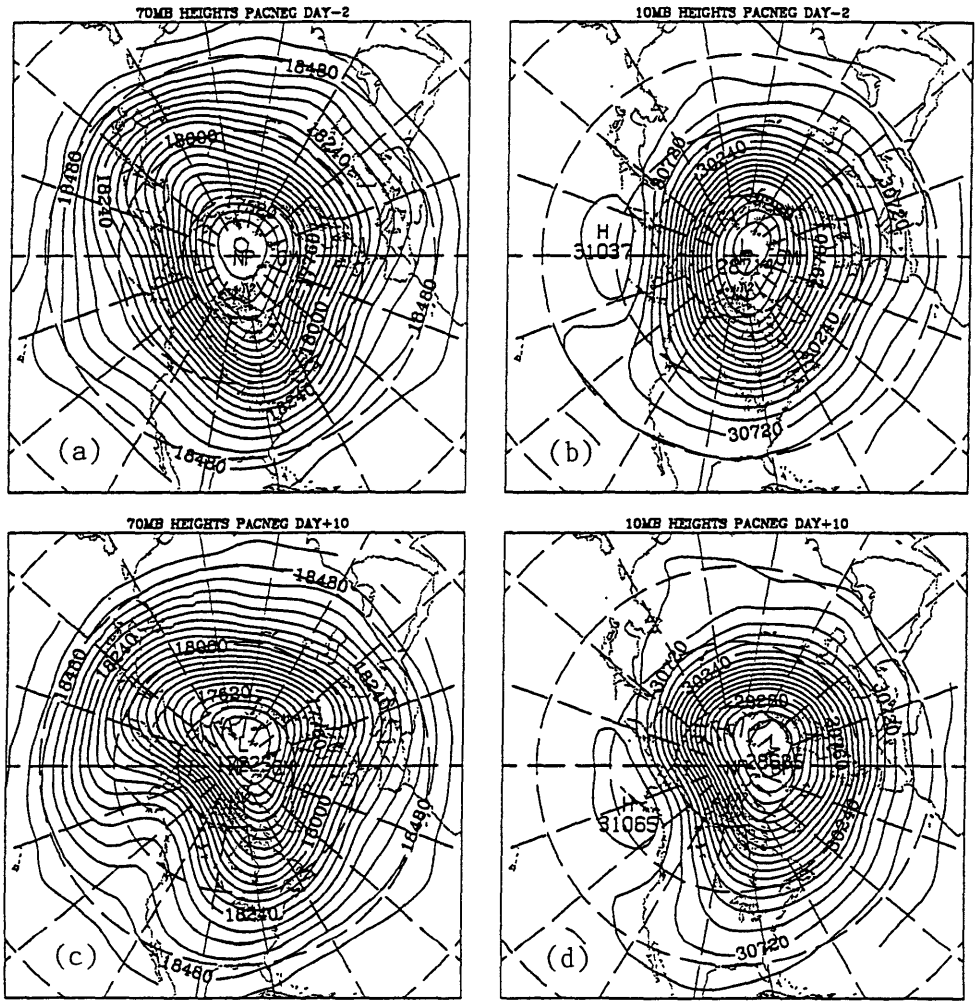

Fig. 3.9 Composite mean time evolution of geopotential heights (in meters) for the PACNEG cases for (a) 70 mb, day-2; (b) 10 mb, day-2; (c) 70 mb, day+10; and (d) 10 mb, day+10.

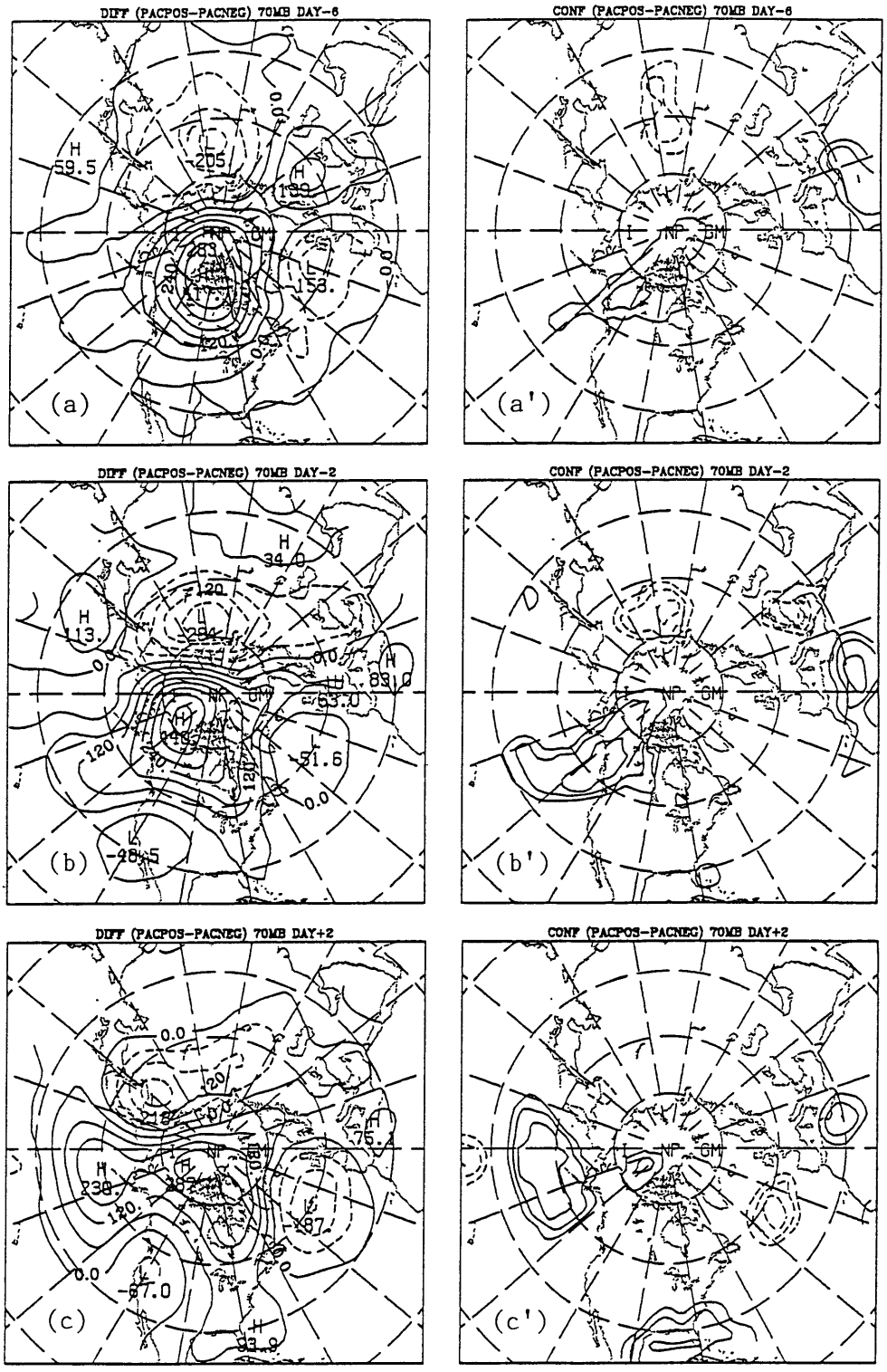

Fig. 3.10 As in Fig. 3.1 for the differences in composite mean 70 mb height anomalies between PACPOS and PACNEG cases at days (a) -6, (b) -2, (c) +2, (d) +6, (e) +10,

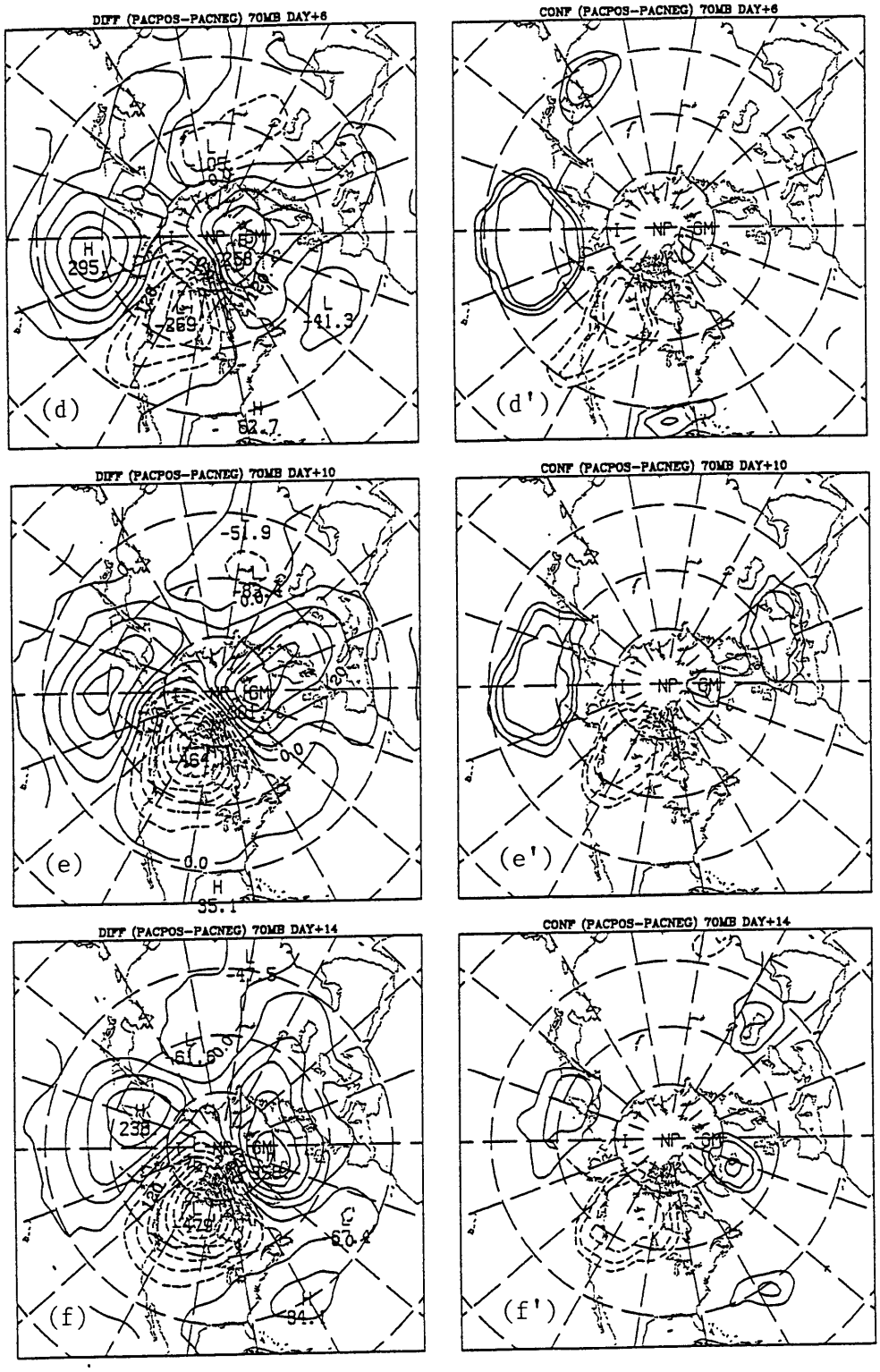

Fig. 3.10 (*Continued*) and (f) +14. Areas where the difference is greater than zero at varying confidence levels are indicated in (a')-(f').

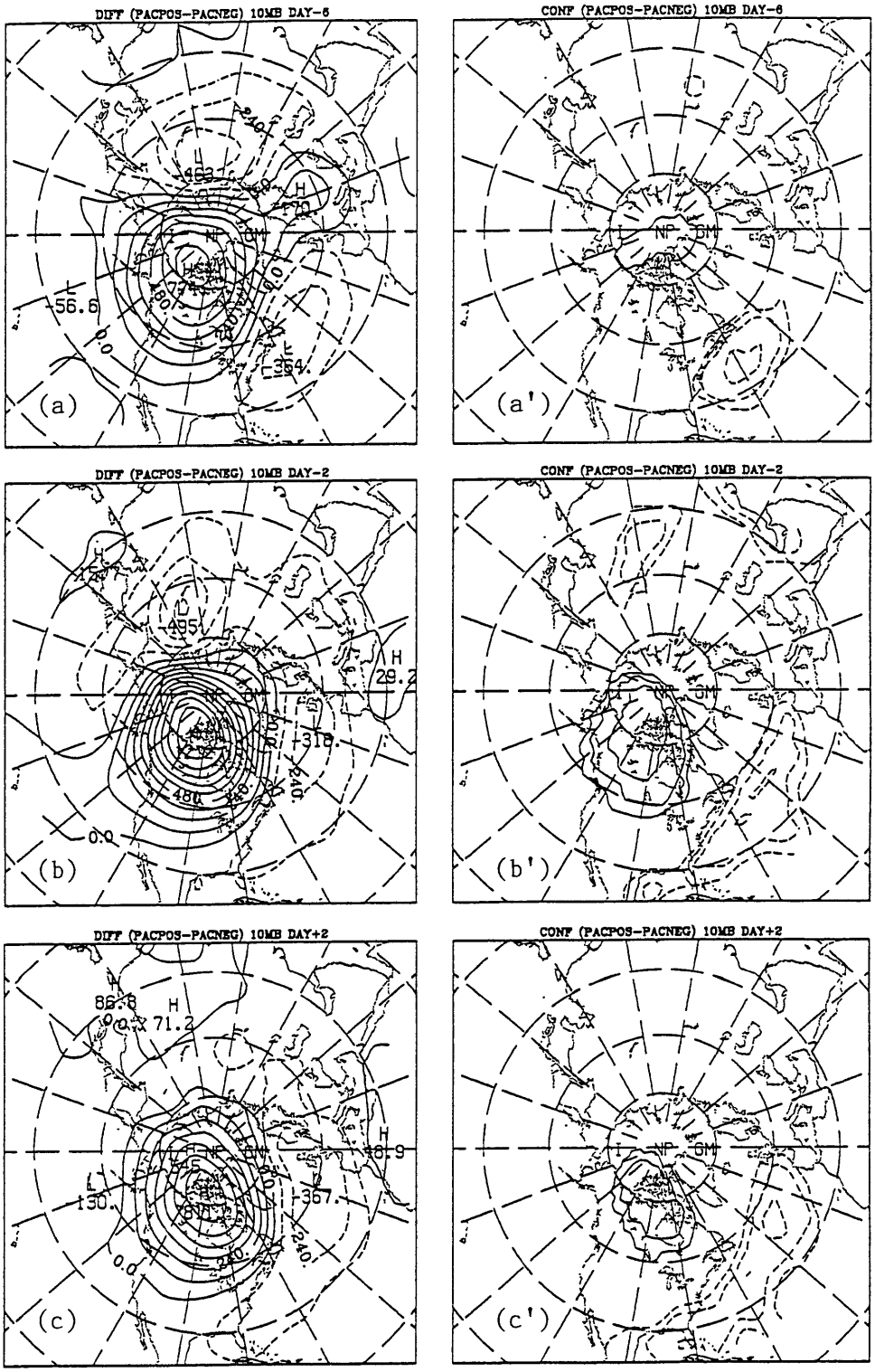

Fig. 3.11 As in Fig. 3.10 for the differences in composite mean 10 mb height anomalies on days (a) -6, (b) -2, (c) +2, (d) +6, (e) +10, and (f) +14.

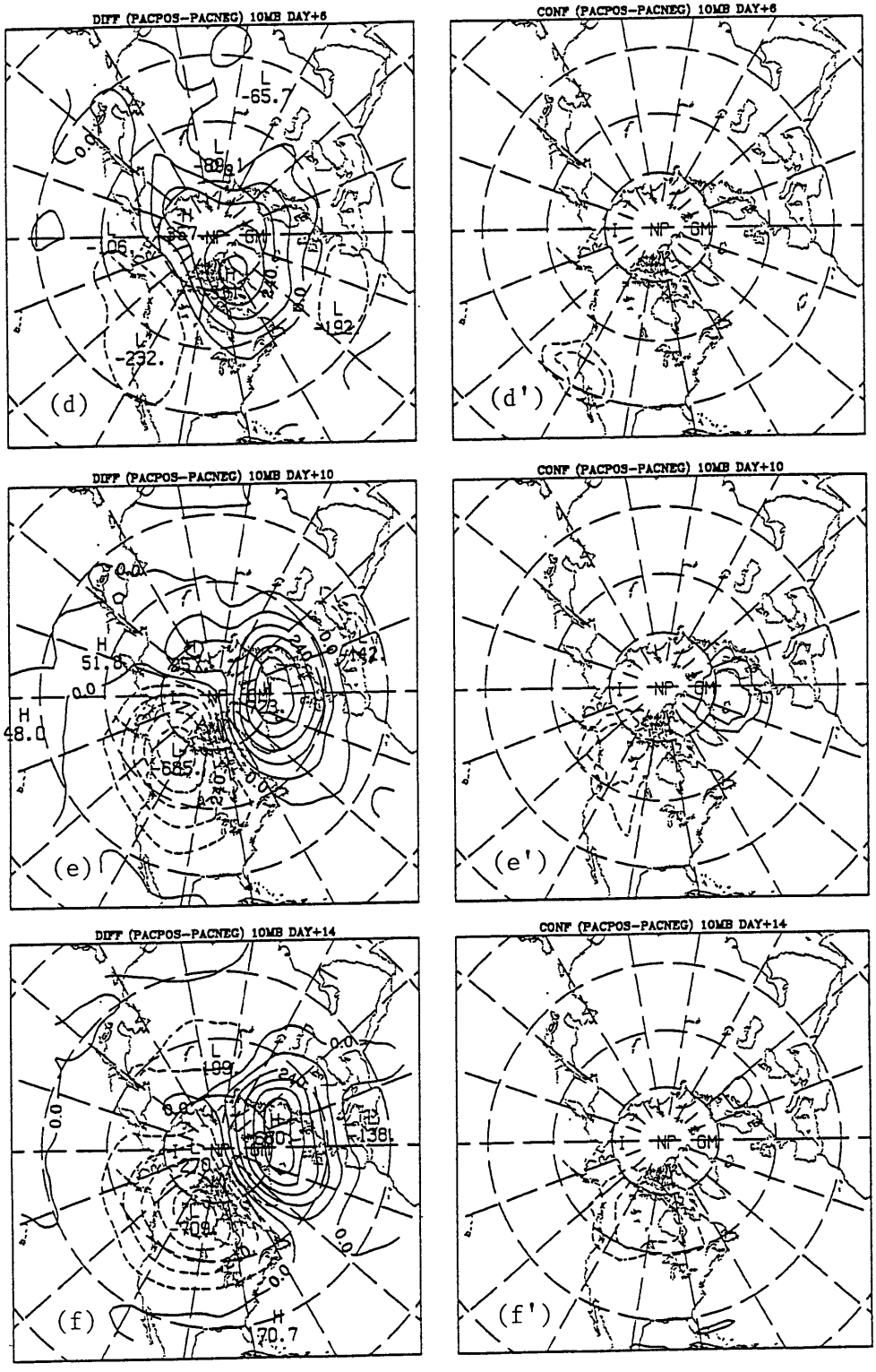

Fig. 3.11 (*Continued*)

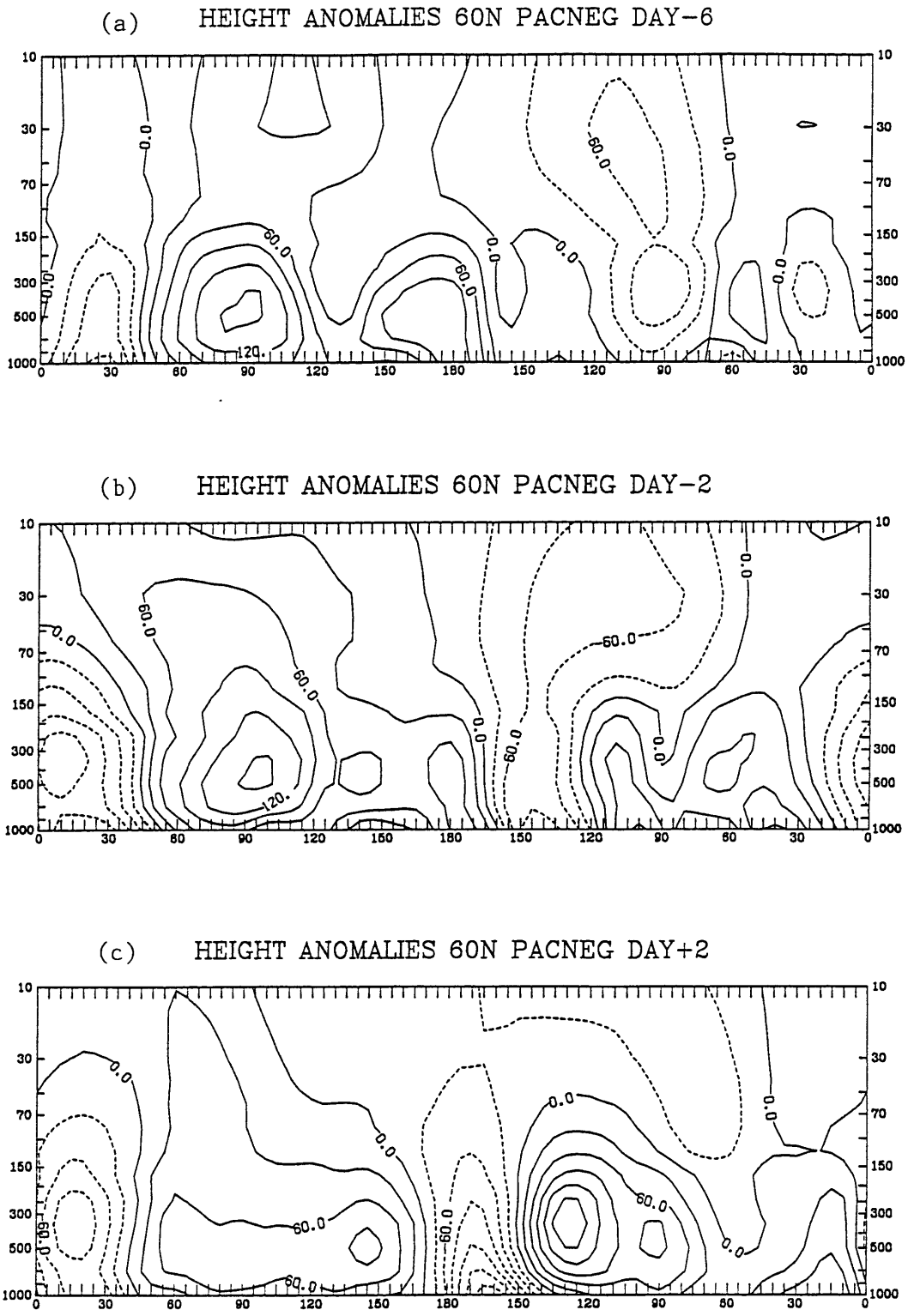

Fig. 3.12 Composite mean longitude-pressure (millibars) cross sections of height anomalies (in meters) for the PACNEG cases at 60°N on days (a) -6, (b) -2, (c) +2, (d) +6, (e) +10, and (f) +14, scaled by the square root of pressure to 300 mb.

(d) HEIGHT ANOMALIES 60N PACNEG DAY+6

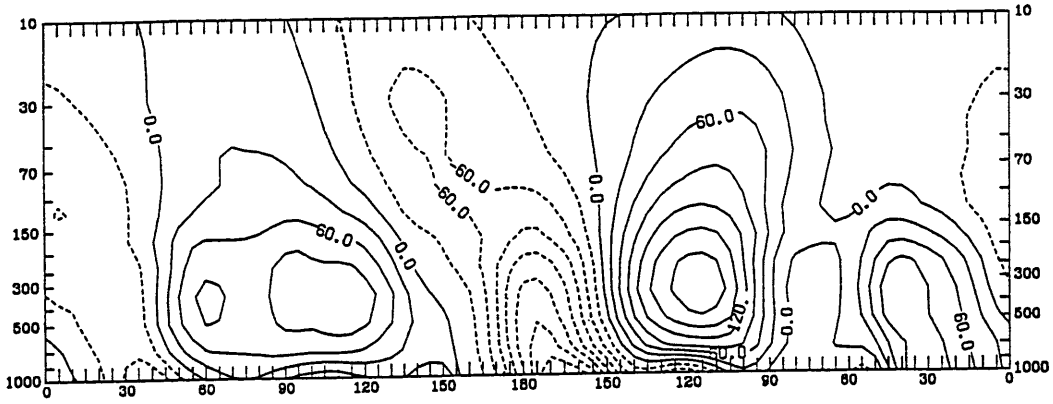

(e) HEIGHT ANOMALIES 60N PACNEG DAY+10

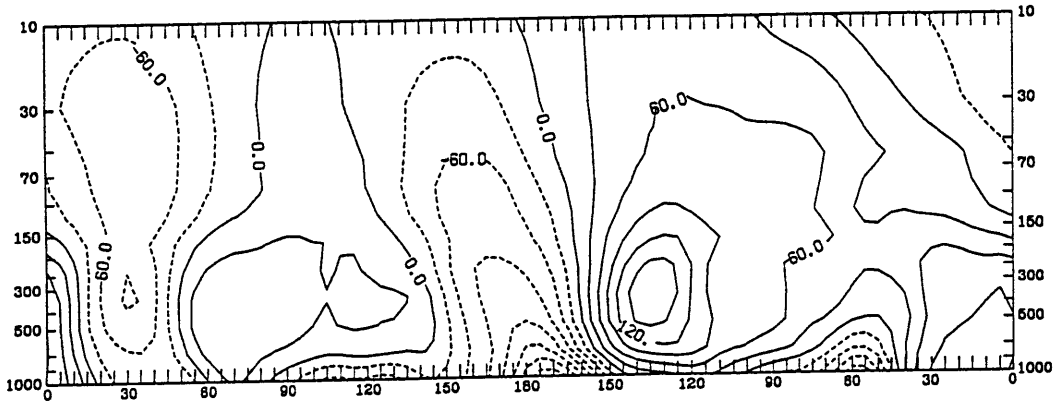

(f) HEIGHT ANOMALIES 60N PACNEG DAY+14

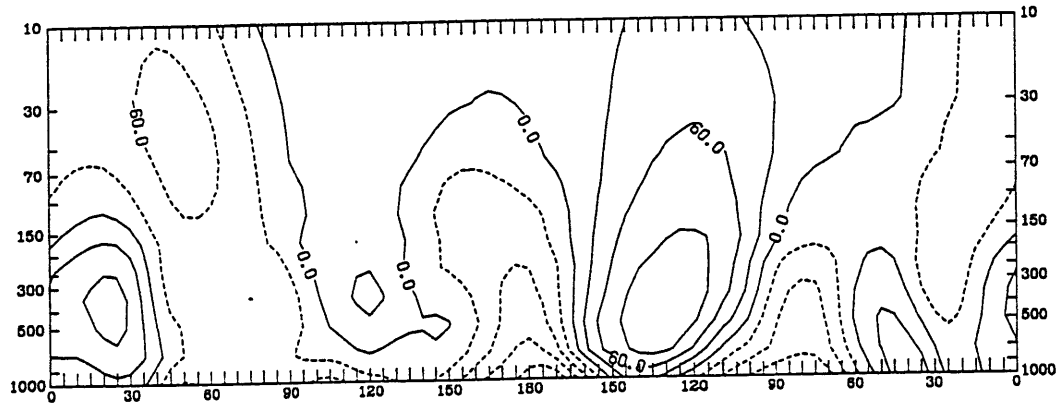

Fig. 3.12 (*Continued*)

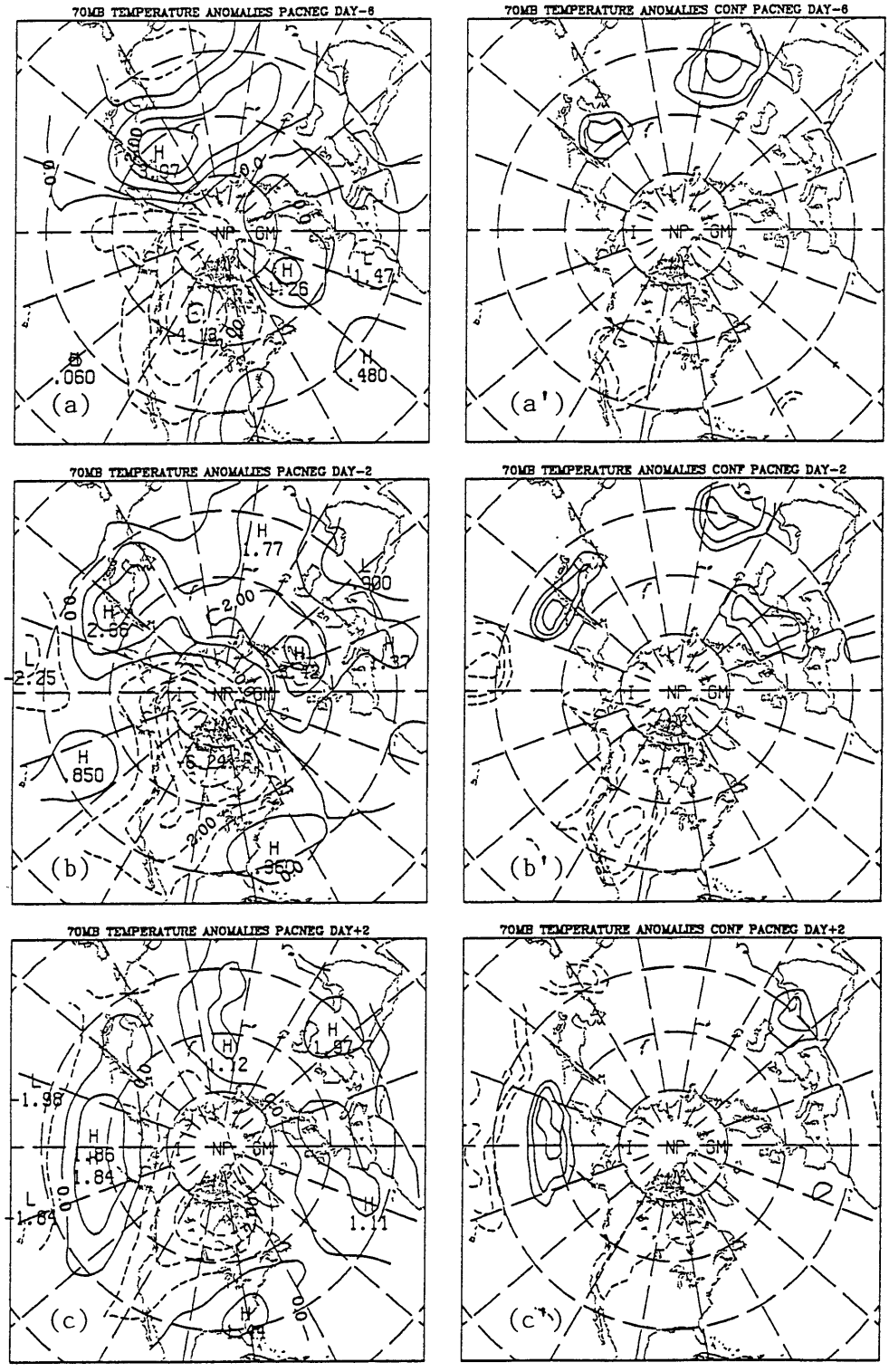

Fig. 3.13 As in Fig. 3.1 for the composite mean time evolution of 70 mb temperature anomalies for the PACNEG cases on days (a) -6, (b) -2, (c) +2, (d) +6, (e) +10, and (f) +14.

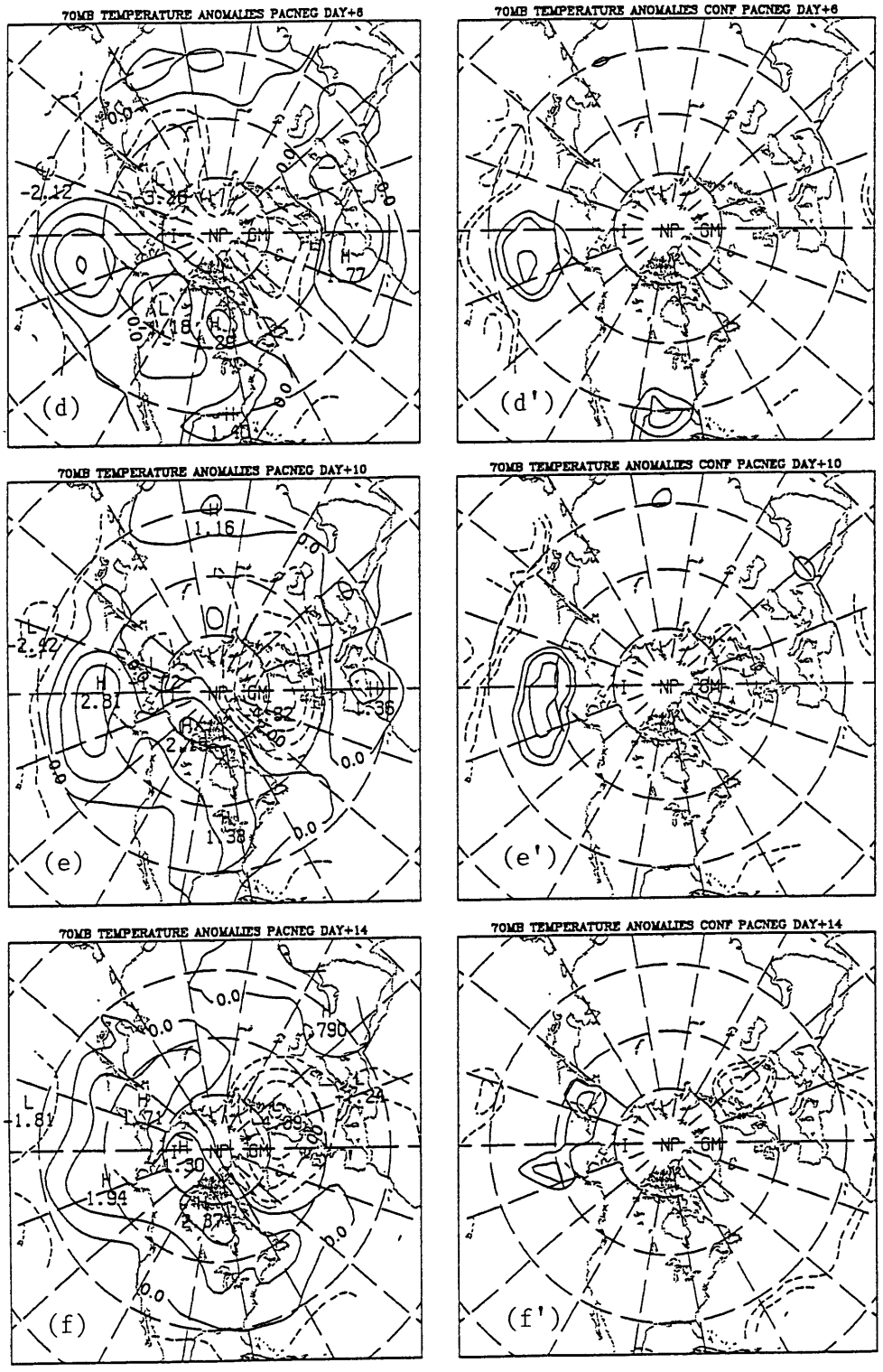

Fig. 3.13 (*Continued*)

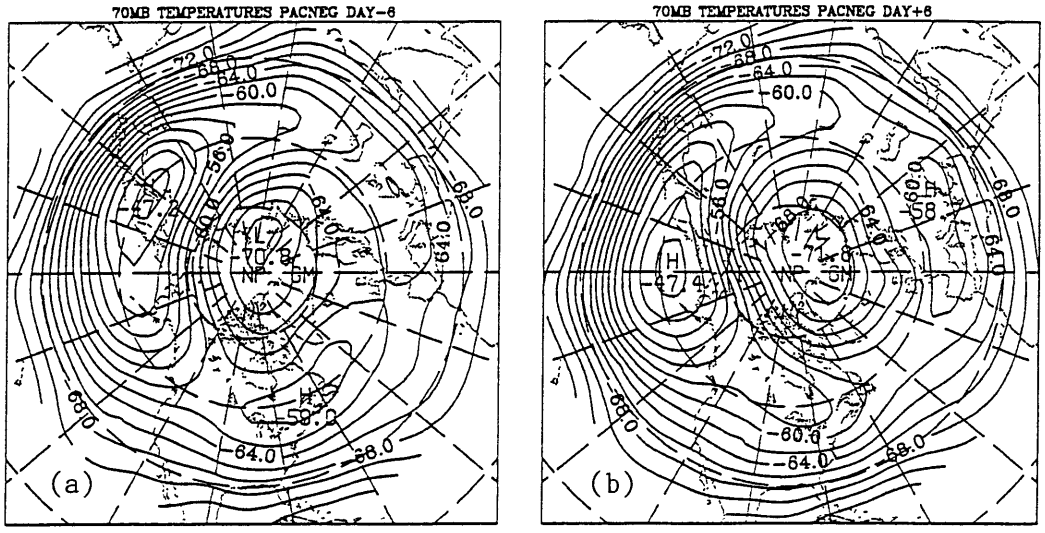

Fig. 3.14 Composite mean 70 mb temperature evolution for the PACNEG cases at days (a) -6, and (b) +6.

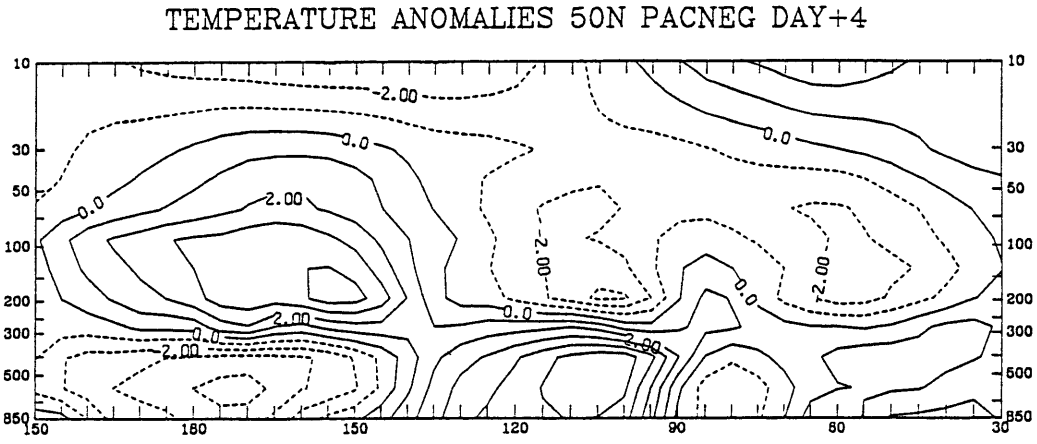

Fig. 3.15 Composite mean longitude-pressure (millibars) cross sections of temperature anomalies (°C) for the PACNEG cases at 50°N on day+4.

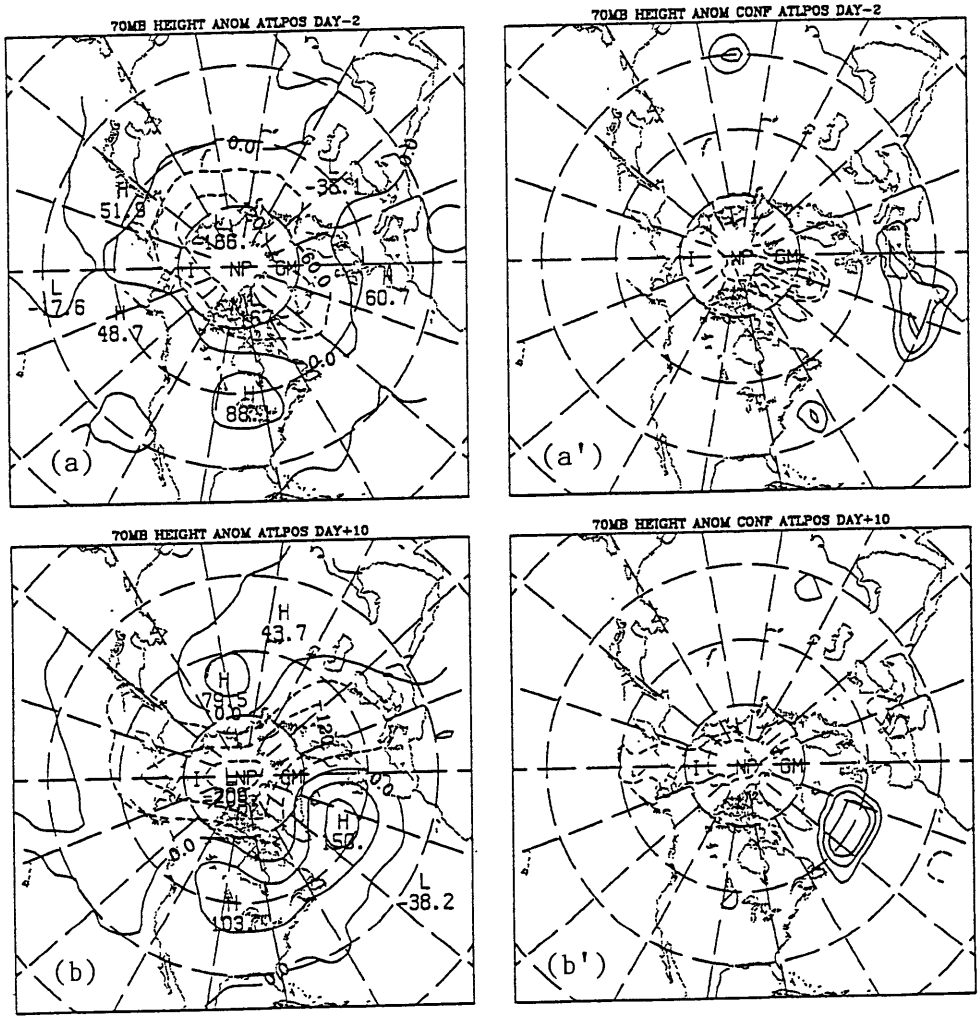

Fig. 3.16 As in Fig. 3.1 for the composite mean time evolution of 70 mb height anomalies from 9 ATLPOS cases on days (a) -2, and (b) +10.

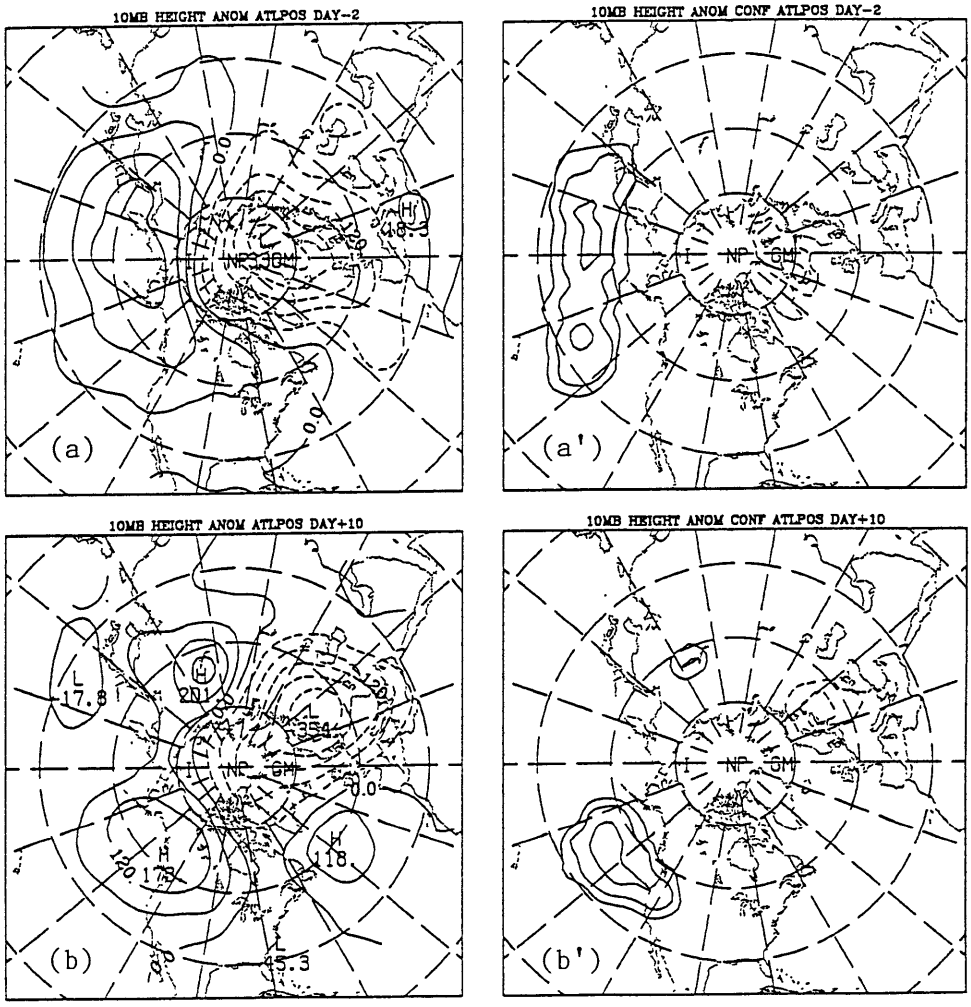

Fig. 3.17 As in Fig. 3.1 for the composite mean time evolution of 10 mb height anomalies for the ATLPOS cases on days (a) -2, and (b) +10.

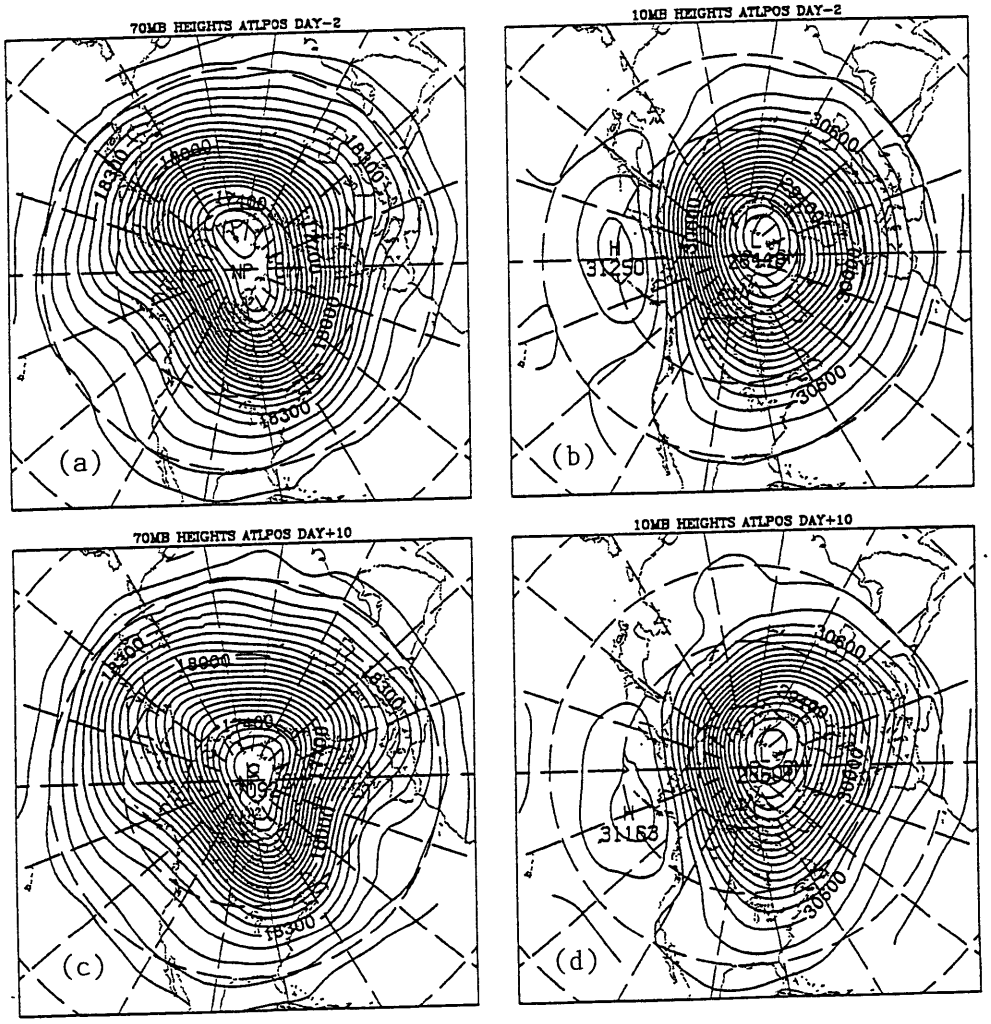

Fig. 3.18 Composite mean time evolution of geopotential heights (in meters) for the ATLPOS cases for (a) 70mb, day-2; (b) 10 mb, day-2; (c) 70 mb, day+10; and (d) 10 mb, day+10.

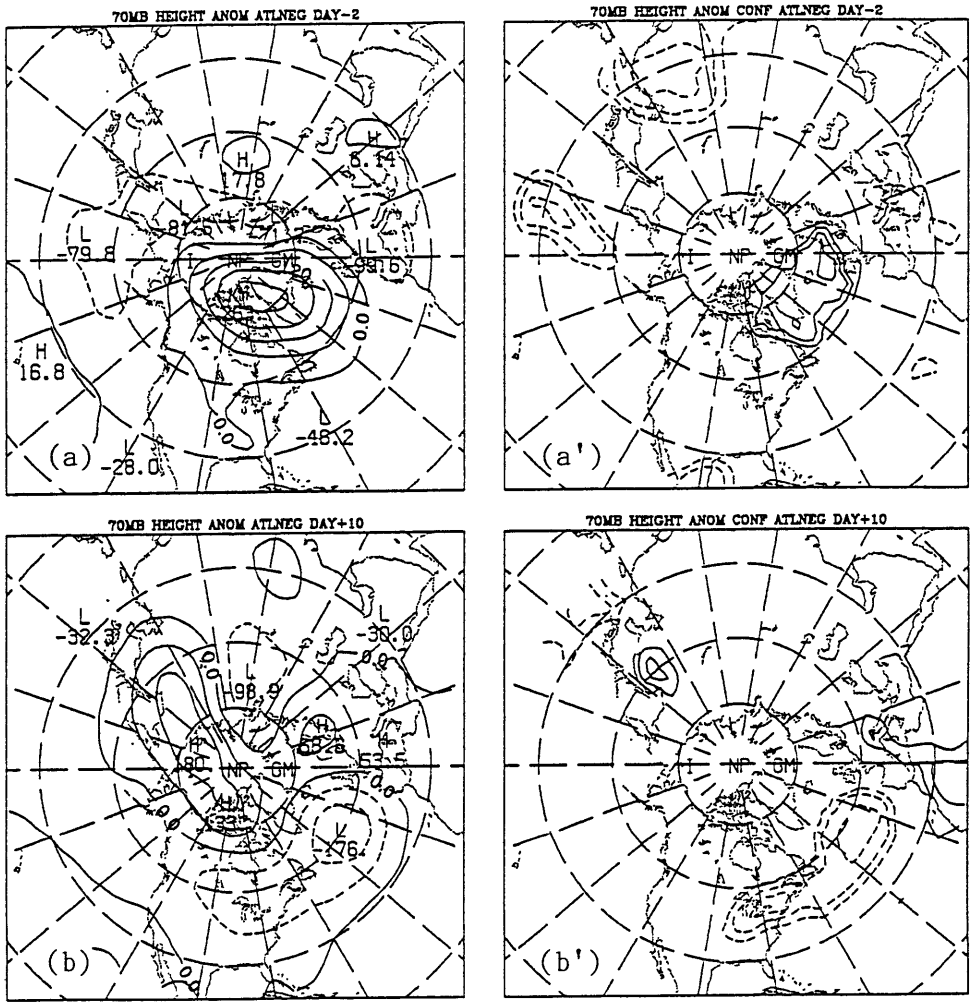

Fig. 3.19 As in Fig. 3.1 for the composite mean time evolution of 70 mb height anomalies from 8 ATLNEG cases on days (a) -2, and (b) +10.

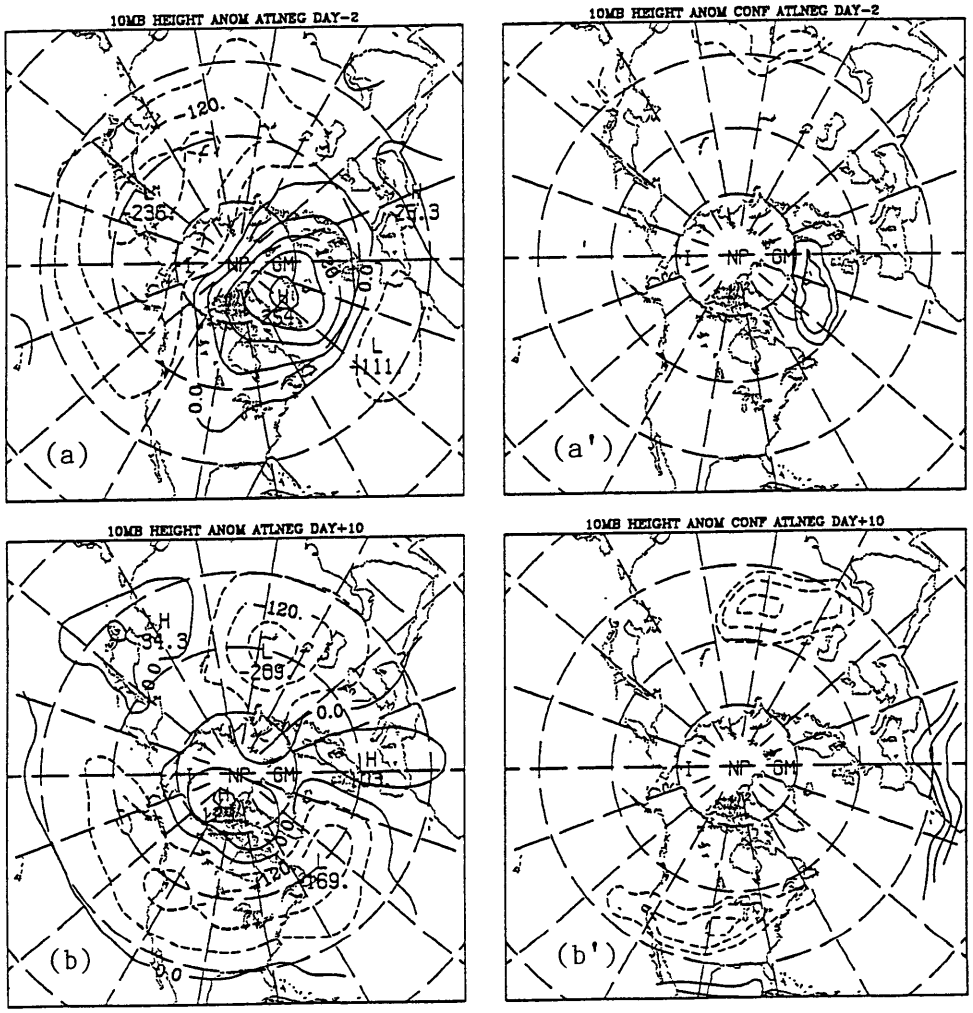

Fig. 3.20 As in Fig. 3.1 for the composite mean time evolution of 10 mb height anomalies for the ATLNEG cases on days (a) -2, and (b) +10.

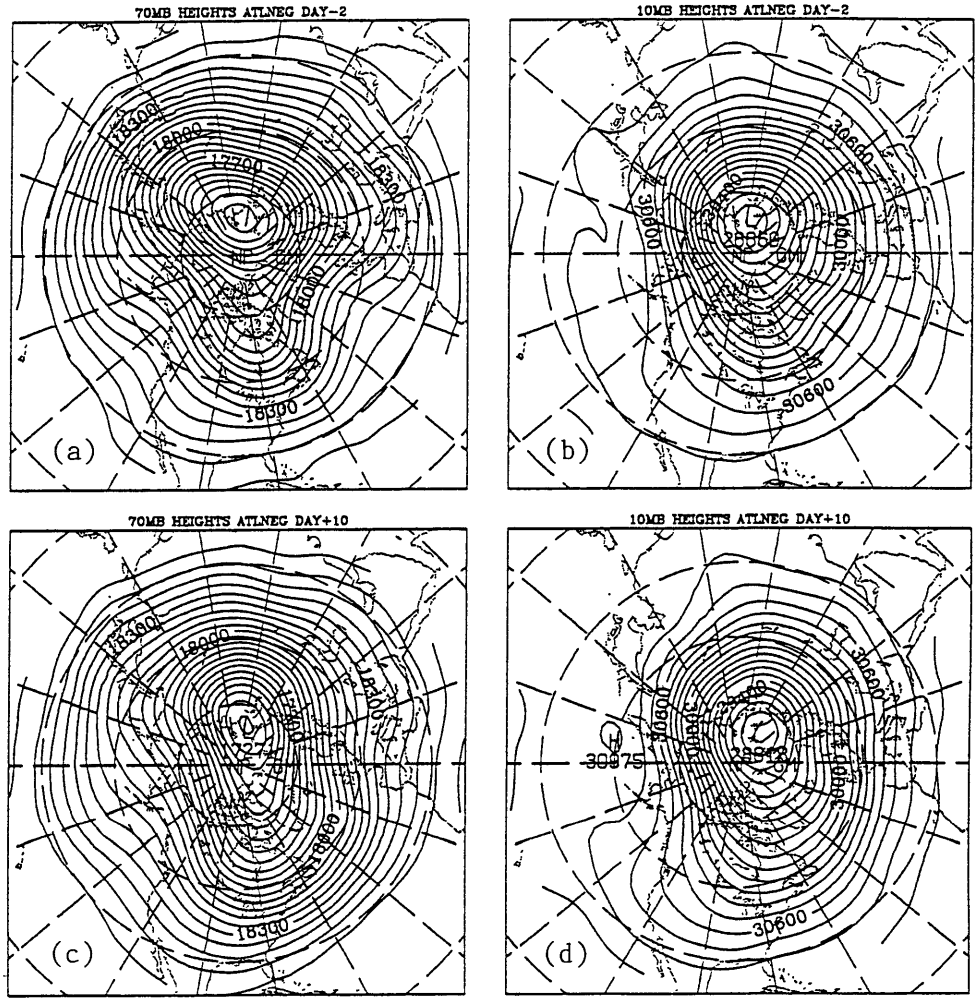

Fig. 3.21 Composite mean time evolution of geopotential heights (in meters) for the ATLNEG cases for (a) 70 mb, day-2; (b) 10 mb, day-2; (c) 70 mb, day+10; and (d) 10 mb, day+10.

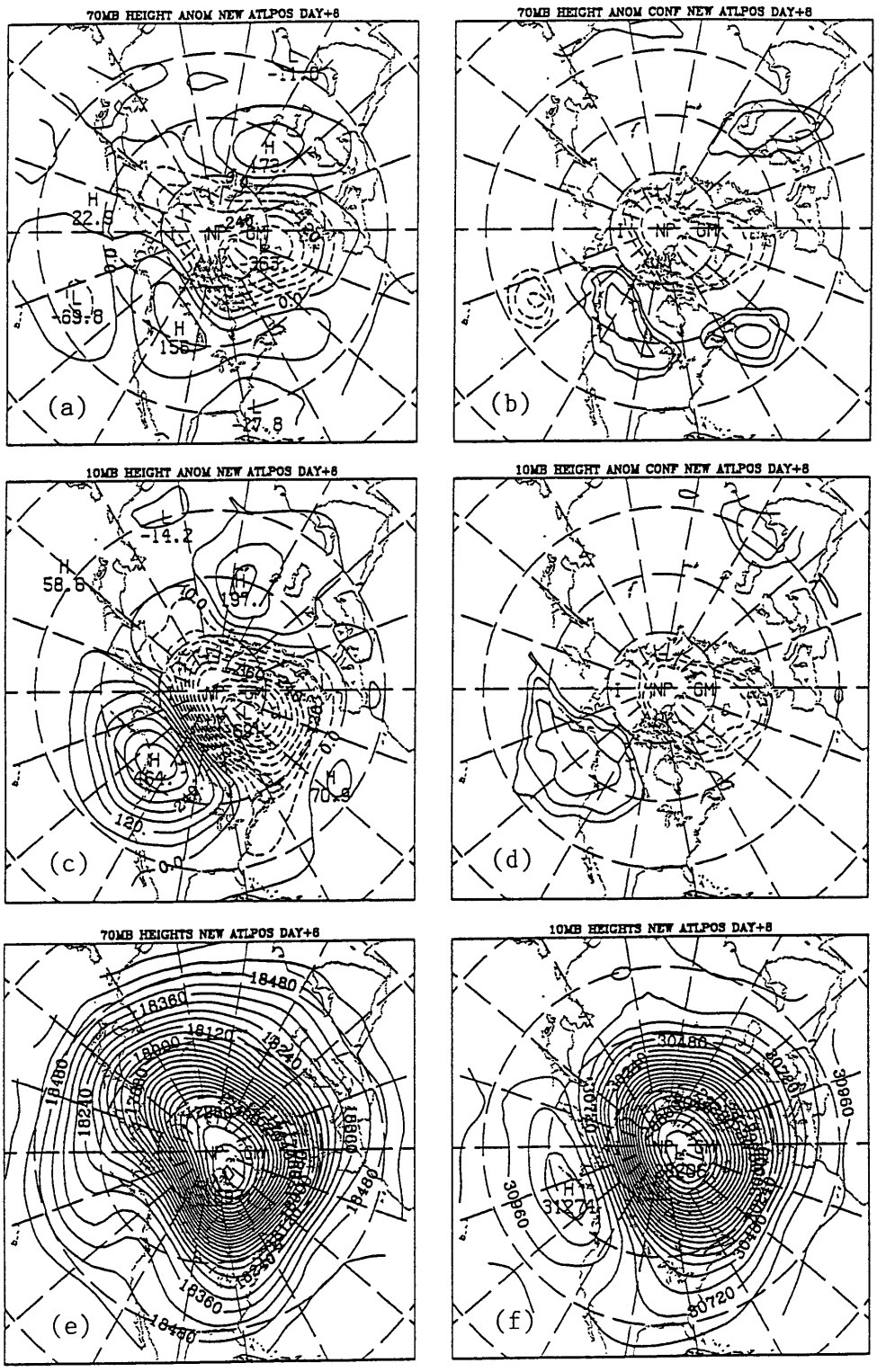

Fig. 3.22 As in Fig. 3.1 for composite means of 9 New ATLPOS cases on day+8: (a) 70 mb height anomalies, (b) confidence levels at which the 70 mb height anomalies are greater or less than zero, (c) 10 mb height anomalies, and (d) as in (b) for 10 mb. Also, (e) 70 mb geopotential heights and (f) 10 mb geopotential heights on day+8.

CHAPTER 4

ZONALLY AVERAGED QUANTITIES

4.1 Overview

Now that the basic features of the anomalies in the stratosphere during tropospheric persistent anomaly cases have been described, we will perform additional diagnostic calculations on the height and temperature data. The calculations performed are the zonal average of squared height anomalies, zonal mean wind anomalies, and Eliassen-Palm flux.

4.2 Zonally Averaged Squared Height Anomalies

Zonally averaged squared height anomalies,

$$\frac{1}{2\pi}\int_0^{2\pi} z'^2 d\lambda$$

were plotted as a function of latitude and pressure for the PACPOS and PACNEG composite anomalies. The anomalies are the same differences between the heights and the climatological normals as in the previous chapter. These squared height anomalies were

scaled by pressure (specifically, p(mb)/300) in order to show the major features at all levels.

Figure 4.1 shows the zonally averaged squared height anomalies for the PACPOS cases. On day -6 (Fig. 4.1a), the large values above 100 mb show the ISPA in the stratosphere at that time. This anomaly gradually decreases throughout the duration of the time series. On day +2 (Fig. 4.1b), strong height anomalies have appeared at the keypoint latitude. A second area is also found near 80°N on day +10 (Fig. 4.1c). Note that there appears to be no major connection between the stratosphere and the troposphere, with a relative minimum at 150 mb. On both day +2 and day +10, the largest values are confined to the troposphere, never extending above 150 mb.

For the PACNEG cases, however, as shown in Fig. 4.2, high values extend upward to 10 mb, with a much greater coherence between the troposphere and the stratosphere. On day -2 (Fig. 4.2a), the ISPA's appear, peaking at 30 mb near 70°N. These ISPA's almost disappear by day +2 (Fig. 4.2b). Also, a strong signal is present in the mid-troposphere near 70°N before onset, and signs of the development of the keypoint anomalies are apparent. Shortly after onset, zonally averaged squared height anomalies peak at 50°N. On following days (Fig. 4.2c-d), the activity over the keypoint latitude builds upward and poleward. Although the activity diminishes with height, it appears that there is a clear link between the troposphere and the stratosphere, for there is no minimum at 150 mb.

The latitude-pressure cross sections of zonally averaged wave activity and the longitude-pressure height anomaly cross sections show that there is something fundamentally different in the stratosphere between the PACPOS and PACNEG cases other than just a reversal of sign. While the PACPOS anomalies indeed extend well into the stratosphere at 120°W, evidence so far shows that the PACNEG anomalies have definite *propagation* into the stratosphere. The greater in-phase relationship between the

stratosphere and troposphere in the longitude-pressure cross sections and the lack of a relative minimum in zonally averaged squared height anomalies near 150 mb suggests that systematic upward propagation is indeed taking place in the PACNEG cases.

4.3 Zonal Mean Wind Anomalies

Zonal mean geostrophic u wind anomalies,

$$\frac{1}{2\pi}\int_0^{2\pi} u_g' d\lambda \qquad\qquad u_g' = \frac{g}{fR_e}\frac{\partial z'}{\partial \theta}$$

were then calculated for the height anomalies.

4.3.1 PACPOS

Zonal mean u wind anomalies are plotted for the PACPOS composite in Fig. 4.3. The plots reveal the strong positive ISPA. Through most of the period, and especially before day 0 (not shown), u winds are much less than normal in the stratosphere, with the weaker than normal polar vortex present before onset. The day -2 (Fig. 3.3a,b) height field for PACPOS shows this distorted and weakened vortex and a very strong ridge over Alaska. Strongest geopotential height gradients are at the pole, so much of the geostrophic wind here is contained in the v component. The center of the vortex is also shallower in the PACPOS cases (28980m) than in the PACNEG cases (28685m). There is a large weakening in the geostrophic u winds, although the winds generally increase

and are closer to normal by day +10 (Fig. 4.3e) since the flow is back to a more zonal state. Even at this time, the vortex is rather weak, so the westerlies remain relatively light.

The tropospheric u wind anomalies strengthen through day +2 (Fig. 4.3c), forming a couplet with negative anomalies south of 38°N and faster than normal u winds from 38°N to 60°N as the jet and storm track shift to the north over the Pacific. This couplet in the troposphere slowly weakens after day +2, never extending significantly upwards. By day +14 (Fig. 4.3f), the couplet has almost completely diminished, and except for a narrow belt of fast winds at 80°N, the stratosphere is still dominated by the weaker than normal westerlies.

4.3.2 PACNEG

In the negative cases (Fig. 4.4), there are substantial changes through the period. At day -2 (Fig. 4.4a) and day +2 (Fig. 4.4b), westerlies are faster than normal in the northern stratosphere, reflecting a strong vortex. The magnitude of the stratospheric wind anomalies is less than in PACPOS cases, as expected, since the magnitude of the ISPA's in PACNEG is less than in the PACPOS cases.

In the troposphere, near the latitude of the keypoint, however, mean u wind anomalies are much smaller than expected, but a couplet pattern nevertheless exists. South of 40°N, u winds are faster, reflecting the strong zonal jet across the Pacific, which is farther south than normal in PACNEG. From 40°N to 60°N, winds are light because the Pacific jet is to the south of this area, and the Aleutians low is deeper during PACNEG events, causing a more easterly flow to its north. The enhanced ridge over western North America also plays a role in this wind anomaly by reducing the u wind there.

On following days, the tropospheric zonal mean u wind anomaly couplet stretches up into the stratosphere, reaching 10 mb by day +12 (Fig. 4.4d). Since the zonal mean wind anomalies are quite light, the confidence of the features just described is not particularly high. Nevertheless, the establishment of a common pattern in both the stratosphere and the troposphere supports earlier arguments that upward propagation occurs in PACNEG cases.

4.4 Eliassen-Palm Fluxes

To discover the true wave propagation characteristics, Eliassen-Palm (EP) fluxes were calculated based on the PACPOS and PACNEG height and temperature composite analyses. Three plots were made. The first plot (Fig. 4.5) is simply the climatological EP flux, which was computed from the climatological data obtained by the Fourier decomposition of the anual cycle (see Chapter 2). This grid was computed by subtracting from the composite height and temperatures their respective anomalies. Although climatology is evaluated at each day for each case, the climatology does not change sufficiently from day to day during the composite period to significantly affect the EP flux vectors. Climatological fields were constructed in this way rather than using a standard winter mean. In this way, the climatology *during the cases* was obtained.

The second plot is the EP flux calculated on the average height and temperature fields for the case composite. The third plot is simply the second plot minus the first.

The formula used for the calculations was:

$$F_y = \overline{u'_g v'_g} \cos\theta \qquad F_z = f\frac{\overline{v'_g T'}}{S}\cos\theta$$

from Edmon, et al. (1980) with the constant R_e (radius of the earth) omitted. Overbars denote zonal averages and primes denote departures therefrom. F_z was scaled by 100/f in order to more readily display vertical propagation.

EP flux calculations performed on the climatological normals of the cases (Fig. 4.5) are similar to the EP flux calculations in Edmon, et al. (1980). There is a strong upward flux of wave activity from 50°N. Wave activity is then refracted equatorward near the tropopause south of this latitude. In the stratosphere, the upward flux continues. There is some small amount of poleward refraction in the lower stratosphere, but the refraction is again equatorward near 10 mb.

Note that these plots were not scaled by pressure and thus do not account for pressure changes with height. If so scaled, the vectors would be too small to see in the stratosphere relative to those in the troposphere. Vectors are scaled similarly for all plots so quantitative differences between composite and climatological EP flux can easily be seen.

Instead of averaging the EP fluxes of each individual case, the EP flux calculations were performed on composite averages over all the cases. In so doing, the magnitude of the EP flux vectors is significantly reduced since contributions to EP flux from incoherent transient disturbances are removed in the compositing procedure.

4.4.1 PACPOS

Figure 4.6 shows the EP fluxes at four day intervals for the PACPOS cases. Vectors plotted in Fig. 4.7 show the difference between the vectors in Fig. 4.6 and those

in Fig. 4.5. On day -6 (Figs. 4.6a, 4.7a), there is a marked strength in upward propagation in the stratosphere and slightly stronger flux into the tropical tropopause region. On day -2 (Figs. 4.6b, 4.7b), the upward flux into the upper stratosphere has weakened considerably as the height anomalies peak there. At the same time (Figs. 4.6b,c; 4.7b,c), fluxes into the equatorial upper stratosphere increase. After this time, the EP fluxes weaken considerably in all parts of the cross section. Finally, by day +10 (Figs. 4.6e, 4.7e) and +14 (Figs. 4.6f, 4.7f), there is considerable poleward refraction in mid-latitudes, but still no anomalously large upward fluxes.

4.4.2 PACNEG

EP flux vectors are plotted for PACNEG cases in Fig. 4.8, and their differences from the EP fluxes of climatology are plotted in Fig. 4.9. In the stratosphere, flux vectors are smaller than normal on day -2 (Figs. 4.8a, 4.9a). This observation is consistent with the relatively zonal flow (weak wave activity) in the stratosphere that exists before onset of PACNEG cases. (See Fig. 3.9a,b for reference). On day +2 (Figs. 4.8b, 4.9b), the EP flux increases in the subtropical upper troposphere, but there is a great deal of equatorward refraction and little activity directed towards the polar stratosphere. By day +8 (Figs. 4.8c, 4.9c), there is more wave activity flux vertically in mid-latitudes, and there is a poleward refraction as well, which directs the vectors right into the stratophere, where the largest 10 mb height anomalies develop in response to the mature PACNEG pattern in the troposphere.

4.5 Discussion

Many features of the PACPOS pattern can be connected with the EP flux characteristics. The strong EP flux in the stratosphere on day -6 (Figs. 4.6a, 4.7a) is consistent with the amplification of the ISPA until day -2 (Figs. 4.6b, 4.7b). On day -2, 10 mb height anomalies reach their maximum at the same time as the EP flux into the upper stratosphere has decreased significantly. Then, with the flux considerably less, the ISPA weakens.

After onset, however, the EP fluxes diminish quite significantly and are weaker than normal throughout most of the Northern Hemisphere. At first, this weakening was a major surprise, since the appearance of anomalies at 10 mb during PACPOS cases led us to believe there was significant upward propagation. After further thought, however, the decreased EP flux can be rationalized.

There are two reasons for weaker than normal EP flux during PACPOS events. First, the PACPOS patterns oppose the climatological geopotential height pattern at 500 mb. This climatological pattern has a trough in the vicinity of the Aleutian Islands (often in the form of a cutoff low), a ridge over western North America, and a trough over eastern North America. The PACPOS events are associated with positive height anomalies in the climatological mean trough positions and negative height anomalies near the mean ridge over the western part of North America. Although the anomaly centers of the PACPOS cases do not match up exactly with the climatological mean trough and ridge positions, the net effect of these anomalies on the flow, globally, is to be associated a more zonal flow (reduced stationary waves).

Second, the PACPOS events decrease the zonal extent of the trough in the western and central Pacific . In PACNEG events, this trough may extend all the way from eastern Asia into the Gulf of Alaska, but in the PACPOS cases, the ridge that builds in the central

North Pacific keeps the trough confined to the western North Pacific. This reduction in scale may be associated with reduced vertical propagation into the stratosphere.

With a more zonal flow and lack of large scale planetary wave activity propagating upward out of the troposphere, the stratospheric flow appears to relax into a more zonal state, as is seen at 10 mb between day -2 and day +10. We conclude this simple relaxation back to a zonal state is responsible in a large part for the anomaly pattern at 10 mb. If the 10 mb flow were completely zonal (i.e. no geostrophic v wind), then the resulting height anomaly pattern would be qualitatively similar to, but slightly out of phase with, the 10 mb height anomalies in the PACPOS cases. Forcing of the 10 mb anomalies by greater wave activity in the troposphere, as was first hypothesized, therefore does not appear to be responsible.

On the other hand, the enhancement of the climatological mean pattern by the PACNEG events (deepening of the Aleutian low, building of the western North American ridge, and deepening of the eastern North American trough) results in enhanced EP fluxes upwards and polewards.

From the theory of vertical propagation of planetary waves (Holton 1979), waves of larger scale are favored for upward propagation. In the PACNEG cases, the mean trough over the western and central Pacific has a larger scale, stretching from the east coast of Asia to as far as the Gulf of Alaska. Increased scale of this trough may favor greater upward propagation.

In order to test the above arguments, zonal height anomalies were plotted for PACPOS and PACNEG cases for 500 mb, 70 mb, and 10 mb. The zonal height anomalies are defined as the difference between the geopotential height at a grid point and the average geopotential height of all grid points at the same latitude. With this plot, the amplitude of the ridges and troughs can be quantified and compared with the amplitudes of climatological mean ridges and troughs. When the plots of climatological zonal height

anomalies (Fig. 4.10) are compared with the PACPOS and PACNEG height anomalies at corresponding levels (Figs. 3.1c-f,3.7c-f) one can see that the PACPOS and PACNEG anomalies are nearly 90° out of phase with the climatological mean trough and ridge positions, rather than exactly 180°. Thus, it appears that PACPOS and PACNEG patterns would neither reinforce nor diminish the climatological mean pattern, but rather, would shift it westward or eastward.

However, when comparing the PACNEG zonal height anomalies and the PACPOS zonal height anomalies (Fig. 4.11) with each other and with the climatological zonal height anomalies (Fig. 4.10), one can see that many of the arguments may have some merit. First of all, the PACNEG pattern (Fig. 4.11a') indeed enhances the 500 mb climatological mean ridges and troughs (Fig.4.10a). The amplitude of the western North American ridge in the PACNEG cases is twice its climatological value. In the PACPOS cases (Fig. 4.11a), there is essentially no western North American ridge. However, there *is* a ridge over the Aleutians whose amplitude is larger than that of the climatological mean western North American ridge. The plots also confirm that the trough over the western Pacific has less amplitude and is much shorter in PACPOS. It is much stronger and zonally elongated in PACNEG. Overall, the troughs and ridges during PACNEG are still in the same place as the climatological mean troughs and ridges. PACPOS ridges and troughs, on the other hand, are not completely in phase with climatological mean troughs and ridges, particularly over the Pacific and western North America.

At higher levels of the atmosphere, the ridge and trough positions of PACPOS cases more closely match ridge and trough positions of PACNEG cases, and the main difference between the two is in amplitude. By 10 mb, the PACNEG ridge (Fig. 4.11c') is centered within 10° longitude of the PACPOS ridge (4.11c). The amplitude of the eastern Pacific/western North American ridge is greater at all levels in the PACNEG cases than it is in either the PACPOS cases or climatology. In fact, it is almost double that of

the PACPOS ridge.

Secondly, cross sections of the zonally averaged squared zonal height anomalies are displayed in Fig. 4.12. The formula to compute them is the same as in section 4.2, except that z' is defined here as the deviation of geopotential heights from the zonal average. These plots provide further evidence that the ridges and troughs have larger amplitude in PACNEG and relatively small amplitude in PACPOS. Values in PACPOS (Fig. 4.12b) are generally less than those in the climatological cross section (Fig. 4.12a), and the cross section of the PACNEG cases (Fig. 4.12c) has the largest values at all levels.

4.6 Summary

While 70 mb and 10 mb height anomalies (Figs. 3.1 and 3.2) and longitude-pressure cross sections (Fig. 3.4) are suggestive of upward propagation of the keypoint anomalies and the first downstream anomalies in PACPOS events, a more careful look at other quantities, such as zonally averaged squared height anomalies, zonal mean wind anomalies, and EP flux suggests a lack of significant upward propagation. Many features in wave activity and zonal mean wind that developed in the troposphere in the PACPOS events do not appear later in the stratosphere. In the zonally averaged squared height anomaly cross sections (Fig. 4.1), a relative minimum is seen near 150 mb, suggesting an incoherent stratosphere and troposphere. Finally, EP flux cross sections (Fig. 4.7) confirm weaker than normal upward propagation in the PACPOS cases. In the stratosphere, many features of the PACPOS pattern can be qualitatively reproduced by simply making the flow zonal, as if all forcing was shut off from below.

In the PACNEG cases, on the other hand, the climatological mean trough and

ridge positions over the Pacific and North America are enhanced, and EP flux cross sections (Fig. 4.9) show increased upward wave activity propagation during these events. Also, the smooth decrease of zonal mean squared height anomalies with height (Fig. 4.2), as well as the appearance of the zonal mean u wind anomaly pattern in the stratosphere (Fig. 4.4), show a connection between the troposphere and the stratosphere that is nearly absent in the PACPOS cases. Finally, in longitude-pressure cross sections of height anomalies (Fig. 3.12), the troposphere and the stratosphere are remarkably coherent from day +6 to day +10 in the PACNEG cases around most of the latitude circle, a characteristic that is not apparent in the PACPOS cases.

Therefore, we suggest that PACNEG cases amplify the climatological mean height pattern and lead to stronger than normal wave propagation into the stratosphere, while the PACPOS cases, in a net sense, cancel out the climatological mean trough and ridge positions. In so doing, the PACPOS events make the stratosphere "blind" to thermal and topographic forcing and allow the stratospheric flow to relax back to a more zonal flow.

In all the above analyses, however, calculations were formed on composites of many cases. Doing calculations on individual cases and then averaging the results could give a markedly different picture. For this reason, it is worthwhile to look at a few cases individually.

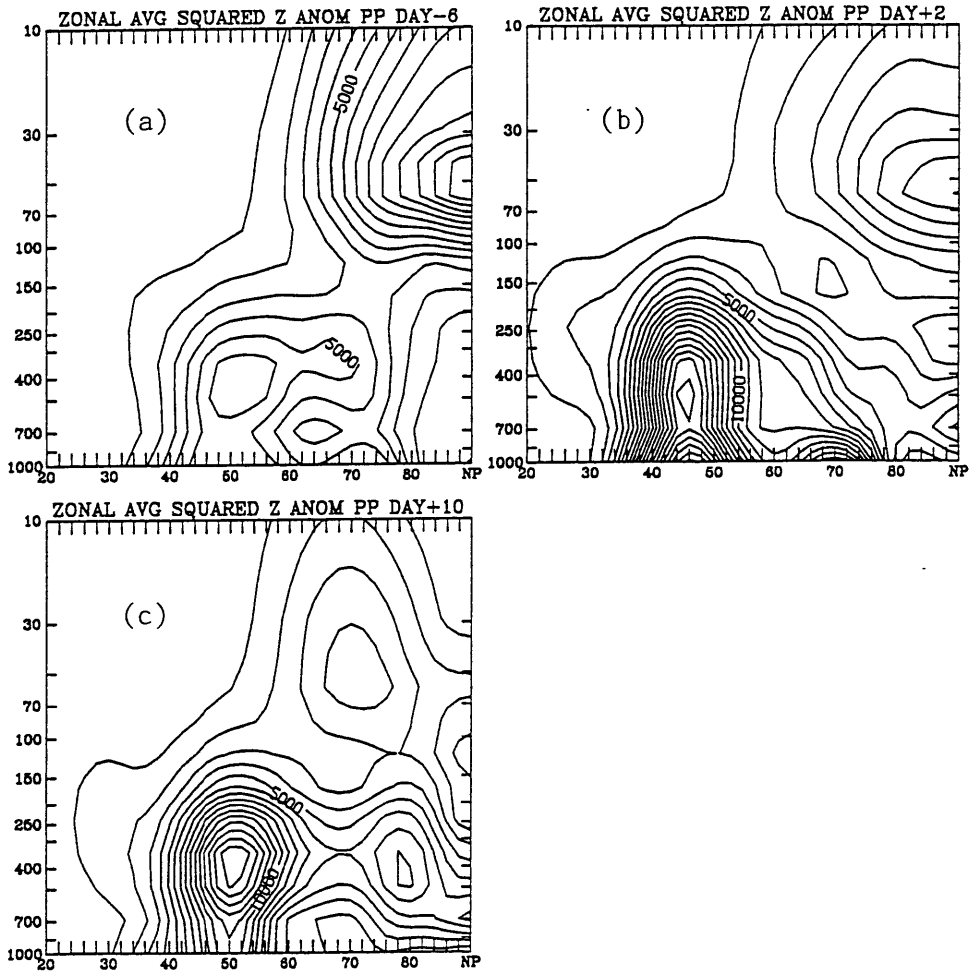

Fig. 4.1 Latitude-pressure (millibars) cross sections of zonally averaged squared height anomalies (in meters squared) for the PACPOS cases on days (a) -6, (b) +2, and (c) +10, scaled by pressure to 300 mb. Zonal average is around the entire latitude circle.

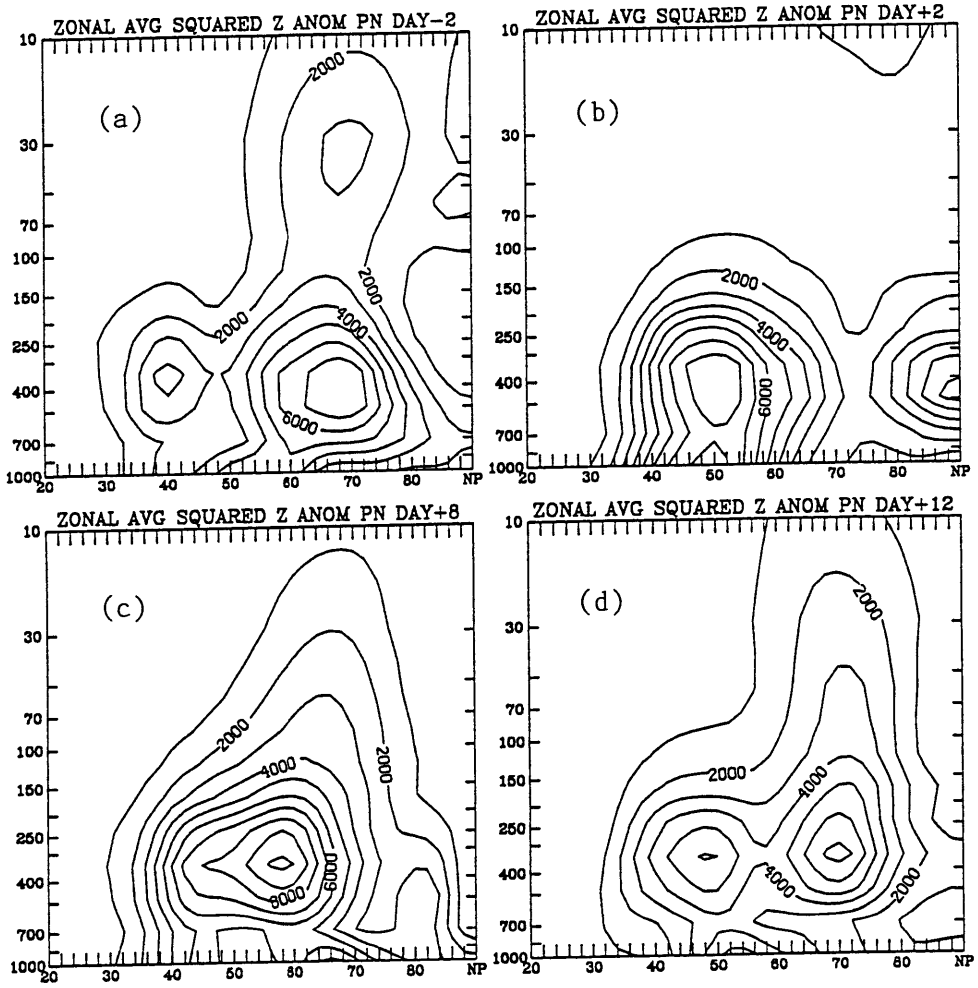

Fig. 4.2 As in Fig. 4.1 for zonally averaged squared height anomalies for the PACNEG cases on days (a) -2, (b) +2, (c) +8, and (d) + 12.

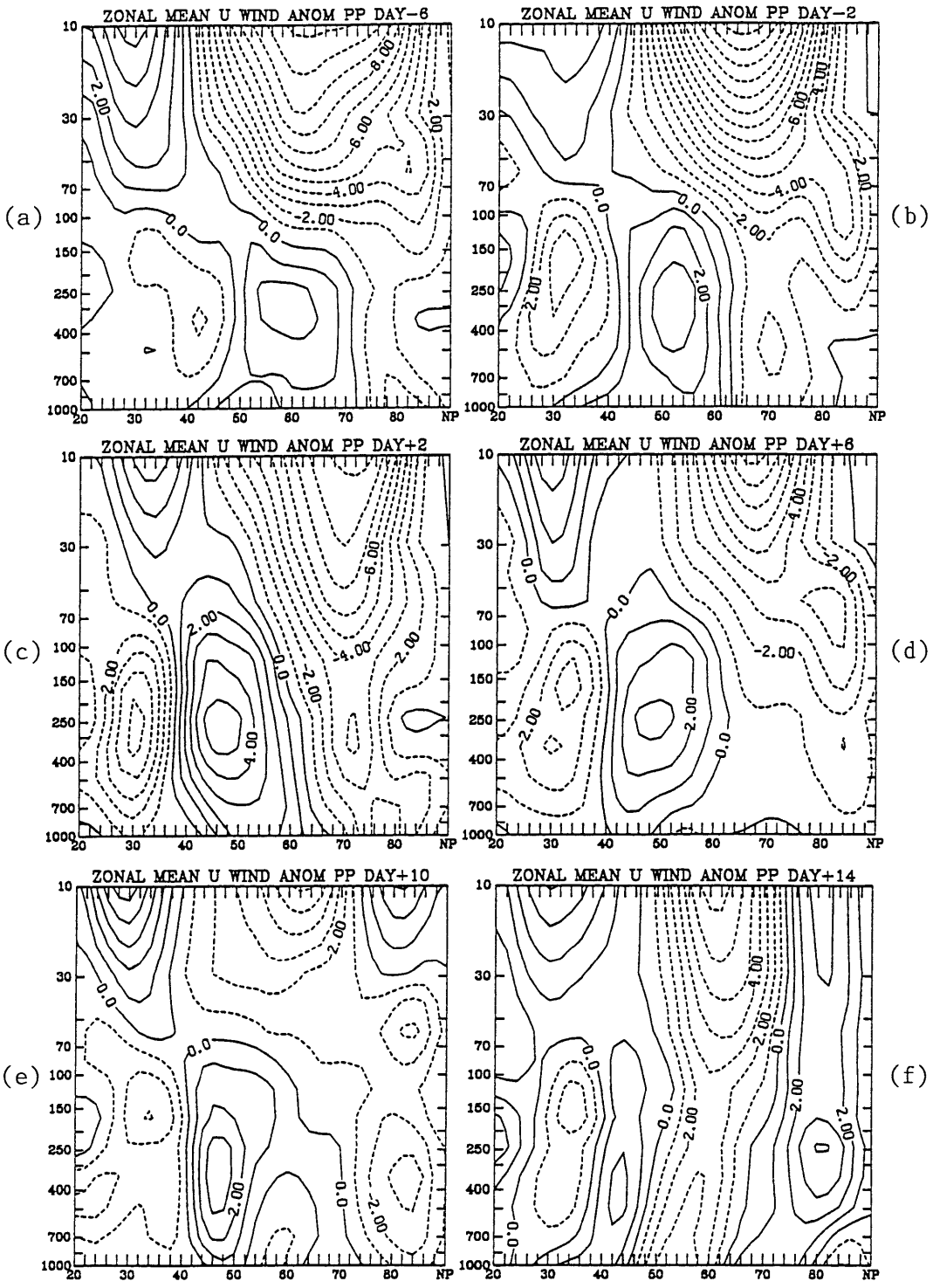

Fig. 4.3 Latitude-pressure (millibars) cross sections of zonal mean geostrophic u wind anomalies for the PACPOS cases on days (a) -6, (b) -2, (c) +2, (d) +6, (e) +10, and (f) +14.

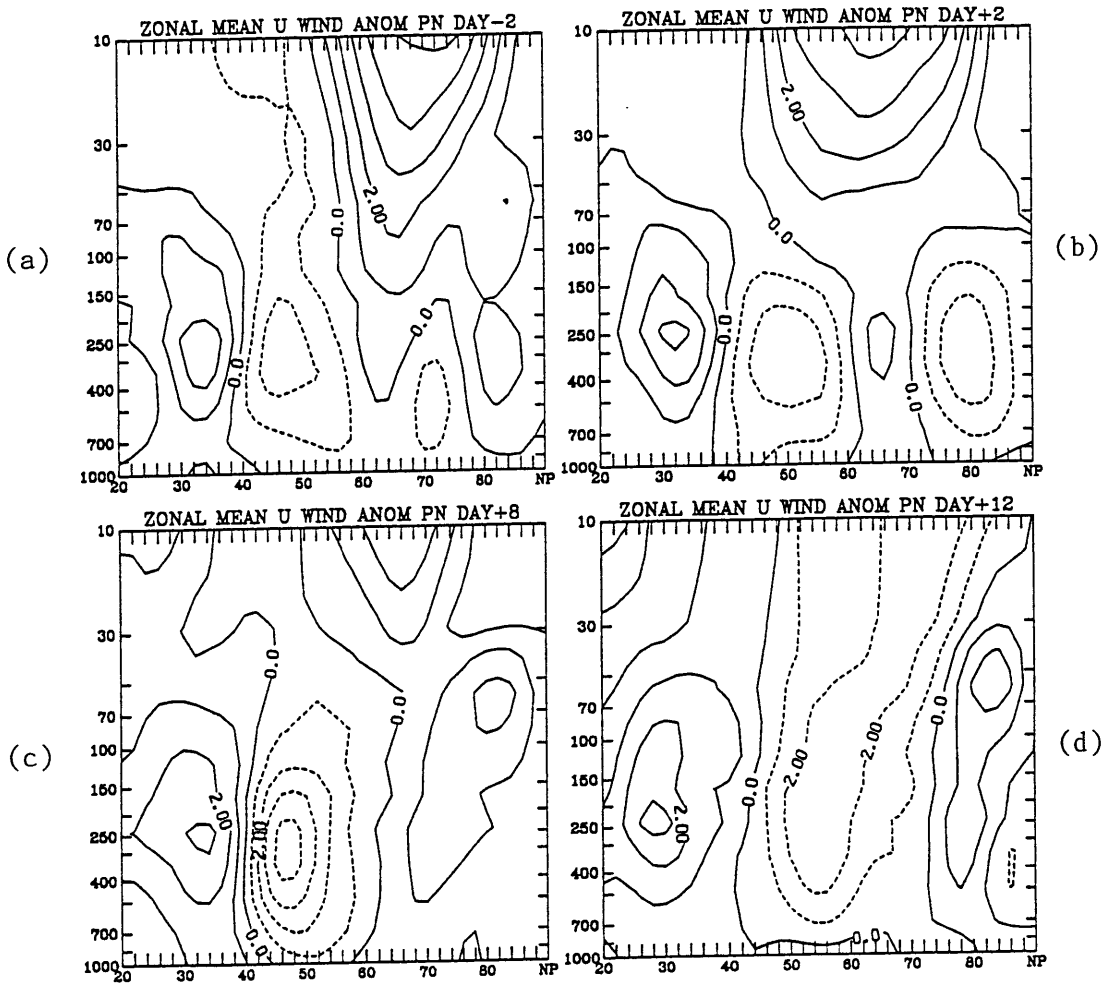

Fig. 4.4 As in Fig. 4.3 for the zonal mean geostrophic u wind anomalies for the PACPOS cases on days (a) -2, (b) +2, (c) +8, and (d) +12.

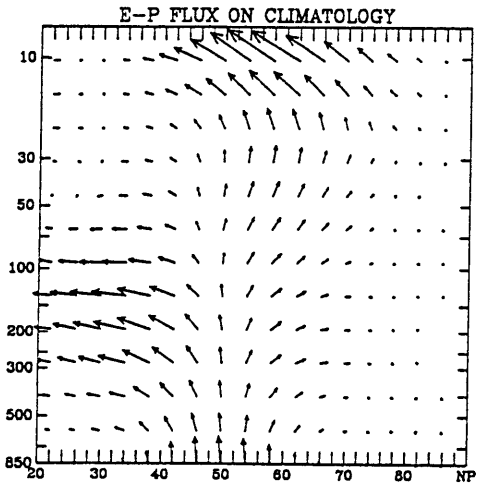

Fig. 4.5 Latitude-pressure cross sections of Eliassen-Palm flux (units: like m^2s^{-2}) for climatology during Pacific cases. The longest vector is 26 units. See text for explanation.

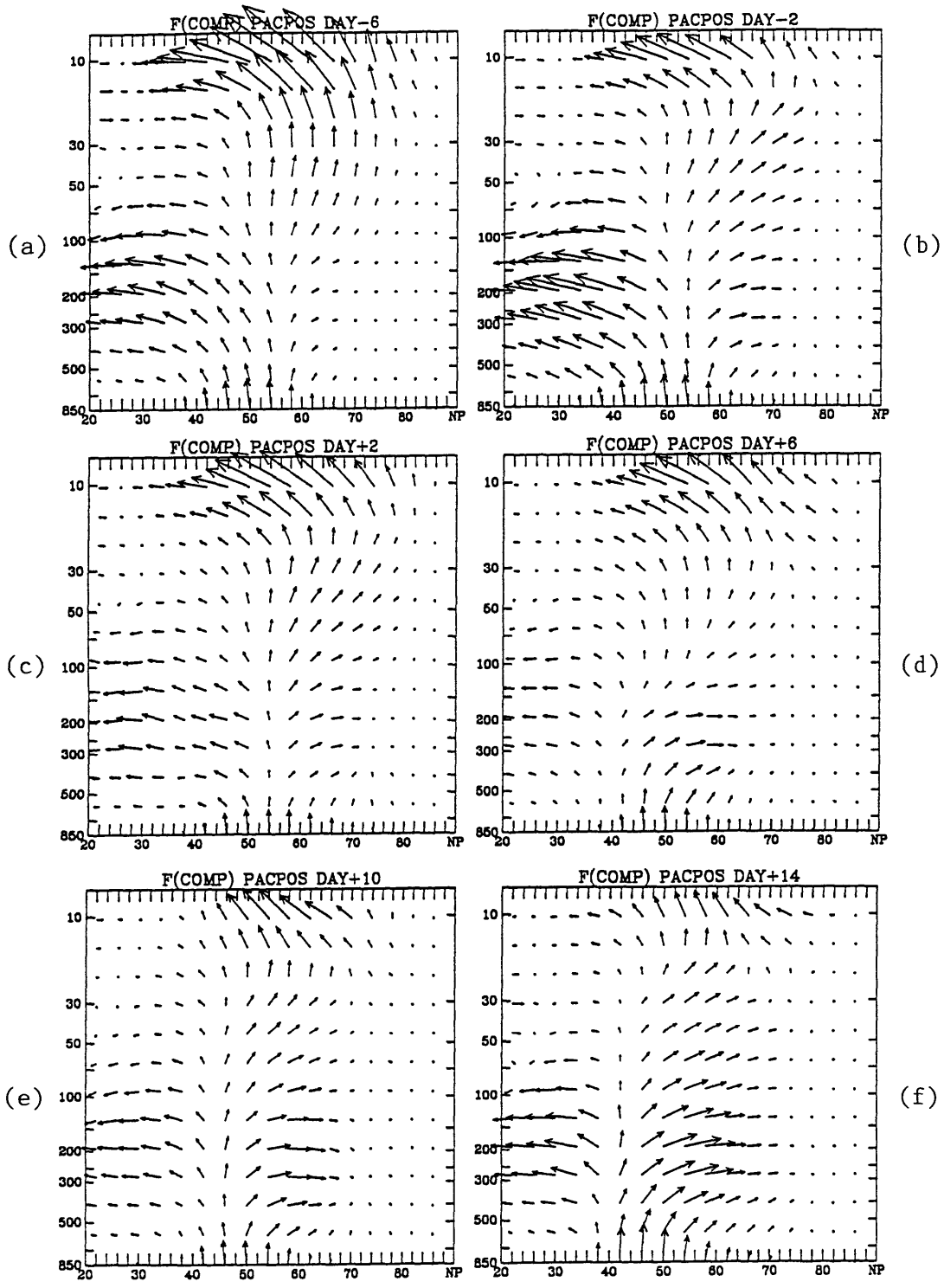

Fig. 4.6 Latitude-pressure cross sections of Eliassen-Palm flux (units: like m^2s^{-2}) for the PACPOS cases on days (a) -6, (b) -2, (c) +2, (d) +6, (e) +10, and (f) +14. Largest vector is 78 units with vectors scaled the same as in Fig. 4.5.

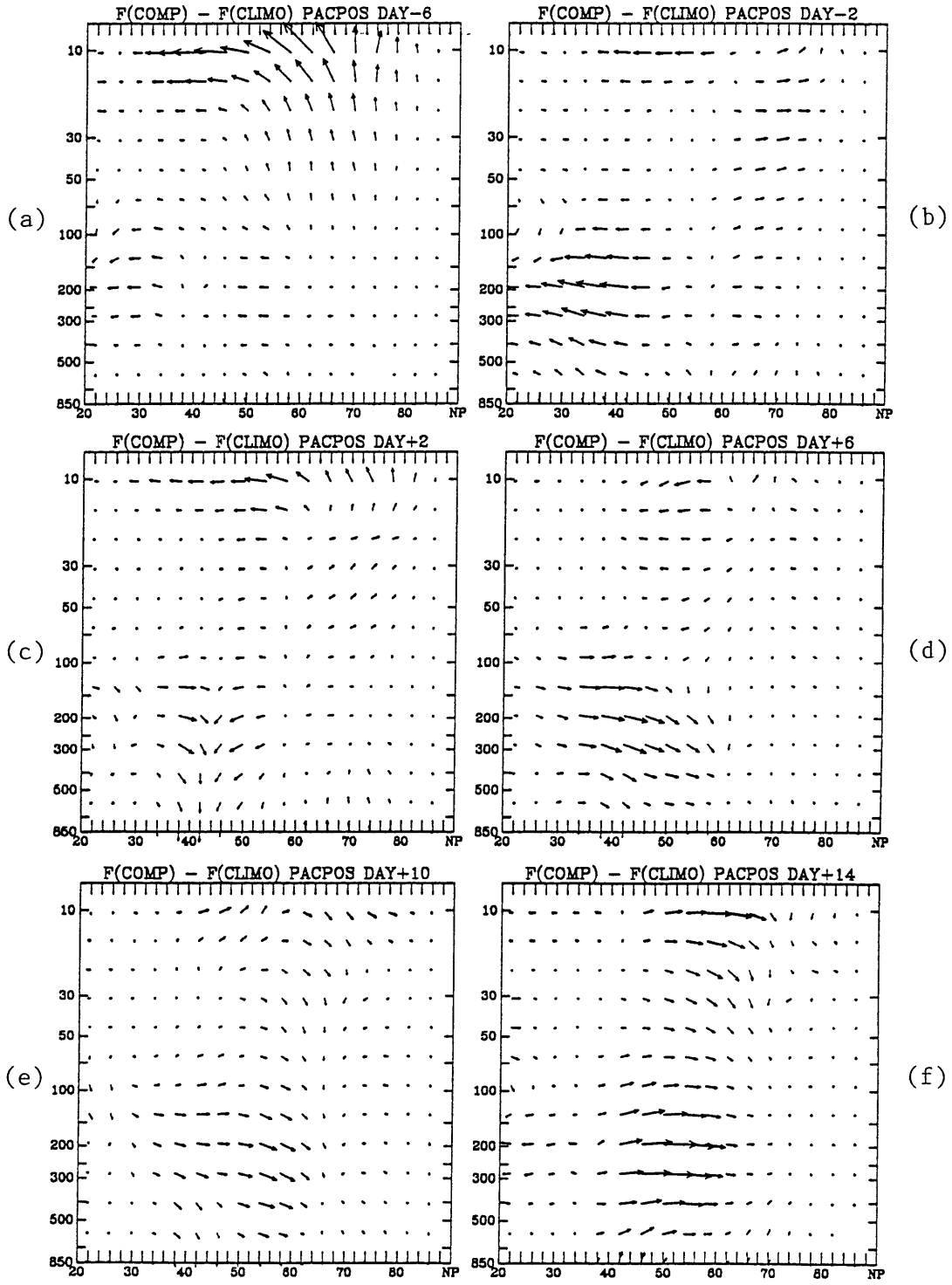

Fig. 4.7 Difference between the E-P flux of PACPOS cases (Fig. 4.6) and the E-P flux of climatology (Fig. 4.5) on days (a) -6, (b) -2, (c) +2, (d) +6, (e) +10, and (f) +14, with vectors scaled the same as in Fig. 4.5.

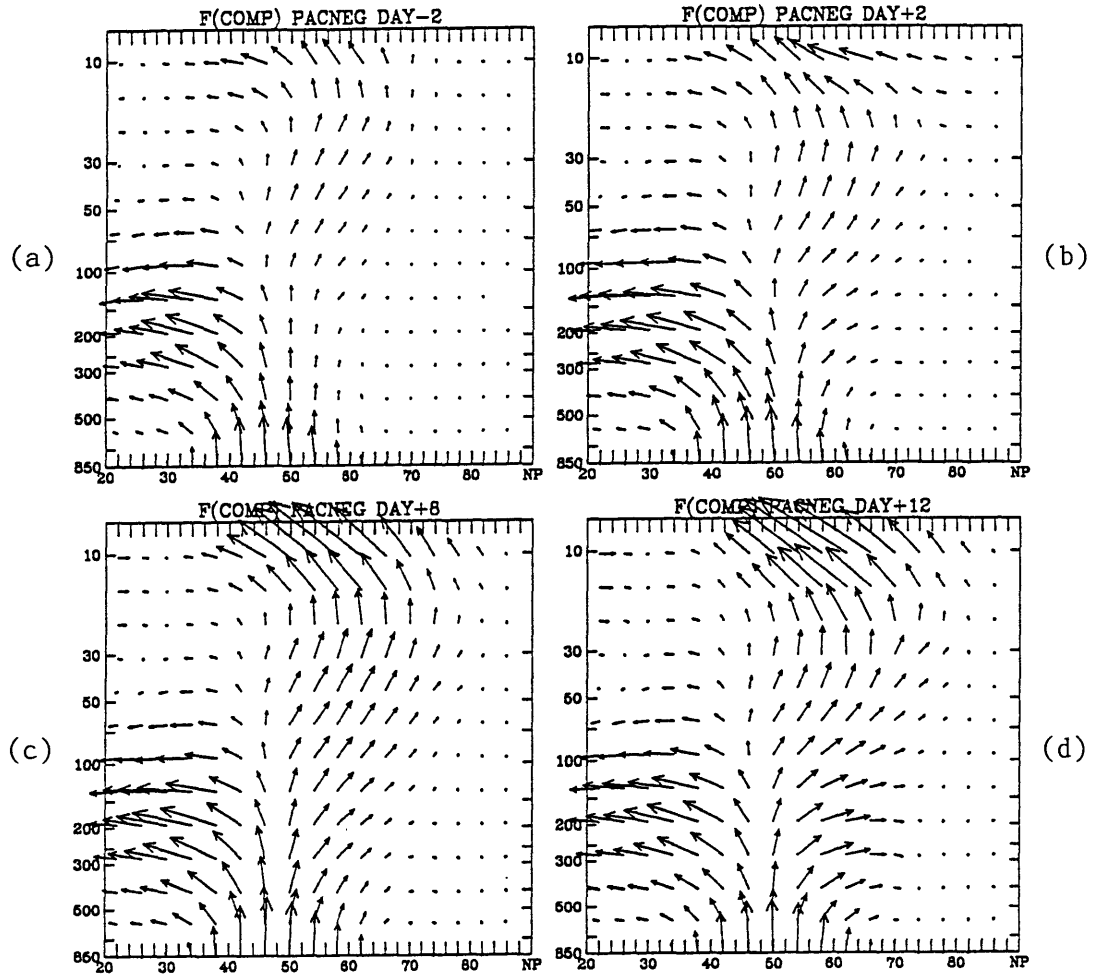

Fig. 4.8 As in Fig. 4.6 for the E-P flux calculated from the composite mean heights and temperatures for the PACNEG cases on days (a) -2, (b) +2, (c) +8, and (d) +12. Largest vector is 69 units.

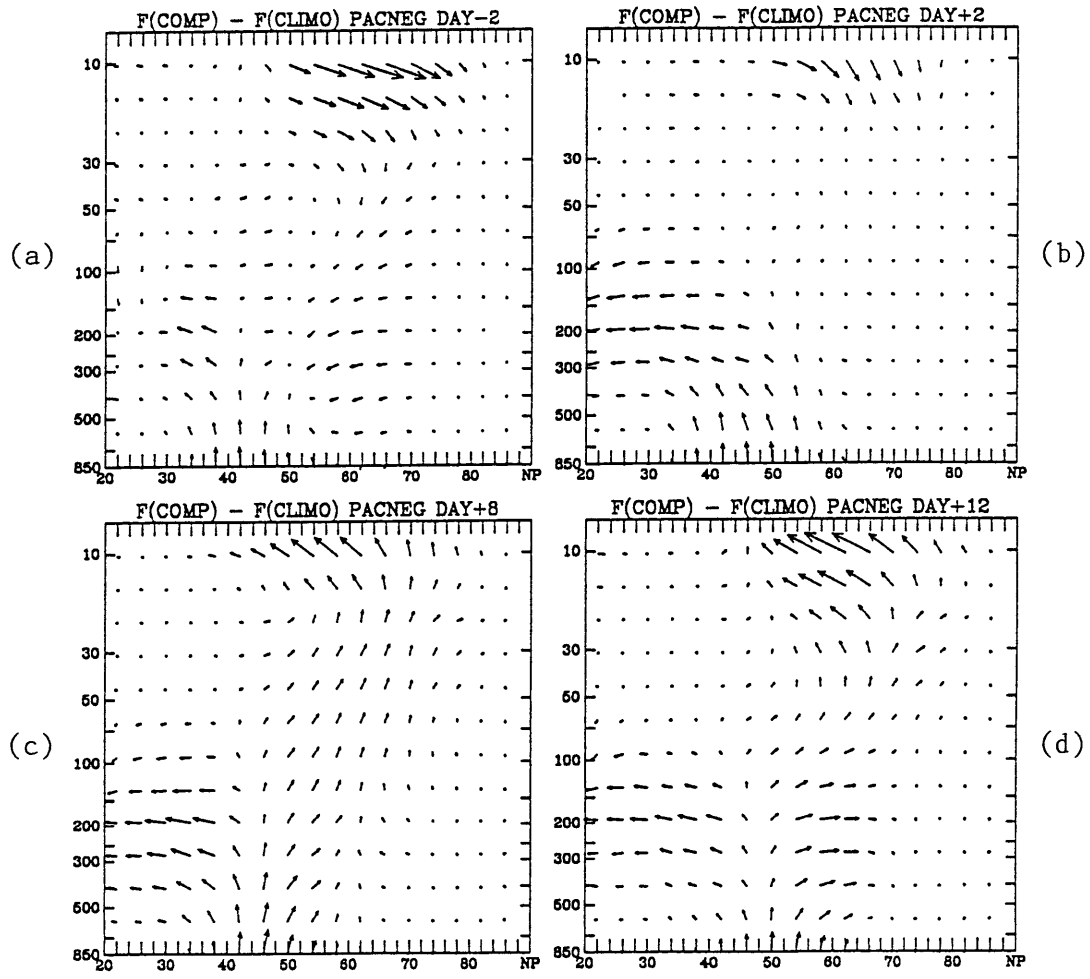

Fig. 4.9 As in Fig. 4.7 for the difference between the E-P flux of PACNEG cases (Fig. 4.8) and the E-P flux of climatology (Fig. 4.5), for days (a) -2, (b) +2, (c) +8, (d) +12. with vectors scaled the same as in Fig. 4.8.

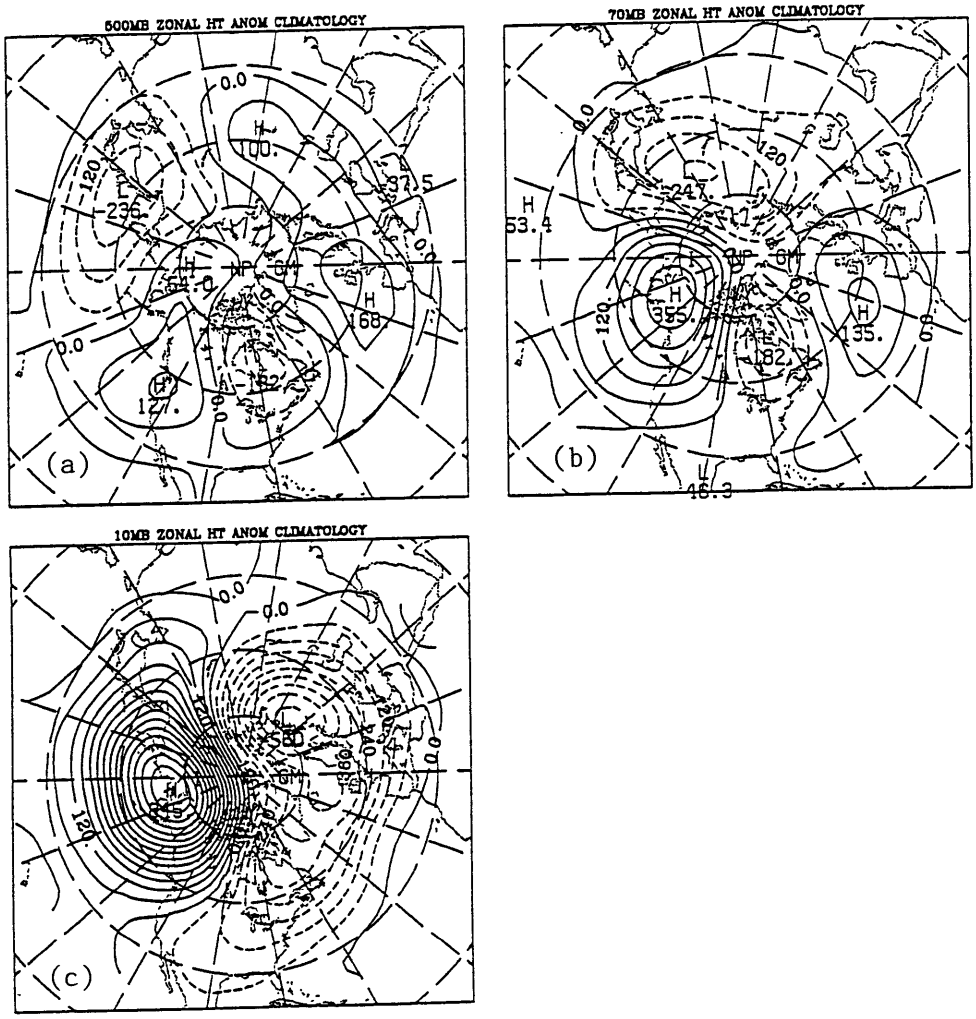

Fig. 4.10 Zonal height anomalies for the composite mean climatological geopotential heights during Pacific persistent anomaly cases at (a) 500 mb, (b) 70 mb, and (c) 10 mb. See text for explanation.

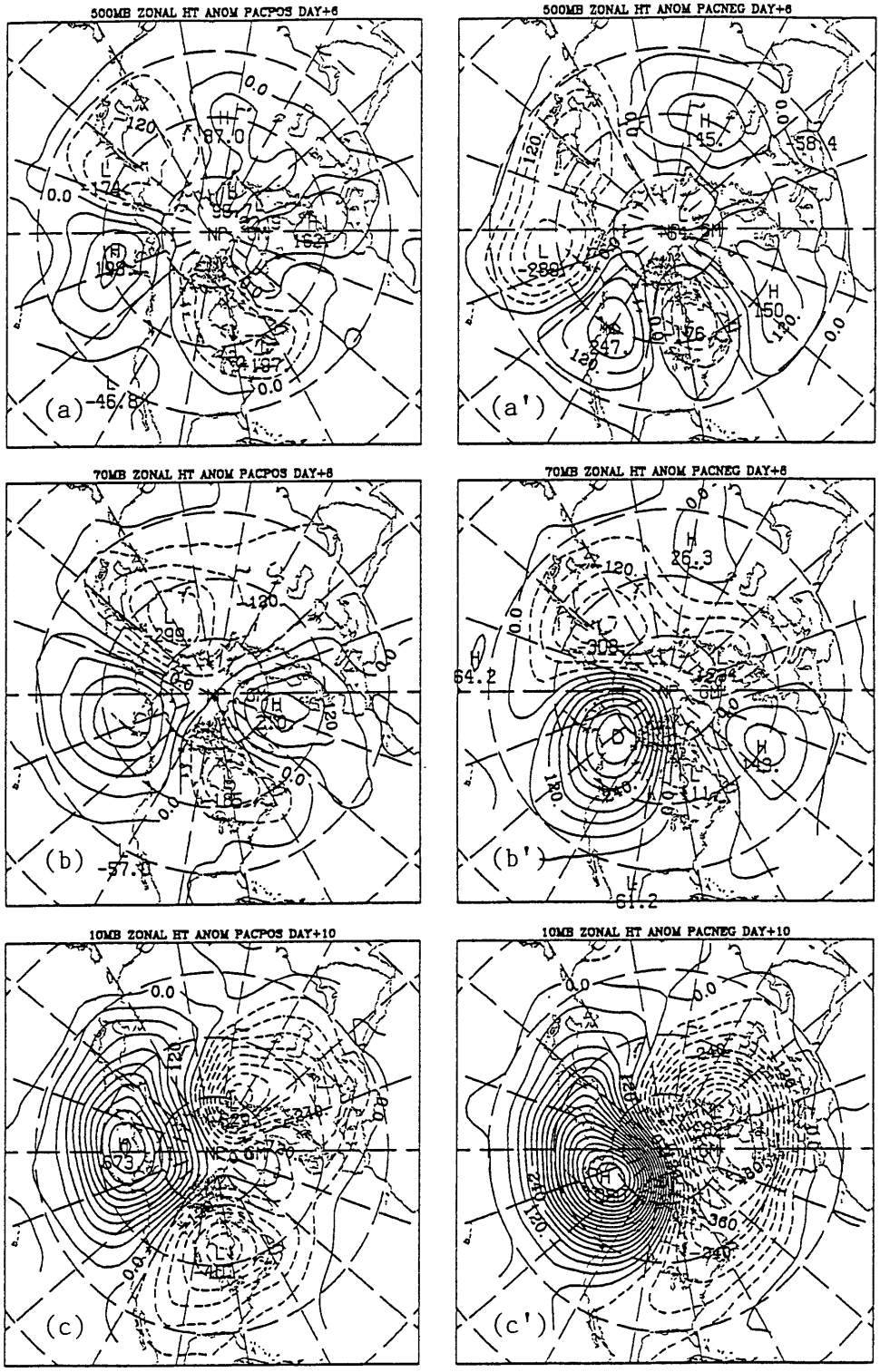

Fig. 4.11 As in Fig. 4.10 for the composite mean zonal height anomalies of the PACPOS cases for (a) 500 mb, day+6; (b) 70 mb, day+8; (c) 10 mb, day+10; and (a')-(c') as in (a)-(c) for the PACNEG cases.

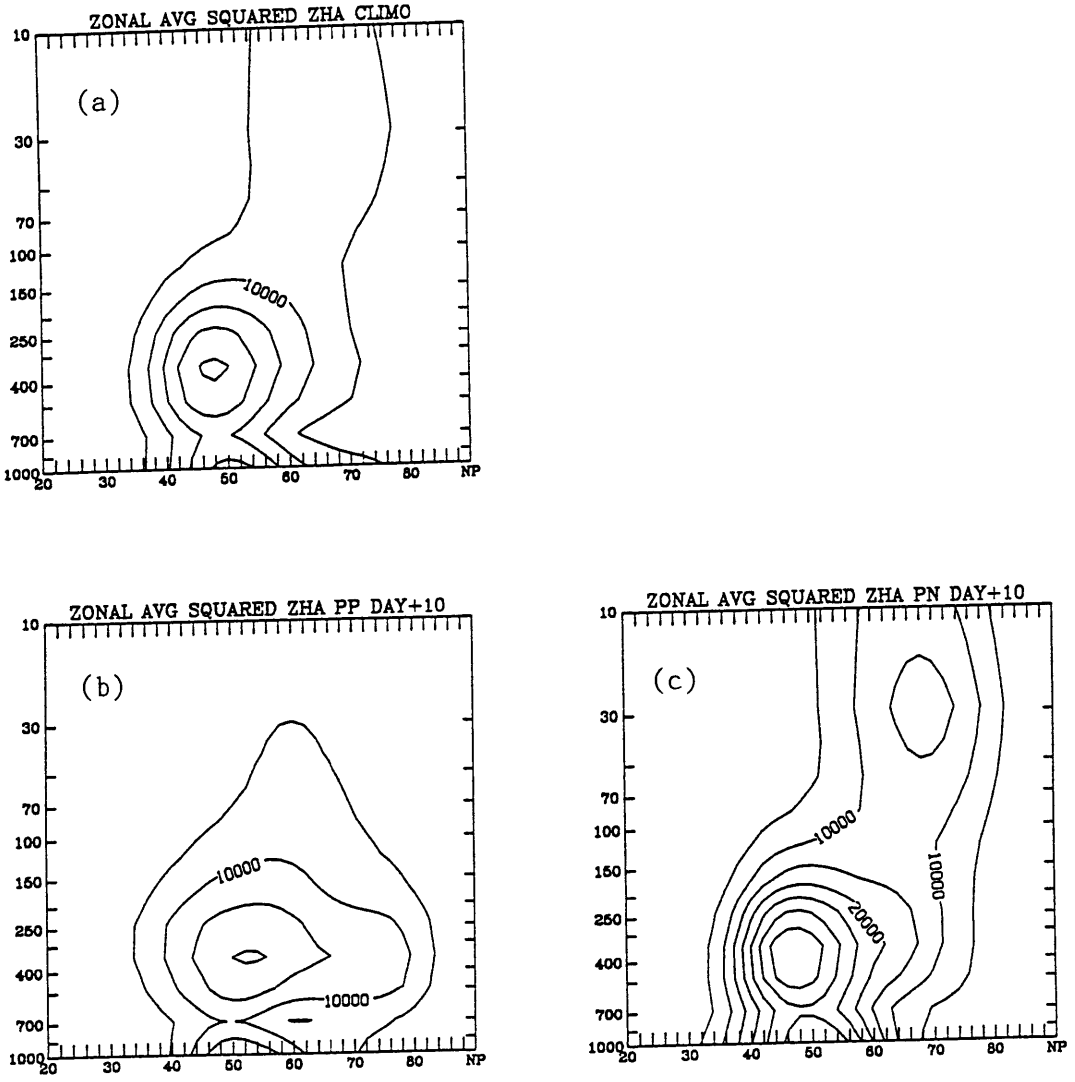

Fig. 4.12 Latitude-pressure (millibars) cross sections of the zonal average, around the latitude circle, of the square of the zonal height anomalies (as in Fig. 4.10) at all 14 levels of data for (a) climatology during Pacific persistent anomaly cases and day+10 of (b) PACPOS, (c) PACNEG, scaled by pressure to 300 mb. (Units: meters squared.)

CHAPTER 5

ASSOCIATION OF PERSISTENT ANOMALIES WITH MAJOR STRATOSPHERIC WARMINGS

5.1 Overview

Major stratospheric warmings occur on the order of once every couple of years in the Northern Hemisphere. A stratospheric warming is defined to be major if at 10 mb or lower, the zonal mean temperature increases from 60°N to the pole and there is an associated breakdown of the polar vortex with circulation reversal. During major warmings, then, there are net zonal easterlies in the vicinity of the pole. Labitzke (1981b) provides a summary of major warming events from 1967 through 1980. A similar summary is given in Labitzke (1982) with the 1980-1981 winter included.

During the period of this study, there were five known major stratospheric mid-winter warmings, four of which occurred during, or within two days of, a persistent anomaly event. The fifth occurred during an event at the new Pacific keypoint. Since persistent anomaly events are associated with waves of large scale, and, at least in PACNEG events, enhanced upward propagation of planetary wave activity, it is worthwhile to look at cases in which major warmings occurred.

For each case, a time series of the development of the major warming is shown at 500 mb and at least one stratospheric level. The 500 mb heights are plotted so that

changes in the 500 mb height field can be compared to the changes that are occurring in the stratosphere. Then, longitude-pressure cross sections of the height anomalies at 60°N are plotted on two selected days in order to show the vertical structure. In these cross sections, anomalies are scaled to the square root of pressure in order to more clearly show growth or decay with height. Finally, EP flux cross sections are shown for each day of the time series to further examine evidence of wave propagation. Our purpose in this section is to show the general direction of EP flux vectors and to review the major warming events. More thorough studies of sudden stratospheric warmings are found in the references for this section.

5.2 ATLPOS Case 1

The first of these major warmings occurred around 2 February 1973, day +10 of ATLPOS case 1. Quiroz (1975) studied the thermal properties of the warming from satellite infrared data, and the energetics of this event are discussed by Crane (1979). Crane finds that the maximum rate of warming is first found in the upper stratosphere and then descends to lower levels. However, there also is strong energy flux through the 50 mb level at the same time that the upper stratosphere is warming quickly.

Our analyses show that circulation reversal occurs at 10 mb, but not in the lower stratosphere. 10 mb and 70 mb heights are shown in Fig. 5.1 for this event, and 500 mb heights are shown in Fig. 5.2. In addition, longitude-pressure cross sections of height anomalies are displayed for days +8 and +12 in Fig. 5.3. On day +6, the ATLPOS pattern is visible in the 70 mb (Fig. 5.1a') and 500 mb (Fig. 5.2a) height fields. There is a large scale ridge over the Atlantic, and another is found over the west coast of North America. Between them, over eastern North America, there is a trough. Two days later

(Fig. 5.1b, b'), the trough is also seen at 10 mb as the Pacific ridge at that level builds. Then, the 10 mb Pacific ridge suddenly builds northward (Fig. 5.1c), appearing to be the primary factor causing the warming event. Longitude-pressure cross sections (Fig. 5.3) reveal that this ridge is the same as the one at 70 mb. The ridge at 70 mb undergoes sudden intensification on day +12 (Fig. 5.1d') in response to a new pattern that is developing over the Pacific. This pattern is most easily visible at 500 mb (Fig. 5.2c,d) in the form of a developing trough in the western Pacific and an amplifying ridge downstream over the Gulf of Alaska. Throughout the time series, the large scale ridge over the eastern Atlantic remains more or less intact as synoptic-scale troughs pass through it.

The longitude-pressure cross sections, in combination with the 10 mb height fields suggest that this warming is associated with two anomalous large scale ridges: the larger than normal climatological ridge over the Pacific and the anomalous ridge over the eastern Atlantic. On day +8 (Fig. 5.3a), the ridge over the Pacific shows up as a positive anomaly located between 90°W and 120°W, and the keypoint ATLPOS anomaly appears at 30°W and is the largest in magnitude of any anomaly in the cross-section, suggesting it plays a significant role in triggering the warming, even though the height fields (Fig. 5.1) show that the Pacific ridge is larger. The Pacific ridge does not appear larger in the longitude-pressure cross sections of the anomalies because it is generally a climatological feature, so its presence is not really anomalous.

A couple of other points may be worth noting. First, over 170°W, the anomalies are negative, indicating that the pattern over the Pacific and North America is like one in a PACNEG case, although the anomalies do not satisfy the criteria for a PACNEG case at this time. Secondly in these cross sections, it appears that the same wavenumbers dominating the troposphere are much smaller than the ones dominating the stratosphere. Thus, much of the wave activity that originates in the troposphere is trapped, as should

be expected.

EP flux vectors are plotted in Fig. 5.4 for the same days shown in the case height fields. On day +6 (Fig. 5.4a), some enhanced upward propagation of wave activity is occurring, but the refraction is equatorward overall. By day +8 (Fig. 5.4b), the vectors point more or less vertically, and although there is no major poleward refraction of wave activity, this vector pattern is still anomalous, with convergence of EP flux in the polar stratosphere at this time, decelerating the westerlies. Day +10 (Fig. 5.4c) shows the vectors turning back to the equator with convergence in the subtropical stratosphere. On day +12 (Fig. 5.4d), wave activity is refracted towards 30°N, where there is strong convergence of EP flux.

5.3 PACNEG Case 5

During January 1977, a major stratospheric warming occurred after about a week into a PACNEG event. The corresponding circulation reversal at 70 mb took place between 5 January and 9 January, and the vortex was split into three pieces. Over the pole there was an amazingly strong anticyclone, which eventually extended down to the surface and up to at least 10 mb. Since this is one of the most dramatic warming events known, it has been the subject of several studies. Quiroz (1977), Taylor and Perry (1977), Labitzke et al. (1977), and Houghton (1978) performed the earliest analyses on this event.

A more rigorous study came from O'Neill and Taylor (1979). This warming was actually the third of three warmings, of which the first two occurred in late November and December 1976. They identify the large Atlantic blocking ridge that is found on 24 December, which plays a major role in the second of the three warmings. This second

warming was nearly a major warming, but just before circulation reversal was about to take place, wave activity suddenly diminished. Another large Atlantic blocking ridge became established by 7 January. This ridge, in cooperation with a deep east Asian trough, formed a wavenumber 1. The Atlantic ridge eventually moved northward and covered the pole. O'Neill and Taylor also argue that southward momentum transport by planetary waves is a crucial aspect of this warming. In a later paper, O'Neill and Youngblut (1982), rather than using the traditional momentum transport ideas, stress the convergence of EP flux. They also introduce a quantity Q (refractive index) which helps to show the direction in which the waves are likely to propagate.

Our analysis of 70 mb heights shows the Atlantic ridge, but there is also a strong ridge that builds over the northeast Pacific and northwestern North America as a secondary PACNEG anomaly. Shown in Fig. 5.5 is the 70 mb time evolution from day +2 to day +12, accompanied by the 500 mb geopotential heights for the same times. The 70 mb level was chosen for display because of its relative proximity to the tropopause and also because the most dramatic high-latitude circulation reversal takes place there. The 10 mb heights were omitted because the event is not as dramatic there. The anticyclone decays upward and is much a smaller feature there. On day +2 (Fig. 5.5a), the vortex looks smaller than normal due to its decrease during recent days by the strong wave activity of the second warming which, incidentally, occurred during PACNEG case 4. At this time, the vortex is reforming after nearly being split into two pieces. Then (Fig. 5.5b-c,b'-c'), a sharp ridge builds just off the west coast of North America. This ridge then amplifies rapidly and cuts off by day +10 (Fig. 5.5e). On day +12 (Fig. 5.5f), the vortex is split into three pieces, with an anticyclone centered over the pole in a strong major warming event.

The 500 mb heights (Fig. 5.5a'-f') over this time period are very similar to the 70 mb heights. The ridge over the west coast of North America builds as the broad,

PACNEG trough digs in to its west. Also noticeable are the strong trough over interior North America (a secondary PACNEG anomaly) and ridge over the central and eastern Atlantic.

Longitude-pressure cross sections are displayed in Fig. 5.6. There is a large discrepancy between the troposphere and the stratosphere regarding the scale of ridges and troughs. As is usually the case, smaller scales are dominant in the troposphere. In other major warming cases, which we will look at briefly, both the troposphere and the stratosphere are dominated by wave 2. Day +4 at 60°N (Fig. 5.6a) shows a strong trough over the keypoint and a ridge to the east. By day +8 (Fig. 5.6b), a ridge/trough/ridge series is to the east of the keypoint latitude. Note how strong the Atlantic ridge near 45°W is, as in O'Neill and Taylor (1979). This is the strongest anomaly in the cross section, but one must remember again that the ridge over the west coast of North America is a climatological feature and is actually much larger than it appears on the longitude-pressure cross section.

EP flux vectors, plotted in Fig. 5.7, show the dramatic changes in wave activity flux that are responsible for this warming. On day +2 (Fig. 5.7a), the upper stratosphere shows large amounts of northward momentum flux south of 55°N. (The EP flux vectors point in the opposite direction of the momentum flux.) There is also large upward EP flux north of this latitude from the previous PACNEG/warming event. The lower stratosphere is beginning to show some signs of poleward refraction from 55°N to 80°N. In the troposphere, strong upward EP flux from 35°N to 55°N is refracted equatorward. On day +4 (Fig. 5.7b), equatorward refraction of the wave activity coming out of the lower troposphere continues, but the direction of propagation in the stratosphere has changed dramatically. There is now strong flux directed towards the pole, as discussed by O'Neill and Youngblut (1982). Such poleward-directed vectors converge strongly, so there is a dramatic deceleration of the westerlies in high latitudes at this time. The

poleward-pointing vectors show the southward transport of momentum, in agreement with the ideas of O'Neill and Taylor. By day +6 (Fig. 5.7c), the equatorward refraction in the troposphere has all but completely stopped, and wave activity is now concentrated almost completely into high latitudes, where there is convergence of the vectors at all levels. On following days (Fig. 5.7e-f), the vectors converge more in the troposphere and the activity in the stratosphere diminishes because the easterlies prevent upward propagation. Wave activity is now concentrated into the polar troposphere, where it is trapped by the easterlies above. The deceleration is now greatest in this area as the circulation reversal works its way downward.

The 500 mb and 70 mb height analyses also show that the developing PACNEG pattern is supplying much of the southward momentum flux and poleward heat flux that are important aspects of major warmings. This is especially obvious on days +4 and +6 (Figs. 5.5b-c,b'-c') as the PACNEG trough digs in and the ridge rapidly builds to its east. Note how strong the southerly 500 mb and 70 mb winds are over the Aleutian Islands. The anomaly patterns associated with the PACNEG 5 case, therefore, appear to have an important role in this warming.

5.4 PACPOS Case 3

In February 1979, a major stratospheric warming occurred that split the vortex into two nearly equal halves. The zonal mean u wind became easterly by 21 February (day +18 of PACPOS case 3). This case is the subject of many studies on the subject of stratospheric warmings. In the first of these studies, Quiroz (1979) looks at the interaction between the troposphere and the stratosphere during the warming by analyzing waves 1 and 2. Palmer (1981a,1981b) uses EP fluxes and EP flux convergence to

diagnose certain aspects of the warming. The concept of wave focusing is discussed in McIntyre (1982). Dunkerton and Delisi (1986) perform a diagnosis of this event using potential vorticity, and Labitzke (1981a) studies the importance of zonal wave 1 in preconditioning the stratosphere for the warming

The 70 mb and 500 mb heights are shown for this case in Fig. 5.8. The 10 mb height field undergoes similar changes to those at 70 mb and therefore is not shown. On day +14 (Fig. 5.8a), 70 mb heights look fairly normal for a PACPOS event, appearing very similar to day +10 of the composite of PACPOS cases (Fig. 3.1e) shown earlier. There is a ridge over the central Pacific and a trough over western North America and the eastern Pacific. The vortex is very elongated and has two centers. On day +16 (Fig. 5.8b), enhanced ridging is observed over the central Pacific and the central Atlantic, and it increases on day +17 (Fig. 5.8c), in agreement with the analysis of this warming by Quiroz (1979). By day +18 (Fig. 5.8d), the pattern has developed to the point that the vortex appears to be pinched into two nearly completely separate parts.

The corresponding 500 mb heights (Fig. 5.8a'-d') show the strengthening of the ridge over the extreme north central Pacific at the same time as the major warming occurs. Also by day +18 (Fig 5.8d'), a pair of strong troughs is present over the western Pacific and east coast of Asia. On following days, these troughs build eastward, becoming zonally elongated over the Pacific, while the ridge cuts off and drifts poleward. A strong ridge over the central Atlantic also appears prominantly during the development. The Atlantic and Pacific ridges together form a visible wave 2 pattern in higher latitudes as in Quiroz (1979).

Longitude-pressure cross sections are shown in Fig. 5.9 for days+17 and +18 at 60°N. The Atlantic ridge is a stronger anomaly than the Pacific ridge (Fig. 5.9a), but this difference in strength gradually disappears (Fig. 5.9b). The most remarkable feature of these cross sections is that the troposphere and the stratosphere are completely in phase.

Both are overwhelmingly dominated by a wavenumber two. There is also a slight westward tilt with height. Such a pattern is indicative of strong upward propagation.

Indeed, EP flux cross sections, plotted in Fig. 5.10, show the enhanced upward flux of wave activity into the polar stratosphere. The cross sections on days +14, +16, and +18 are on the same days as the first three cross sections in Palmer (1981a), and agree with his analyses. On day +14 (Fig. 5.10a), there is a small amount of flux refracted poleward in the troposphere, but the vectors then turn back equatorward by 50 mb. On day +16 (Fig. 5.10b), the flux at 30-50 mb is more vertical and is turning northward. Note that there is some convergence of the vectors near the pole in the stratosphere, although the magnitude of the vectors is hard to judge since vectors are not properly scaled. By day +17 (Fig. 5.10c), wave activity is strongly focused into the pole, in agreement with the ideas presented in McIntyre (1982). Convergence of the EP fluxes is very strong here, producing strong deceleration just at the time the polar vortex is most rapidly breaking down. The vectors then turn slightly equatorward by day +18 (Fig. 5.10d), when the circulation reversal is well established, preventing upward propagation into the regions where winds are easterly.

Thus, even though there is another strong anomaly involved in this warming, namely the ridge over the Atlantic, the PACPOS pattern indeed plays a large role because of its large scale wave contribution to the pattern. Such a statement contradicts the idea put forward in the previous chapter that PACPOS cases are associated with weaker than normal upward wave activity flux. However, during previous days of this PACPOS case, the EP flux actually *is* weak between 200 mb and 50 mb. The enhanced wave activity occurs just a few days before the warming.

5.5 PACPOS Case 6 and PACNEG Case 11

In December 1984, a major warming occured in the two days between a PACPOS event and a PACNEG event. By December 28, zonal mean winds at 70 mb north of 70°N were easterly. This is the earliest in the season such a major warming has ocurred, so it is a particularly dramatic example. Preliminary analyses of this event were done by Labitzke et al. (1985a, 1985b). Later, Randall and Boville (1987) looked at other diagnostics, such as zonal mean wind, EP flux, root mean square heights (around latitude circles), and a refractive index, Q.

70 mb and 500 mb heights are plotted in Fig. 5.11 on days +12 (25 December) and +14 of PACPOS case 6 and days -1.5 and -2.5 of PACNEG case 11. Day -1.5 of PACNEG case 11 is one day after day +14 of PACPOS case 6. By inspection, one can see throughout the period the amazing similarity in the large scale pattern between the two levels.

A deep vortex lies over Canada both at 500 mb and 70 mb. The PACPOS ridge is firmly in place at both 70 mb (Fig. 5.11a) and 500 mb (Fig. 5.11a') on day +12. At the same time, a strong trough, which will soon develop into the PACNEG case, is developing off the Asian east coast at 500 mb. Two days later, the trough has moved eastward, and the ridge is building ahead of it at both 70 mb (Fig. 5.11b) and 500 mb (Fig. 5.11b'). The trough continues to build eastward, intensifying and building the 500 mb ridge to the point that it cuts off to form an anticyclone (Fig. 5.11d'). In the meantime, another strong ridge has developed at 20°E-20°W, and at 70 mb, the circulation reversal near the pole has occurred by day -1.5 of PACNEG case 11 (Fig. 5.11d). The large scale troughs centered over eastern North America and eastern Asia, in connection with the aforementioned ridges, form a dominant wave 2 pattern that is strongly upward-propagating.

Longitude-pressure cross-sections for PACPOS case 6 on day +12 (Fig. 5.12a) and for PACNEG case 11 on day -1.5 (Fig. 5.12b) show why this pattern is associated with upward-propagating waves. The cross sections are almost identical to those presented for the PACPOS 3 warming. The dominant wave 2 permeates all levels of the atmosphere up to 10 mb, and there is a slight westward tilt to the waves. Again, instead of the PAC primary or secondary anomaly, the strongest anomaly at the time of the warming is on the opposite side of the Northern Hemisphere. This time, the strong ridge is found farther east over western Europe.

EP flux cross sections are shown in Fig. 5.13. As is typical for the PACPOS cases, the upward flux during the first ten days of this PACPOS case (not shown) is relatively weak but then increases. On day +12 (Fig. 5.13a), the normal equatorward refraction near 200 mb is visible. Between 30 mb and 50 mb, the vectors are beginning to increase and turn poleward. On PACPOS 6 day +14 (Fig. 5.13b) and PACNEG 11 day -2.5 (Fig. 5.13c), wave activity is directed right into the polar region. At this time, strong deceleration of the westerlies is occurring. The strong flux into polar latitudes continues on day -1.5 (Fig. 5.13d). If the vectors were scaled the same among all the cases in this chapter, this case would have the largest vectors.

This case is similar to PACPOS 3. A ridge is present over the Atlantic and Pacific during both cases. Also similar are the trough in the western Pacific during PACPOS 3 and the trough over the same area that develops into a PACNEG pattern in this case, building the ridge over the central Pacific and causing it to cut off as it drifts northward.

5.6 SUMMARY

The common feature in each of these events is a strong positive anomaly over the

Atlantic or western Europe concurrently with a ridge over the north central or northeast Pacific. In each case, the strongest anomaly at the time of the warming was over the Atlantic or western Europe.The fact that in all these warmings there were major positive height anomalies over both the Atlantic and Pacific is interesting. It appears that this may be the difference between lesser warmings, in which the vortex is simply "pushed" off the pole and distorted, and the major warmings, in which the vortex breaks down. The appearance of the wave 2 pattern may help to focus wave activity into the pole from both sides. Further analysis using wave propagation diagnostics in Plumb (1985) may provide more detailed clues as to the role of the persistent anomaly patterns in these warmings.

There were two PACNEG events in this section of case studies, but there were just as many PACPOS events that were associated with major warmings. This is somewhat inconsistent with the thinking that PACPOS events are associated with weak upward wave activity flux. The fact that the warmings occurred at the end of PACPOS cases, as a trough deepened in the western Pacific, somewhat weakens this apparent contradiction.

In any case, it is evident that persistent anomalies are often associated with enhanced upward propagation of planetary wave activity and hence, may be related to major stratospheric warmings. It appears that certain conditions in the stratosphere are necessary for the focusing of wave activity into the polar region (O'Neill and Youngblut, 1982) while persistent anomaly events are associated with anomalously strong large scale wave activity that can propagate into the stratosphere.

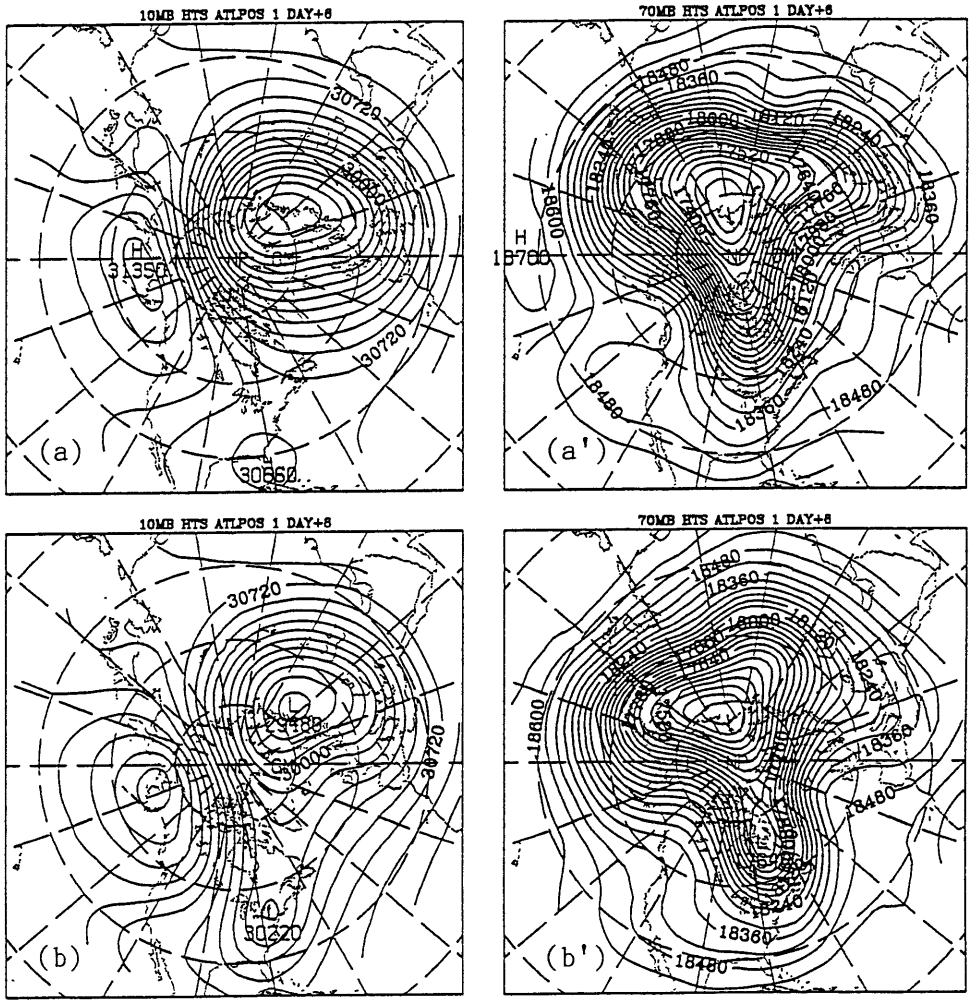

Fig. 5.1 10 mb geopotential heights (in meters) during ATLPOS case 1 on days (a) +6, (b) +8, (c) +10, (d) +12, and (a')-(d') as in (a)-(d) for 70 mb geopotential heights.

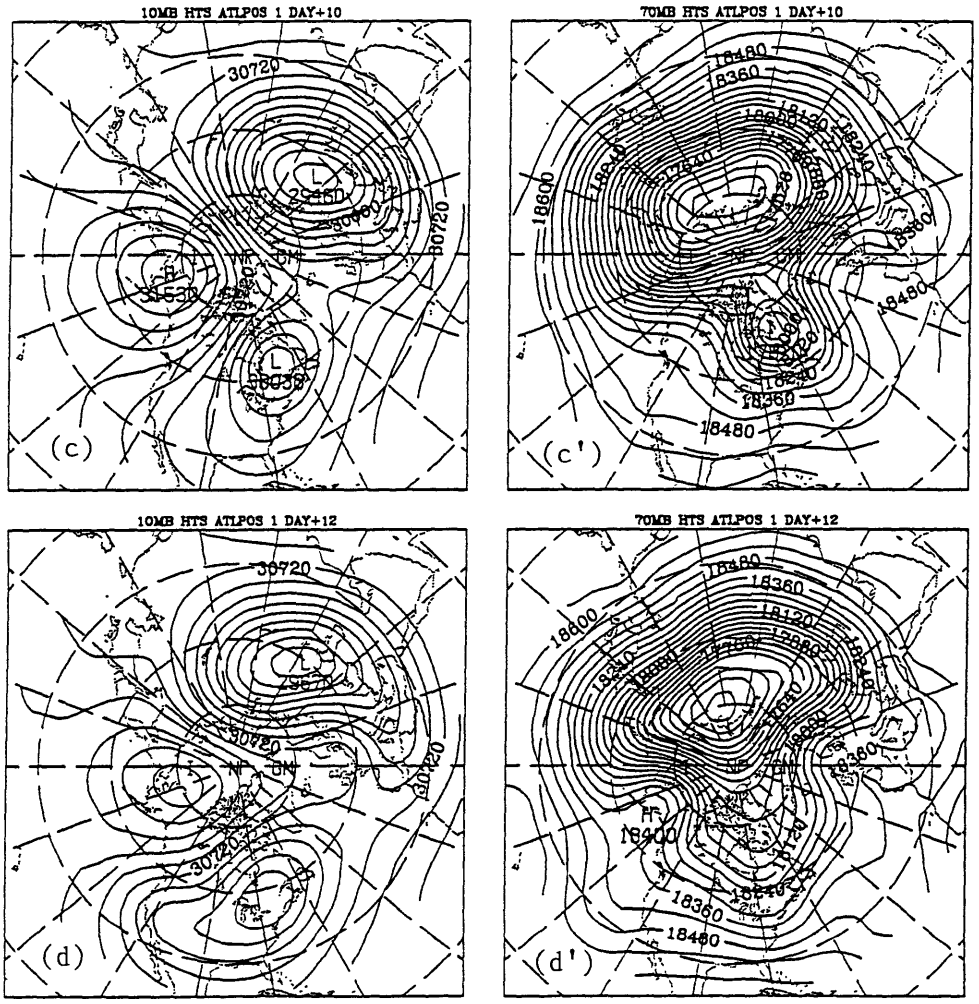

Fig. 5.1 (*Continued*)

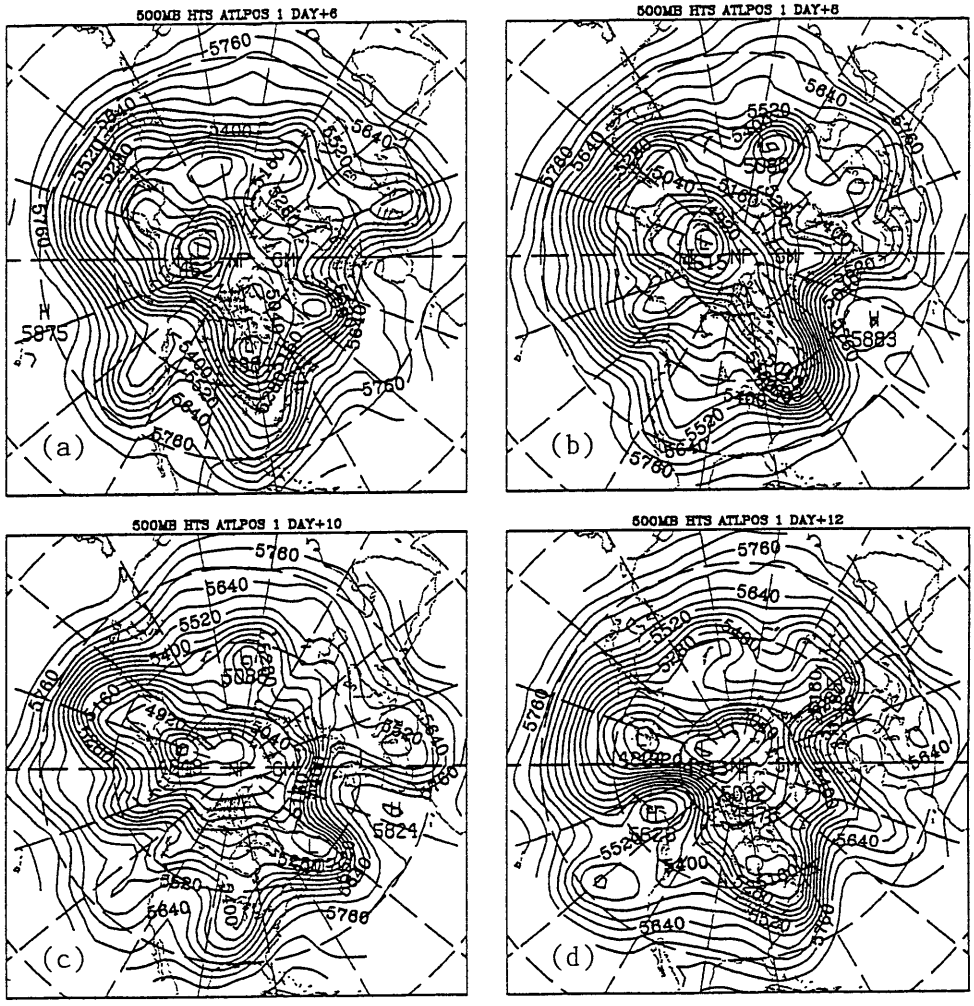

Fig. 5.2 500 mb geopotential heights (in meters) during ATLPOS case 1 on days (a) +6, (b) +8, (c) +10, and (d) +12.

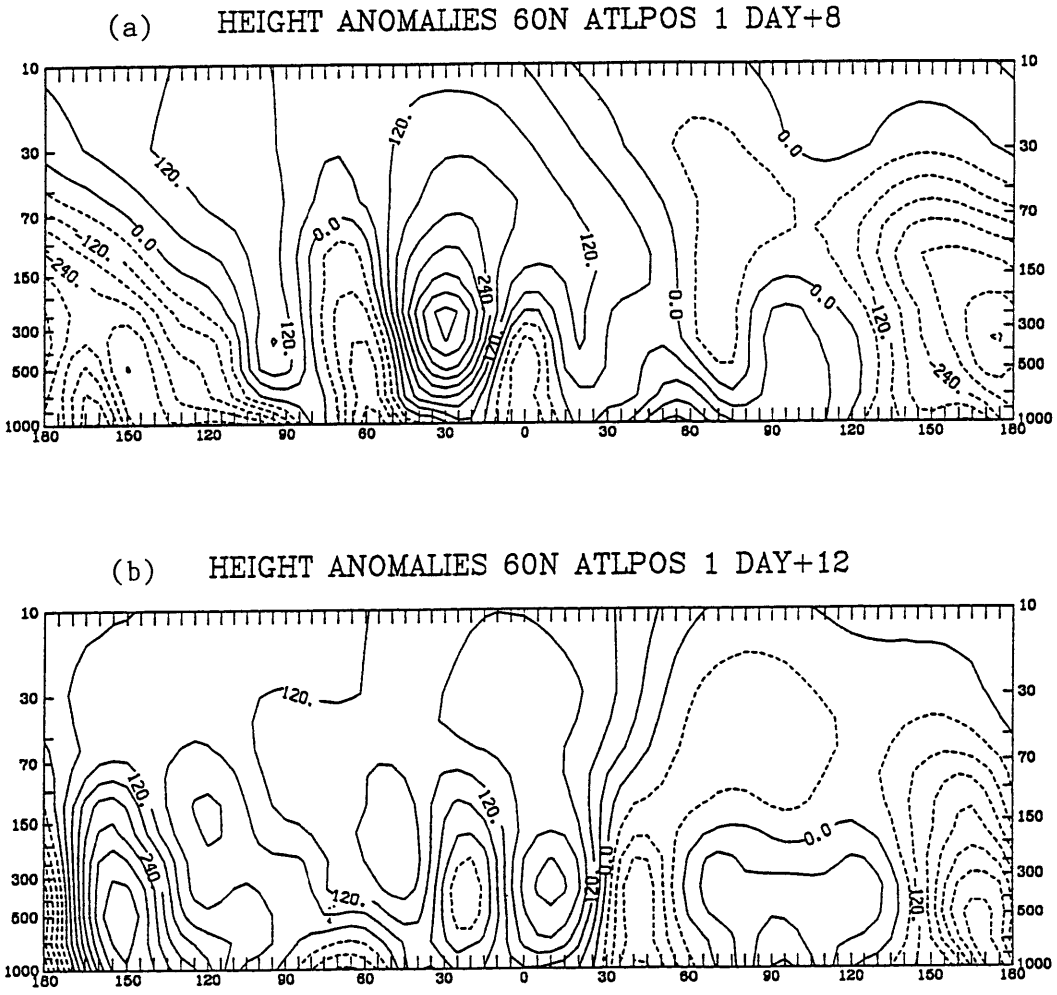

Fig. 5.3 Longitude-pressure (millibars) cross sections of height anomalies during ATLPOS case 1 at 60°N on days (a) +8 and (b) +12, scaled by the square root of pressure to 300 mb.

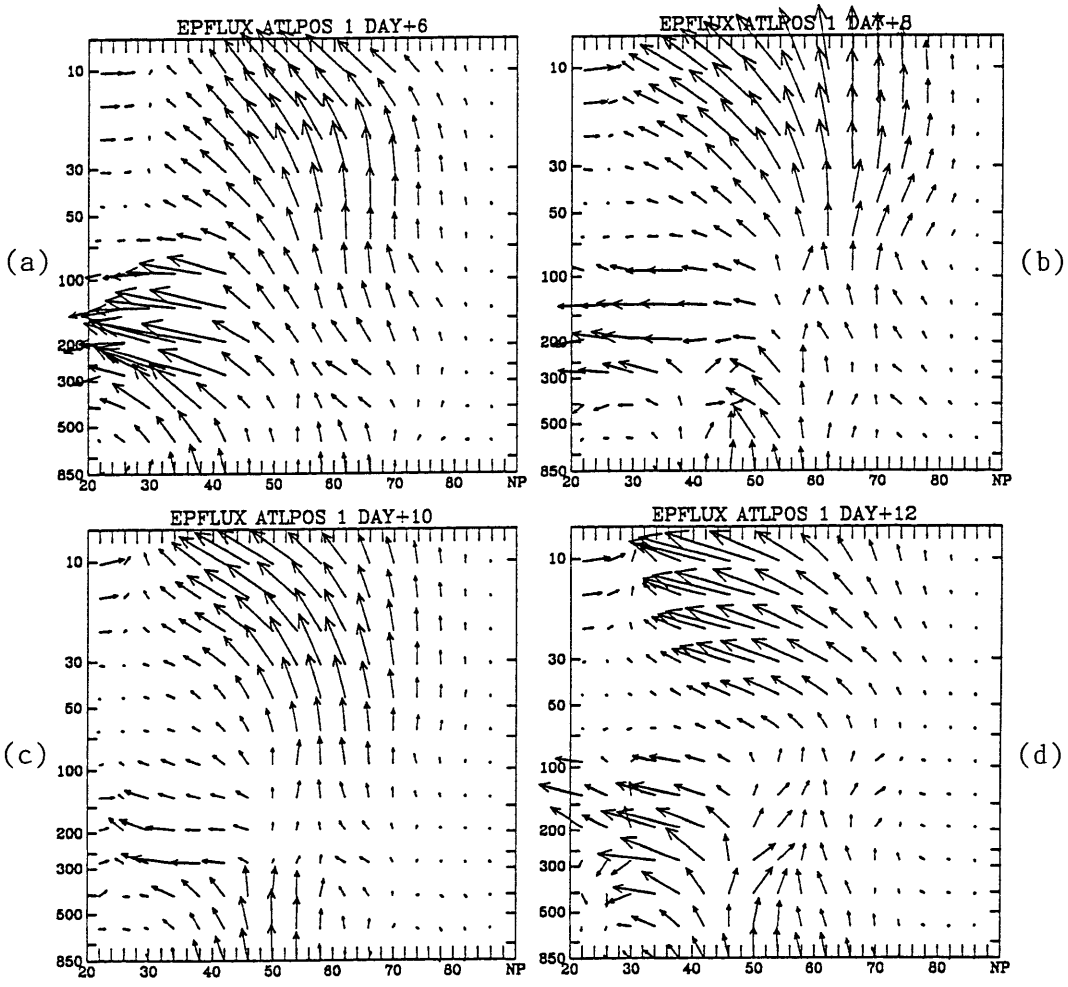

Fig. 5.4 As in Fig. 4.5 for Eliassen-Palm flux during ATLPOS case 1 on days (a) +6, (b) +8, (c) +10, and (d) +12. The largest vector is 140 units.

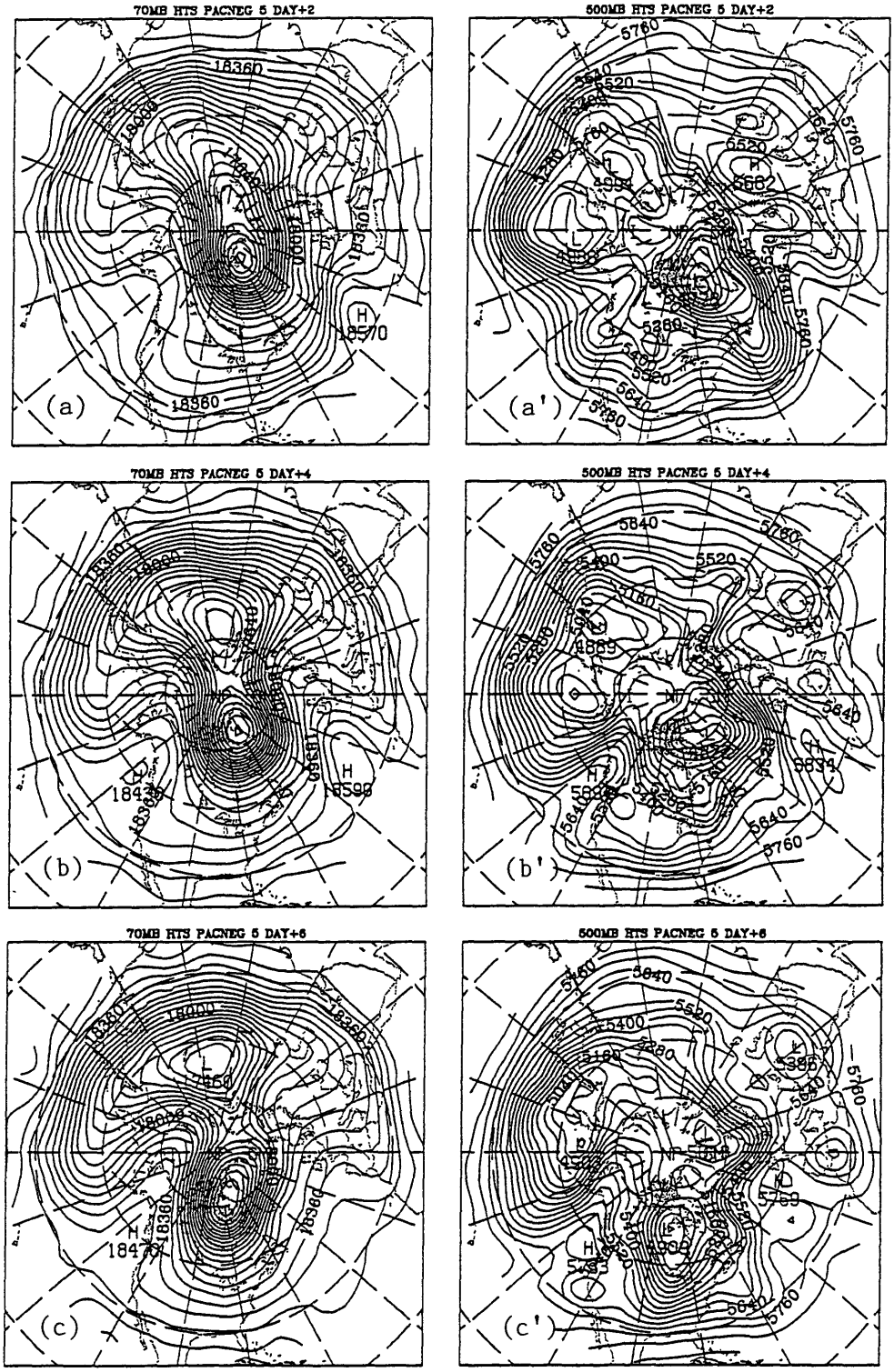

Fig. 5.5 70 mb geopotential heights (in meters) during PACNEG case 5 on days (a) +2, (b) +4, (c) +6, (d) +8, (e) +10, (f) +12, and (a')-(f') as in (a)-(f) for 500 mb geopotential heights.

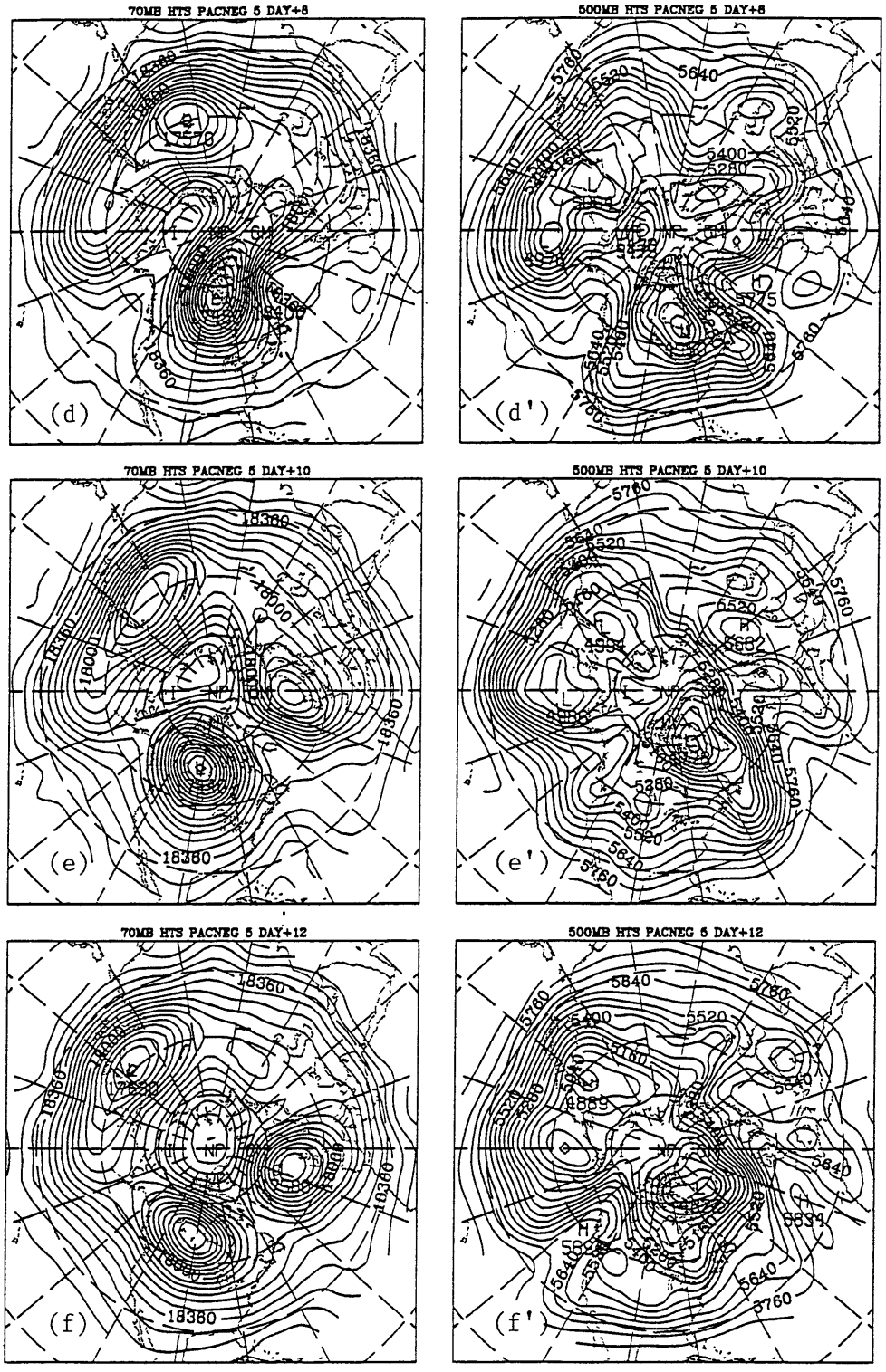

Fig. 5.5 (*Continued*)

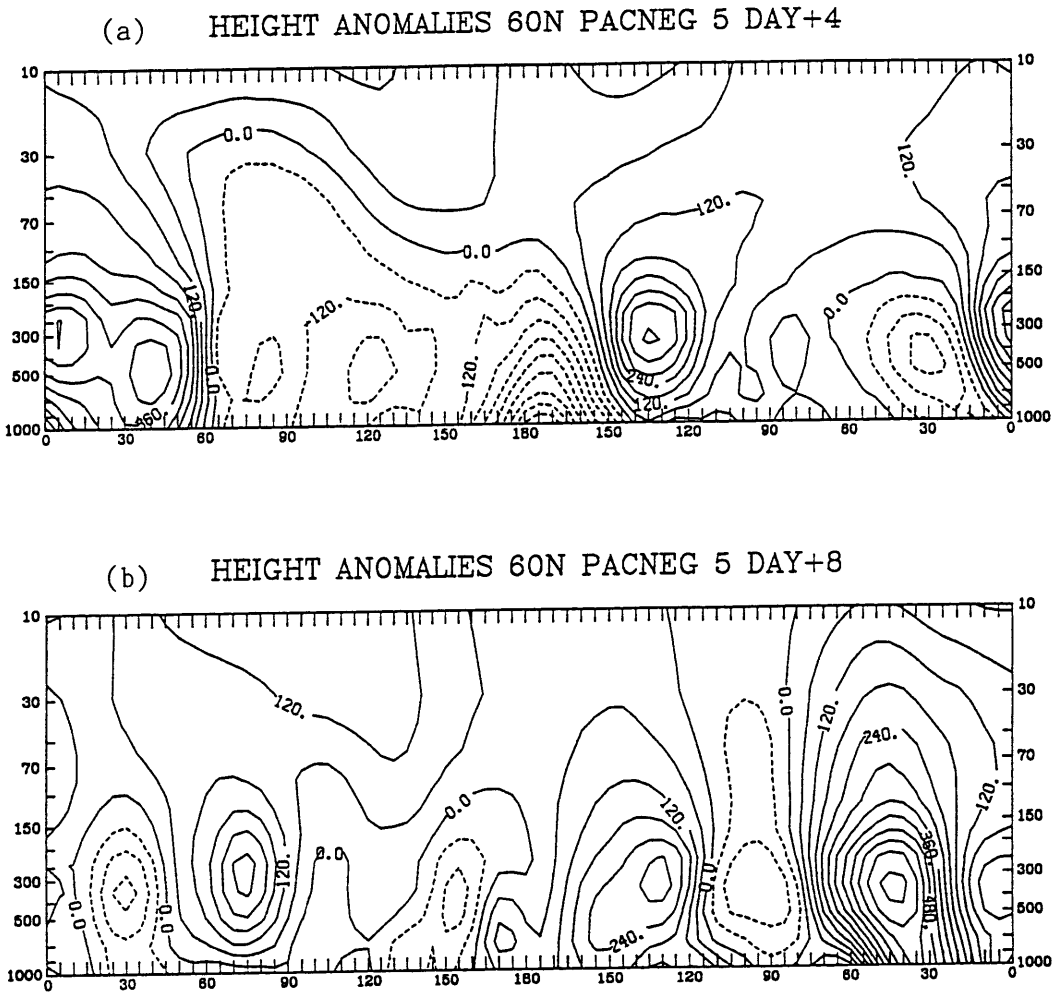

Fig. 5.6 Longitude-pressure (millibars) cross sections of height anomalies during PACNEG case 5 at 60°N on days (a) +4 and (b) +8, scaled by the square root of pressure to 300 mb.

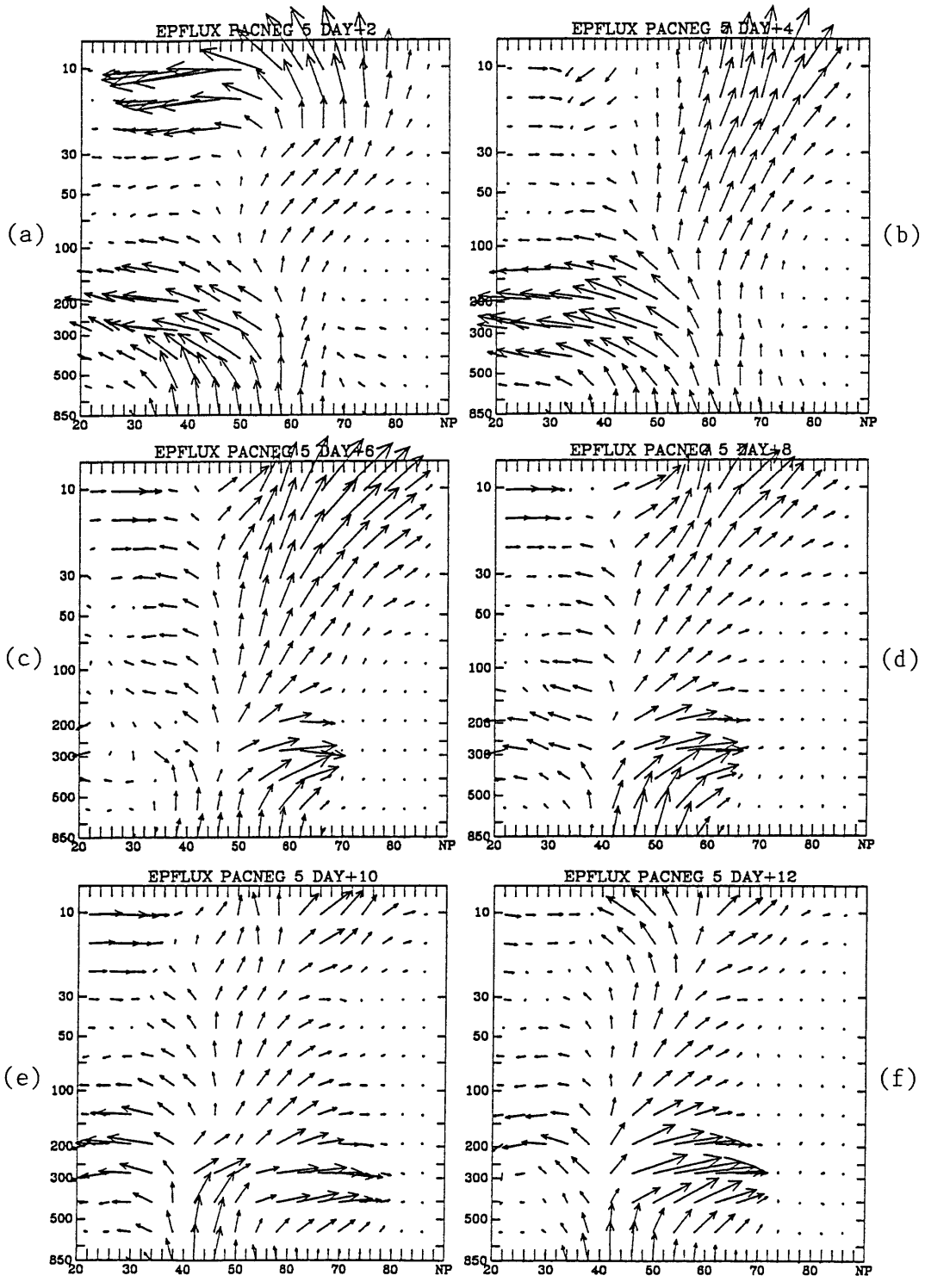

Fig. 5.7 As in Fig. 4.5 for Eliassen-Palm flux during PACNEG case 5 on days (a) +2, (b) +4, (c) +6, (d) +8, (e) +10, and (f) +12. The largest vector is 134 units.

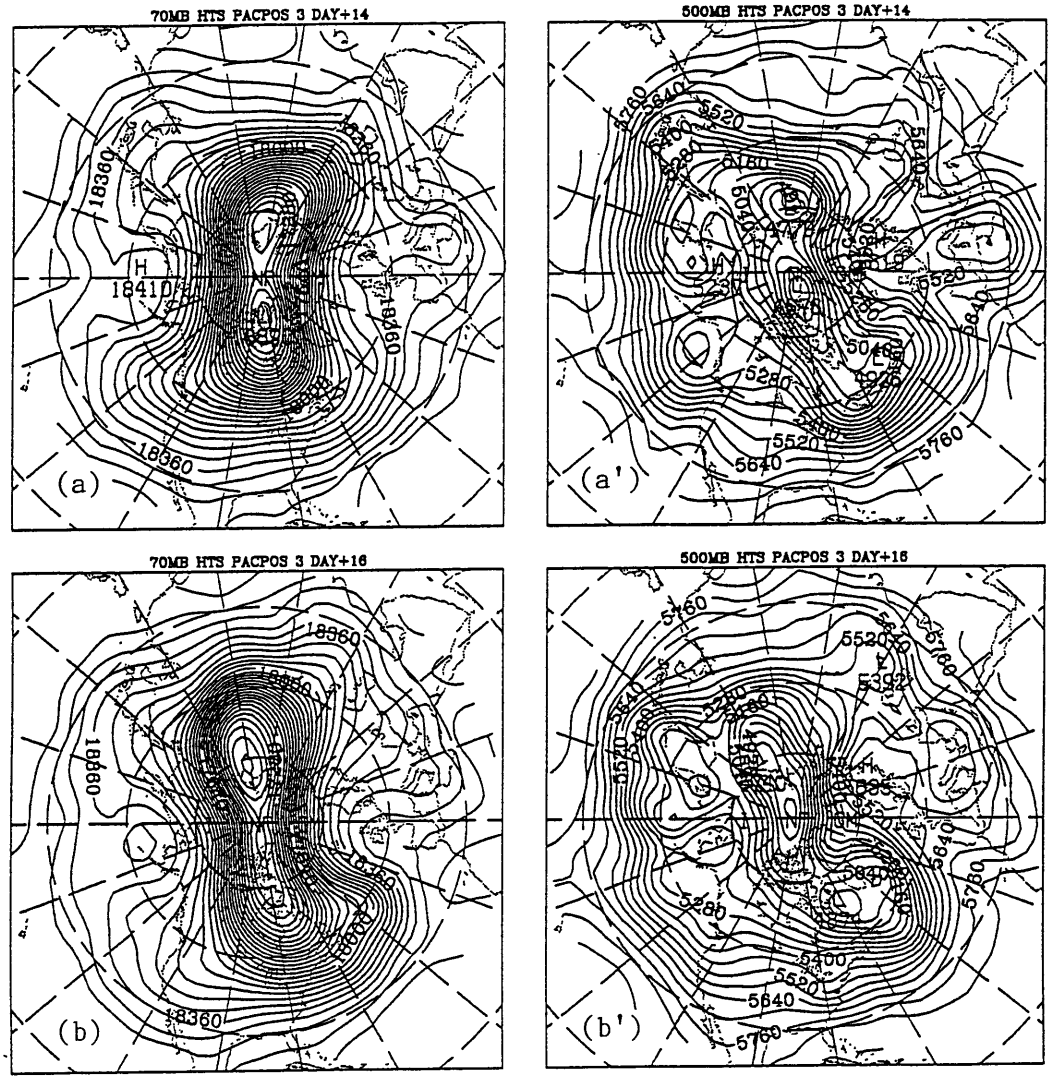

Fig. 5.8 70 mb geopotential heights (in meters) during PACPOS case 3 on days (a) +14, (b) +16, (c) +17, (d) +18, and (a')-(d') as in (a)-(d) for 500 mb geopotential heights.

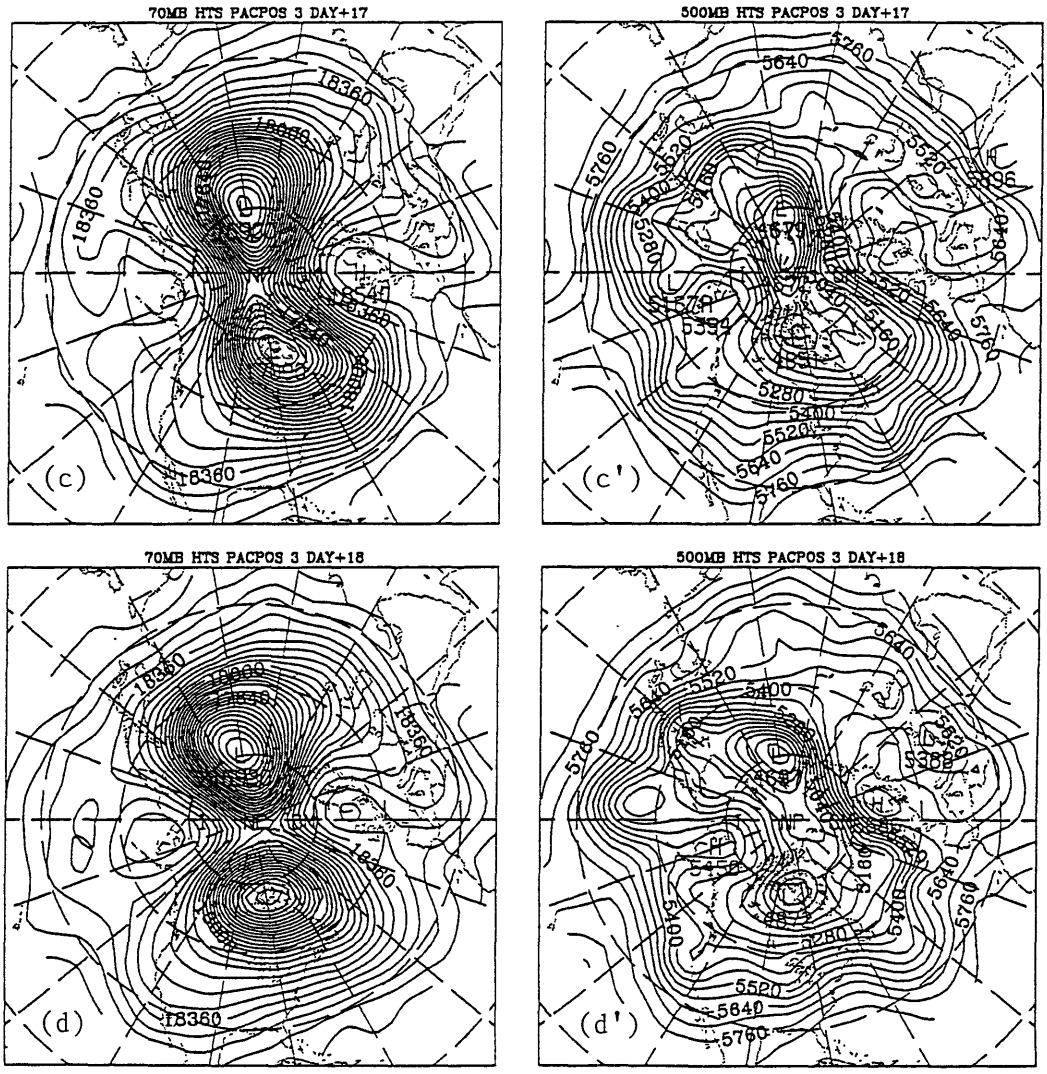

Fig. 5.8 (*Continued*)

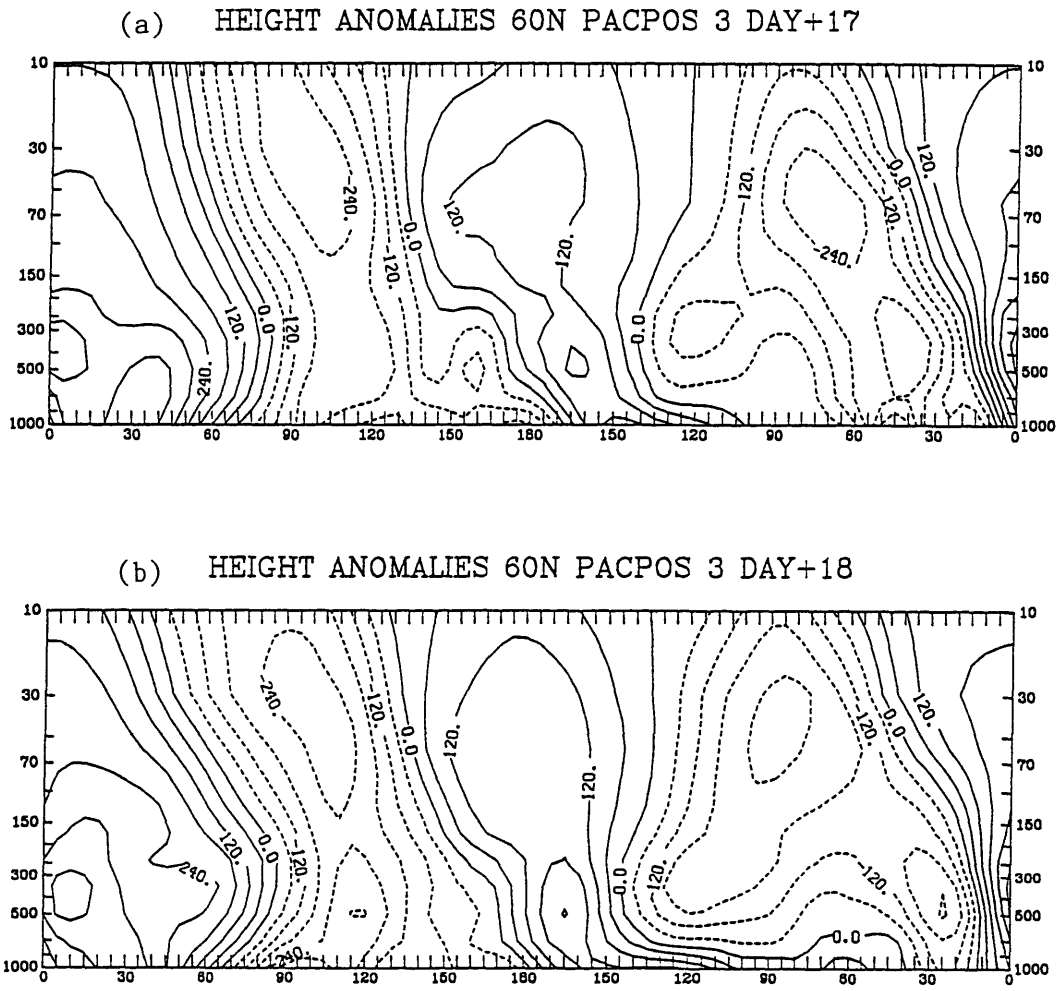

Fig. 5.9 Longitude-pressure (millibars) cross sections of height anomalies during PACPOS case 3 at 60°N on days (a) +17 and (b) +18, scaled by the square root of pressure to 300 mb.

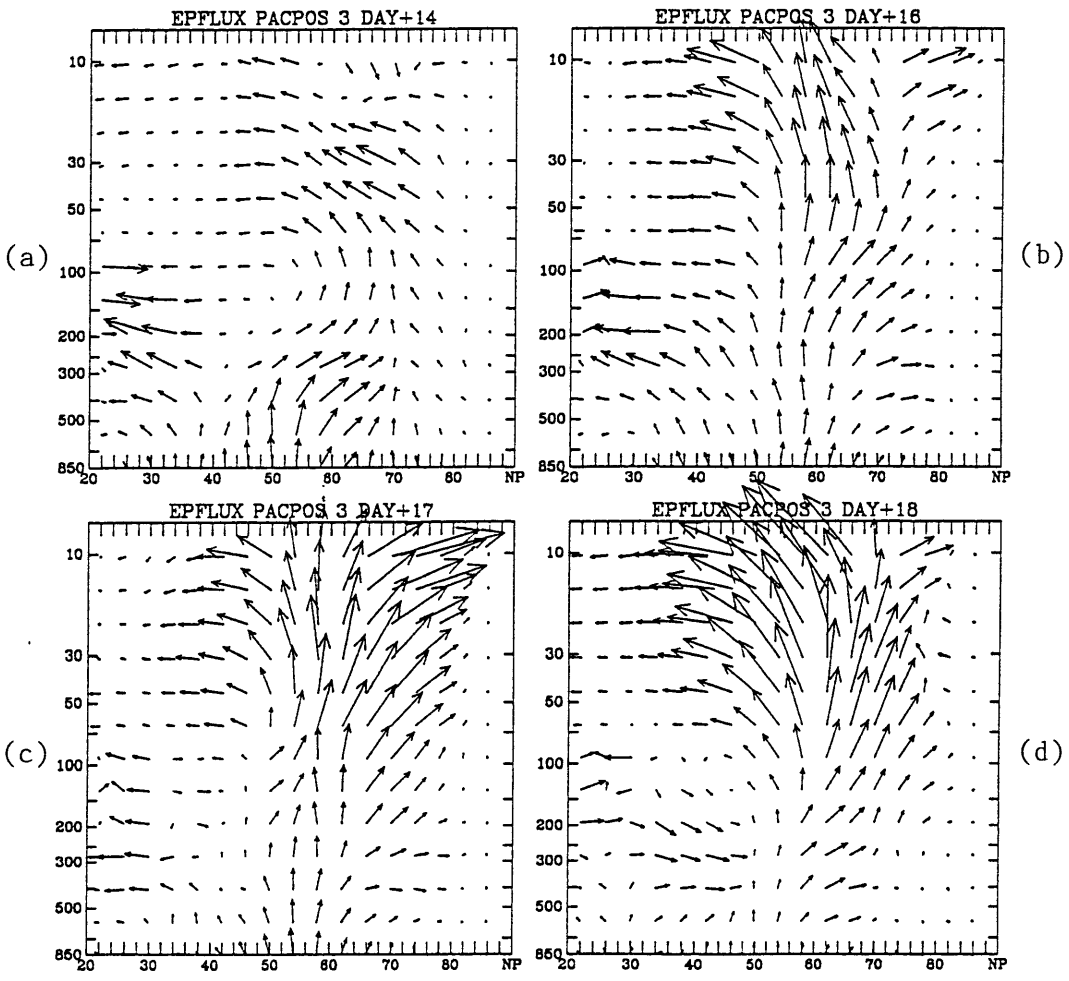

Fig. 5.10 As in Fig. 4.5 for Eliassen-Palm flux during PACPOS case 3 on days (a) +14, (b) +16, (c) +17, and (d) +18. The largest vector is 192 units.

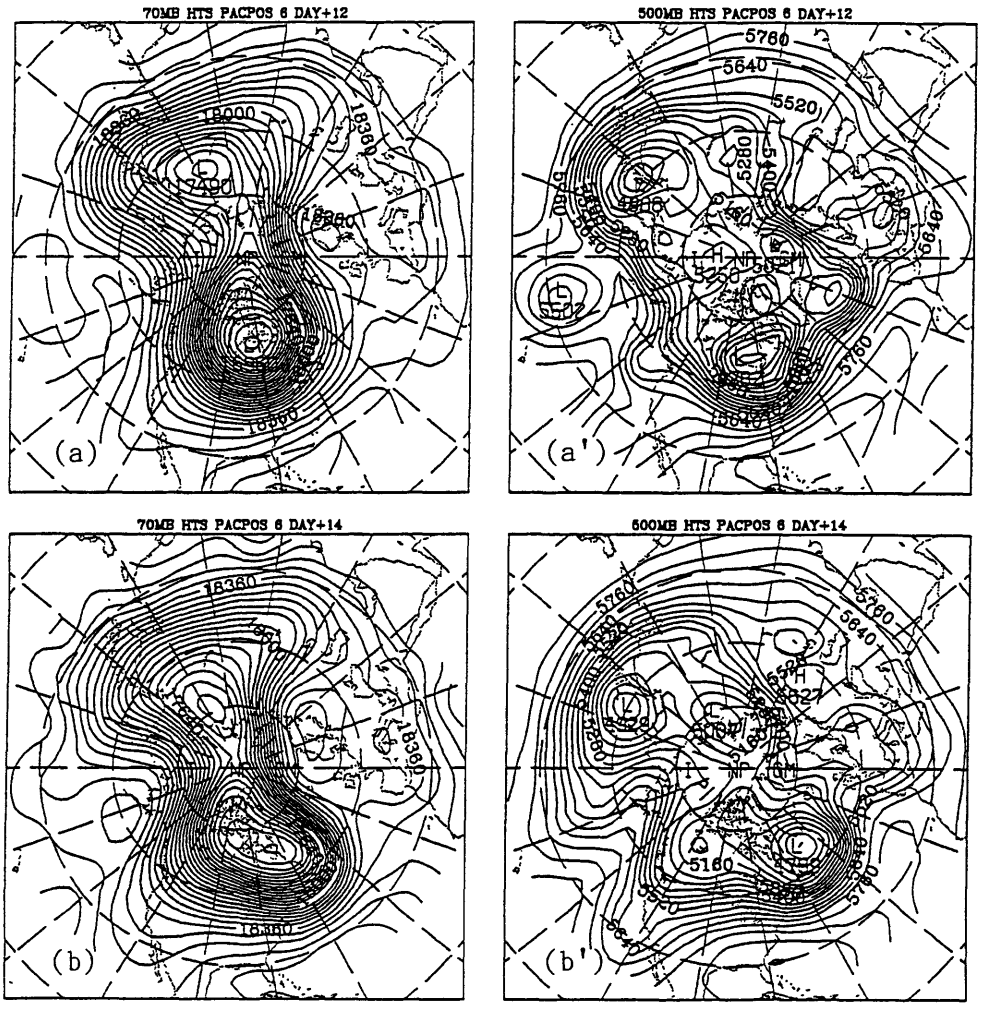

Fig. 5.11 70 mb geopotential heights during PACPOS case 6 on days (a) +12 and (b) +14 and for PACNEG case 11 on days (c) -2.5 and (d) -1.5. (a')-(d') are as in (a)-(d) for 500 mb.

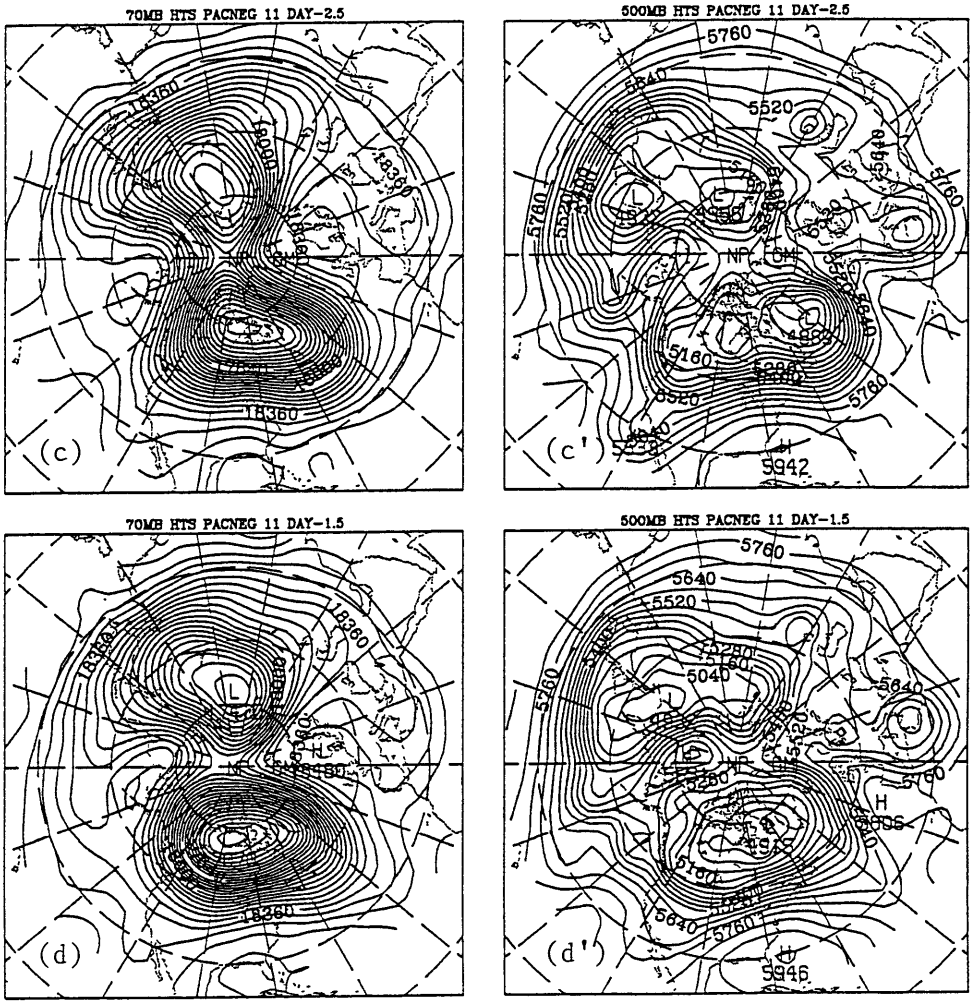

Fig. 5.11 (*Continued*)

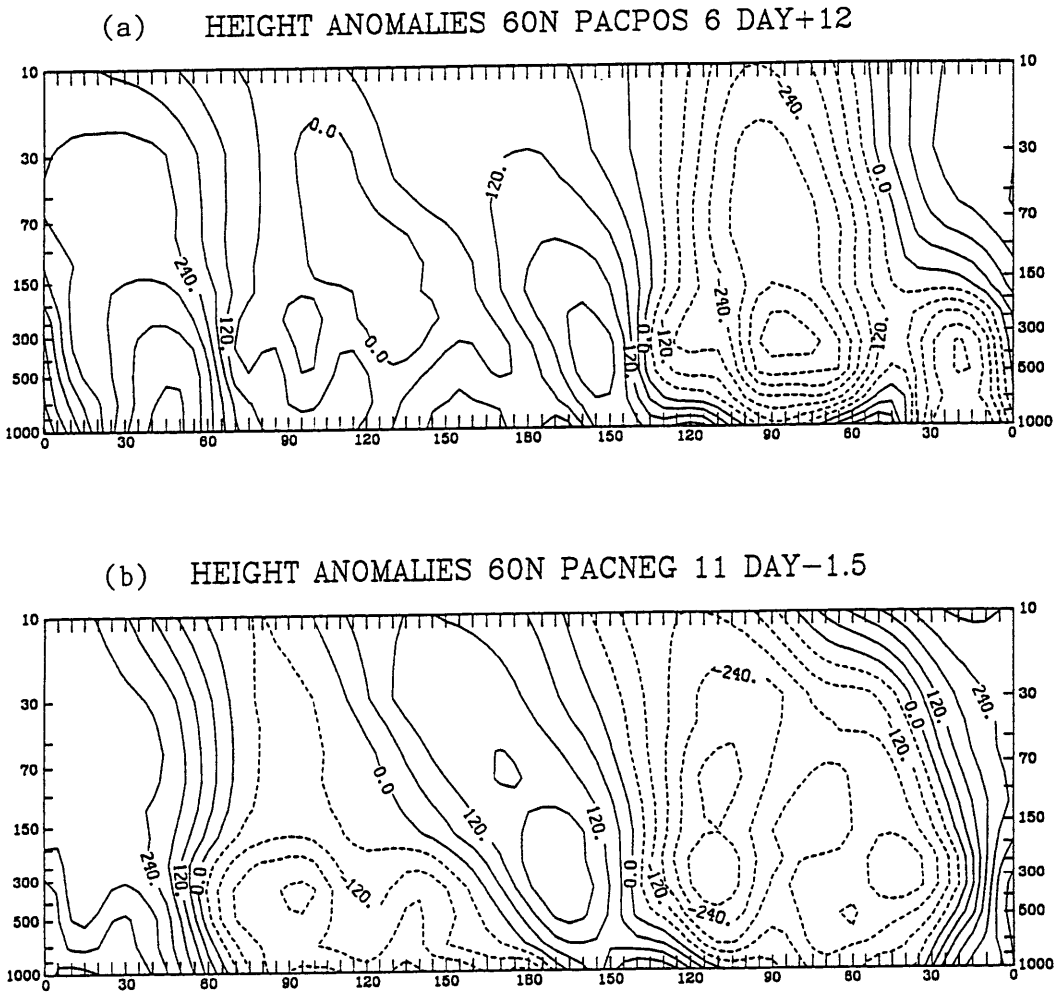

Fig. 5.12 Longitude-pressure (millibars) cross sections of height anomalies on (a) day +12 of PACPOS case 6 and (b) day-1.5 of PACNEG case 11.

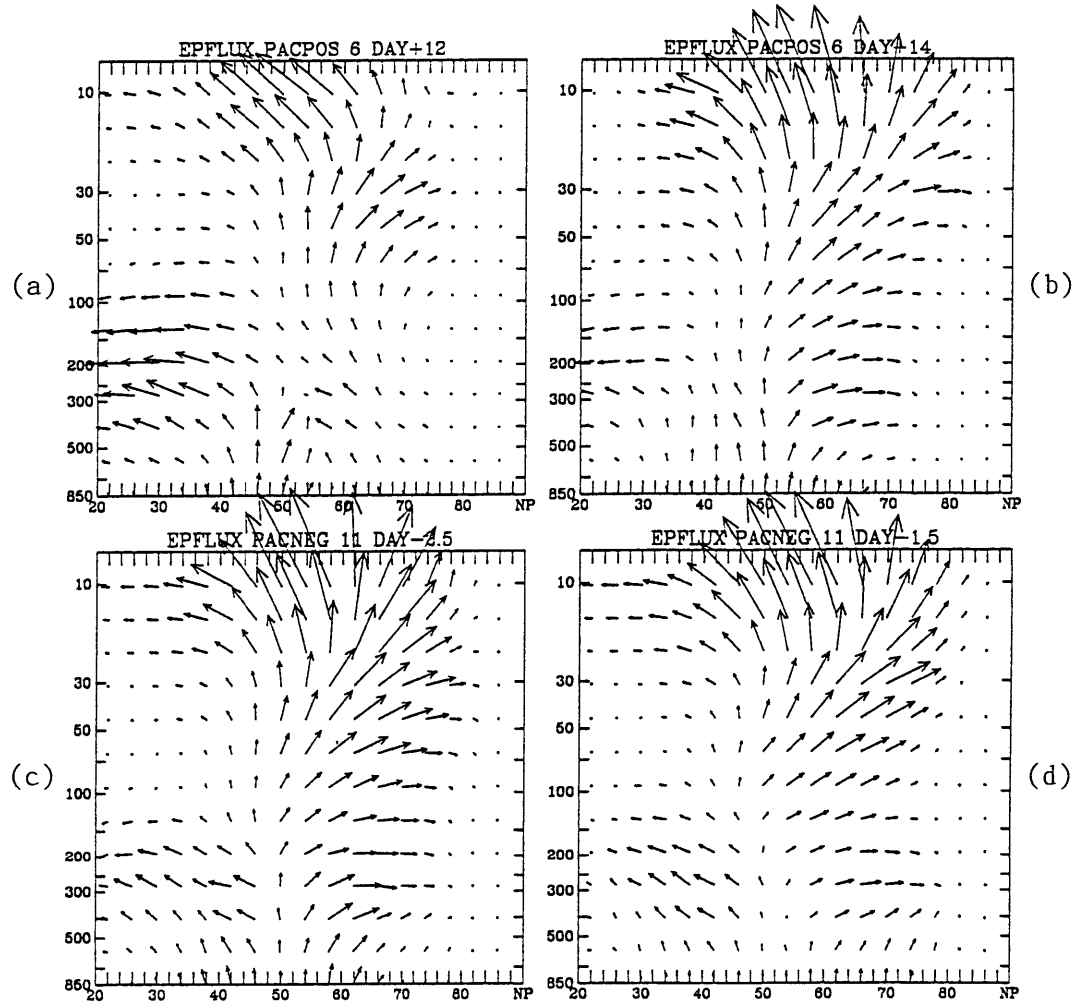

Fig. 5.13 As in Fig. 4.5 for Eliassen-Palm flux during PACPOS case 6 on days (a) +12 and (b) +14 and PACNEG case 1, days (c) -2.5 and (d) -1.5. The largest vector is 264 units.

CHAPTER 6

SUMMARY AND CONCLUSIONS

The previous results indicate that enhanced upward propagation from the troposphere into the middle stratosphere of large scale planetary waves may occur in conjunction with the development of certain persistent anomaly patterns. The Pacific events are associated with the greatest change in the middle stratosphere after case onset, while the Atlantic events appear to have only a small effect on the stratospheric flow, confined mainly to the lower stratosphere. Among the Pacific events, the PACNEG development is associated with enhanced upward propagation of planetary-scale waves, while the PACPOS events are associated with greater trapping of waves in the troposphere. We suggest that the anomaly patterns that develop in the stratosphere during the PACPOS cases result from the flow reducing back to a more zonal state in response to reduced upward flux of planetary wave activity from below.

In the first section, composite analyses of the developments of the PAC and ATL cases were presented. The 70 mb height analyses reveal that the dominant pattern at that level is the same pattern as at 500 mb and therefore, is primarly equivalent barotropic, as discussed in DS and DB, and we would expect this pattern to continue to decay away with height. At 10 mb, an upward-propagating component is found, although only PAC cases display a significant circulation change from day -2 to day +10. The primary anomaly does not appear at 10 mb. Rather, it is the secondary anomaly downstream over western North America that propagates into the middle stratosphere. Longitude-pressure cross sections of PACPOS and PACNEG case composites confirm that the primary

anomaly slowly dies with height, but the downstream anomaly is much less damped. Actual propagation, however, is different between PACPOS and PACNEG, with PACNEG having enhanced upward propagation. In PACNEG case cross sections, the stratosphere and troposphere are coherent and are dominated by wavenumber 2.

The most striking of all the stratospheric features are the initial stratospheric polar anomalies, which exist well before case onset and are strong in both ATL and PAC cases. In fact, they are the most intense and highly significant features at 10 mb. In the PAC patterns, the anomaly is centered over northwestern Canada and has the same sign as the primary anomaly (i.e. PACPOS-- positive ISPA). In PACPOS events, the ISPA has a warm core structure and is seen in the composite height field as a large wavenumber 1 ridge centered over Alaska. The polar vortex is highly distorted and weak. In PACNEG events, the ISPA is negative, and lower than normal heights dominate northwestern Canada. The 10 mb flow is more zonal with a deep, strong vortex. Temperature analyses reveal this feature to have a cold core.

In the Atlantic cases, the ISPA is centered more directly over the pole, and the relationship between the ISPA and the sign of the case is reversed. ATLPOS events have a negative ISPA, and ATLNEG events have a positive ISPA. The ATLPOS cases composited at the new Atlantic keypoint have the strongest and most highly significant of the ISPA's in any of the cases.

How these ISPA's develop is a mystery, because there is little evidence of any counterpart in the troposphere. Perhaps they are forced by random-phase planetary wave activity globally, and this random-phase forcing would explain why the wave activity is not observed in the troposphere. PACPOS and ATLNEG, having the positive ISPA and a weak polar vortex, would be associated with enhanced planetary wave activity in the stratosphere before onset, and the PACNEG and ATLPOS cases would be preceeded by less than normal planetary wave activity at 70 mb and above. Such a hypothesis of

random-phase wave activity explains ISPA's of all the cases quite well, except for the PACNEG cases, in which there is a strong wavenumber 1 ridge centered over Alaska. Such a ridge would not be found if wave activity was truly random in phase.

The existence of the ISPA's and their different relationships with ATL and PAC cases (i.e. positive ISPA with PACPOS and ATLNEG, negative ISPA with PACNEG and ATLPOS) provides some evidence for an association between ATL and POS patterns. It could be that the existence of an ATL case of one sign may favor development of a PAC case of the opposite sign or vice versa. Indeed, there is only a 10% chance that 7 out of the 9 case overlaps being opposite sign could have occurred only from sampling variability. Perhaps the ISPA's are a sign of atmospheric patterns that favor the development of persistent anomalies which otherwise would have been damped. If this is true, the same patterns that favor PACPOS favor ATLNEG development and those that favor PACNEG also favor ATLPOS. However, a larger set of cases is required to rule out sampling variability as an explanation for these overlaps.

Further diagnostic study in Chapter 3 concentrates on PAC cases. 10 mb heights during PAC events undergo a two stage process. First, there is the precursor stage. During this time (before day 0), the ISPA's are strong and highly significant. Then, the ISPA's are gradually replaced by the western North American anomaly, which extends upward from the troposphere.

Diagnostic studies presented in chapter 3 indicate that the way in which these secondary anomalies reach the stratosphere is different between PACPOS and PACNEG events. The patterns revealed by these diagnostics are essentially confined to the troposphere in PACPOS cases, but the same patterns reach upward to 10 mb in PACNEG.

Cross sections of the zonally averaged squared height anomalies show that in PACPOS cases, there is a relative minimum in wave activity near 150 mb. Above that

level, the high values are related to the ISPA's, and below, the development of the tropospheric persistent anomaly pattern results in a maximum of wave activity there. However, it appears that both areas occur separately, with no interaction between them. The tropospheric development remains essentially confined to levels below 100 mb. The same cross sections for PACNEG cases, on the other hand, have no relative minimum at 150 mb. The wave activity decreases upwards smoothly throughout the atmosphere, with one, single wave activity pattern that covers all layers in the last cross section.

Further evidence of this difference in propagation is given by zonal mean wind anomaly cross sections. In both PACPOS and PACNEG events, a couplet of zonal mean wind anomalies develops in the troposphere. In the PACPOS events, this couplet is confined to the troposphere, but in the PACNEG events, it extends up to 10 mb. Also, in the PACPOS events, the stratosphere is dominated by a weaker flow (i.e. weaker polar vortex) throughout the time series, showing the presence of the ISPA before onset and a continued weak (but strengthening) vortex throughout the rest of the case. In the PACNEG events, the polar vortex in the stratosphere originally is strong, but the flow then slows down in response to the convergence of the upward flux of wave activity from below.

Finally, EP flux vectors confirm that there is indeed weaker than normal wave activity flux during the PACPOS events. On day -6, EP flux is quite large and upward at 10 mb and 30 mb during the development of the positive ISPA. As the tropospheric PACPOS pattern develops, EP flux decreases and upward flux remains weak throughout the rest of the time series. There is, however, some anomalously large horizontal flux into high latitudes.

In the PACNEG cases, vectors in the stratosphere are weak before onset. During onset of the tropospheric PACNEG pattern, the EP fluxes in that region increase. After onset, upward fluxes increase at all levels, and there is more concentration of wave

activity into the polar stratosphere, especially on day +8, when the 10 mb positive anomaly over North America is building most rapidly.

Four sudden stratospheric major midwinter warmings were also analysed to see what role the simultaneous persistent anomaly cases may have played in their development. In all cases, it was found that major ridges were present in both the eastern Atlantic and eastern Pacific during the warming, of which the Atlantic ridge was the larger anomaly. The EP fluxes in all the cases were anomalously convergent in the polar stratosphere. It appears that certain conditions are necessary for the focusing of large scale wave activity into the polar regions, and although these conditions are not present in all persistent anomaly cases, when they do occur, the persistent anomaly patterns contribute significantly to the anomalous large scale wave activity.

APPENDIX A

SYMBOLS

f = Coriolis parameter

g = gravitational acceleration

S = static stability of the atmosphere

T = temperature

z = geopotential height

z' = geopotential height anomaly (difference from climatology)

u_g = geostrophic eastward wind

v_g = geostrophic northward wind

θ = latitude

λ = longitude

APPENDIX B

CASE DATES

ORIGINAL KEYPOINTS

Pacific Cases (45°N,170°W)

PACPOS

No.	Yr.	Mo.	Day	UTC	Duration (days)
1	75	1	25	0000	20.0
2	78	12	12	1200	14.0
3	79	2	3	1200	14.0
4	79	12	1	0000	11.0
5	81	12	25	0000	10.0
6	84	12	13	1200	14.5
7	85	2	2	1200	14.5

PACNEG

No.	Yr.	Mo.	Day	UTC	Duration (days)
1	73	12	17	0000	11.0
2	75	12	16	1200	12.0
3	76	1	24	0000	10.5
4	76	12	10	0000	15.0
5	77	1	1	0000	52.5
6	78	2	10	0000	28.5
7	80	2	4	0000	11.0
8	80	12	28	1200	22.5
9	81	12	11	0000	12.5
10	83	1	13	1200	56.0
11	84	12	30	0000	14.0
12	85	12	17	0000	11.5
13	86	1	26	0000	19.5

Atlantic Cases (50°N,25°W)

ATLPOS

No.	Yr.	Mo.	Day	UTC	Duration (days)
1	73	1	23	1200	36.0
2	74	12	29	1200	10.0
3	75	12	3	0000	26.5
4	76	1	8	0000	18.5
5	77	12	26	1200	10.0
6	80	12	26	0000	42.0
7	83	2	2	0000	13.0
8	84	2	5	0000	12.0
9	86	1	23	1200	13.5

ATLNEG

No.	Yr.	Mo.	Day	UTC	Duration (days)
1	74	1	1	0000	14.0
2	74	1	24	0000	10.0
3	77	12	1	0000	11.0
4	78	2	15	1200	16.5
5	78	12	1	0000	14.5
6	81	12	10	1200	26.0
7	83	12	13	0000	12.0
8	85	2	5	0000	10.0

NEW KEYPOINTS

Pacific Cases (42°N,145°W)

New PACPOS

No.	Yr.	Mo.	Day	UTC	Duration (days)
1	79	1	26	0000	12.5
2	82	1	10	1200	13.0
3	82	1	29	1200	12.0
4	84	1	20	1200	14.0
5	84	12	8	1200	12.0
6	85	1	26	1200	13.0
7	85	2	16	0000	19.0

New PACNEG

No.	Yr.	Mo.	Day	UTC	Duration (days)
1	77	12	9	1200	14.0
2	78	1	2	0000	16.5
3	78	2	1	1200	12.5
4	79	1	2	1200	11.0
5	80	2	15	1200	15.5
6	81	1	6	1200	16.5
7	81	12	3	1200	17.5
8	82	12	10	1200	13.5
9	83	1	14	0000	55.5
10	85	1	13	1200	12.0
11	86	2	11	0000	10.0

Atlantic Cases (46°N,35°W)

New ATLPOS

No.	Yr.	Mo.	Day	UTC	Duration (days)
1	77	12	25	1200	10.0
2	78	1	9	1200	11.5
3	80	12	25	1200	31.0
4	82	12	12	0000	12.5
5	83	1	26	1200	18.0
6	83	12	26	0000	21.0
7	84	1	27	1200	14.0
8	86	1	20	1200	16.0

New ATLNEG

No.	Yr.	Mo.	Day	UTC	Duration (days)
1	77	12	1	0000	10.5
2	78	2	14	0000	20.5
3	78	12	1	0000	13.5
4	78	12	22	1200	10.0
5	79	2	2	0000	13.0
6	80	2	6	1200	10.5
7	81	12	24	0000	17.5
8	85	2	2	1200	12.0

REFERENCES

Blackmon, M. L., 1976: A climatological spectral study of the geopotential height of the Northern Hemisphere. *J. Atmos. Sci.*, **33**, 1607-1623.

----, R. A. Madden, J. M. Wallace and D. S. Gutzler, 1979: Geographical variations in the vertical structure of geopotential height fluctuations. *J. Atmos. Sci.*, **36**, 2450-2466.

----, S. L. Mullen and G. T. Bates, 1986: The climatology of blocking events in a perpetual January simulation of a spectral general circulation model. *J. Atmos. Sci.*, **43**, 1379-1405.

Charney, J. G., and P. G. Drazin, 1961: Propagation of planetary-scale disturbances from the lower into the upper atmosphere. *J. Geophys. Res.*, **66**, 83-109.

Crane, A. J., 1979: Aspects of the energetics of the upper stratosphere during the January-February 1973 major warming. *Quart. J. R. Met. Soc.*, **105**, 185-206.

Dole, R. M., 1986a: Persistent anomalies of the extratropical Northern Hemisphere wintertime circulation: Structure. *Mon. Wea. Rev.*, **109**, 784-812.

----, 1986b: The life cycles of persistent anomalies and blocking over the North Pacific. *Adv. Geophys.*, **29**, 31-69.

----, 1989: The life cycles of persistent anomalies. Part I: Evolution of 500 mb height anomalies. *Mon. Wea. Rev.*, **117**, 177-211.

----, and Black, R. X., 1990: Life cycles of persistent anomalies. Part II: The development of persistent negative height anomalies over the North Pacific Ocean. *Mon. Wea. Rev.*, **118**, 824-846.

----, and Gordon, N. D., 1983: Persistent anomalies of the extratropical Northern Hemisphere wintertime circulation: Geopotential distribution and regional persistence characteristics. *Mon. Wea. Rev.*, **11**, 1567-1586.

Dunkerton, T. J., and D. P. Delisi, 1986: Evolution of potential vorticity in the winter stratosphere of January-February 1979. *J. Geophys. Res.*, **91**, 1199-1208.

Edmon, H. J., B. J. Hoskins and M. E. McIntyre, 1980: Eliassen-Palm cross sections for the troposphere. *J. Atmos. Sci.*, **37**, 2600-2616.

Held, I. M., 1983: Stationary and quasi-stationary eddies in the extratropical troposphere: Theory. *Large-scale Dynamical Processes in the Atmosphere*. B. J. Hoskins and R. P. Pearce, Eds., Academic Press, 127-168.

Holton, J. R., 1979: *An Introduction to Dynamic Meteorology*, Second Ed. Academic Press, 391 pp.

Hoskins, B. J., A. J. Simmons and D. G. Andrews, 1977: Energy dispersion in a barotropic atmosphere. *Quart J. Roy. Meteor. Soc.*, **103**, 553-567.

Houghton, J. T., 1978: The stratosphere and mesosphere. *Quart. J. R. Met. Soc.*, **104**, 1-29.

Labitzke, K. B., 1981a: The amplification of wave 1 in January 1979: a characteristic precondition for the major warming in February. *Mon.Wea Rev.*, **109**, 983-989.

----, 1981b: Stratospheric-mesospheric mid-winter disturbances: A summary of observed characteristics. *J. Geophys. Res.*, **86**, 9665-9678.

----, 1982: On the interannual variability of the middle stratosphere during the northern winters. *J. Meteorol. Soc. Japan*, **60**, 124-139.

----, R. Lenschow, B. Naujokat and K. Petzoldt, 1985a: First note in the major stratospheric warming at the end of December 1984. *Beilage zur Berliner Wetterkarte*, SO 1/85, 16 January 1985.

----,----,----,----, B. Rajewski and R. C. Wohlfart, 1985b: The third winter of MAP-Dynamics, 1984/85: A winter with an extremely intense and early major warming. *Beilage zur Berliner Wetterkarte*, SO 24/85, 7 Ocotober 1985.

----, K. Petzoldt, B. Naujokat, E. Klinker and R. Lenschow, 1977: *Beilage zur Berliner Wetterkarte des Institüt für Meteorologie der Freien Universität*, Berlin, 27 Jan. 1977.

Lau, N-C., and M. J. Nath, 1987: Frequency dependence of the structure and temporal development of wintertime tropospheric fluctuations-- comparison of a GCM simulation with observations. *Mon. Wea. Rev.*, **115**, 251-271.

McIntyre, M. E., 1982: How well do we understand the dynamics of stratospheric warmings? *J. Meteorol. Soc. Japan*, **60**, 37-65.

O'Neill, A., and B. F. Taylor, 1979: A study of the major stratospheric warming of 1976/77. *Quart. J. R. Met. Soc.*, **105**, 71-92.

----, and C. E. Youngblut, 1982: Stratospheric warmings diagnosed using the transformed Eulerian-mean equations and the effect of the mean state on wave propagation. *J. Atmos. Sci.*, **39**, 1370-1386.

Palmer, T. N., 1981a: Diagnostic study of a wavenumber-2 stratospheric sudden warming in a transformed Eulerian-mean formalism. *J. Atmos. Sci.*, **38**, 844-855.

----, 1981b: Aspects of stratospheric sudden warmings studied from a transformed Eulerian-mean viewpoint. *J. Geophys. Res.*, **86**, 9679-9687.

Plumb, R. A., 1985: On the three-dimensional propagation of stationary waves. *J. Atmos. Sci.*, **42**, 217-229.

Quiroz, R. S., 1975: The stratospheric evolution of sudden warmings in 1969-74 determined from measured infrared radiation fields. *J. Atmos. Sci.*, **32**, 211-224.

----, 1977: The tropospheric-stratospheric polar vortex breakdown of January 1977. *Geophys. Res. Lett.*, **4**, 151-154.

----, 1979: Tropospheric-stratospheric interaction in the major warming event of January-February 1979. *Geophys. Res. Lett.*, **6**, 645-648.

Randall, W. J., and B. A. Boville, 1987: Observations of a major stratospheric warming during December 1984. *J. Atmos. Sci.*, **44**, 2179-2186.

Rex, D. F., 1950a: Blocking action in the middle troposphere and its effects on regional climate. I. An aerological study of blocking. *Tellus*, **2**, 196-211.

----, 1950b: Blocking action in the middle troposphere and its effects on regional climate. II. The climatology of blocking action. *Tellus*, **2**, 275-301.

Taylor, B. F., and J. D. Perry, 1977: The major stratospheric warming of 1976-77. *Nature*, **267**, 417-418.

Wallace, J. M. and D. S. Gutzler: Teleconnections in the geopotential height field during the Northern Hemisphere winter. *Mon. Wea. Rev.*, **109**, 784-812.